

University of Windsor

Scholarship at UWindor

Electronic Theses and Dissertations

Theses, Dissertations, and Major Papers

10-30-2020

Investigation of Heat Recovery Methods from Molten Salts with Phase Change

Bharanidharan Rajasekaran
University of Windsor

Follow this and additional works at: <https://scholar.uwindsor.ca/etd>

Recommended Citation

Rajasekaran, Bharanidharan, "Investigation of Heat Recovery Methods from Molten Salts with Phase Change" (2020). *Electronic Theses and Dissertations*. 8471.
<https://scholar.uwindsor.ca/etd/8471>

This online database contains the full-text of PhD dissertations and Masters' theses of University of Windsor students from 1954 forward. These documents are made available for personal study and research purposes only, in accordance with the Canadian Copyright Act and the Creative Commons license—CC BY-NC-ND (Attribution, Non-Commercial, No Derivative Works). Under this license, works must always be attributed to the copyright holder (original author), cannot be used for any commercial purposes, and may not be altered. Any other use would require the permission of the copyright holder. Students may inquire about withdrawing their dissertation and/or thesis from this database. For additional inquiries, please contact the repository administrator via email (scholarship@uwindsor.ca) or by telephone at 519-253-3000ext. 3208.

Investigation of Heat Recovery Methods from Molten Salts with Phase Change

By

Bharanidharan Rajasekaran

A Thesis
Submitted to the Faculty of Graduate Studies
through the Department of Mechanical, Automotive, and Materials Engineering
in Partial Fulfillment of the Requirements for
the Degree of Master of Applied Sciences
at the University of Windsor

Windsor, Ontario, Canada

2020

© 2020 Bharanidharan Rajasekaran

Investigation of Heat Recovery Methods from Molten Salts with Phase Change

By

Bharanidharan Rajasekaran

Approved by

M. Azzouz

Department of Electrical & Computer Engineering

V. Roussinova

Department of Mechanical, Automotive and Materials Engineering

O. A. Jianu, Advisor

Department of Mechanical, Automotive and Materials Engineering

August 20, 2020

DECLARATION OF CO-AUTHORSHIP/ PREVIOUS PUBLICATION

I. Co-Authorship

I hereby declare that this thesis incorporates material that is result of joint research, as follows: Chapter 3, 4 and 5 of the thesis was authored by Bharanidharan Rajasekaran under the supervisions of Professor Ofelia A. Jianu. In all cases, the key ideas, primary contributions, experimental designs, data analysis, interpretation, and writing were performed by the author, and the contribution of the co-author was primarily through the feedback on refinement of ideas and editing of the manuscript.

I am aware of the University of Windsor Senate Policy on Authorship and I certify that I have properly acknowledged the contribution of other researchers to my thesis and have obtained written permission from the co-author to include the above material in my thesis.

I certify that, with the above qualification, this thesis, and the research to which it refers, is the product of my own work.

II. Previous Publication

This thesis includes one original paper that has been previously published/submitted for publication in peer reviewed journals, as follows:

Thesis Chapter	Publication title/full citation	Publication status*
Chapter 3 and 4	Investigation of Thermodynamic Properties of Molten Salts Evaluated by EMF Measurements with Application to Thermochemical Cycles for Hydrogen Production	Submitted to International Journal of Hydrogen Energy
Chapter 5	Numerical Thermal Model of Liquid-to-Solid Phase Change of Free Falling CuCl and AgCl Droplets	Submitted to International Journal of Heat and Mass Transfer

I certify that I have obtained a written permission from the copyright owner(s) to include the above published material(s) in my thesis. I certify that the above material describes work completed during my registration as a graduate student at the University of Windsor.

III. General

I declare that, to the best of my knowledge, my thesis does not infringe upon anyone's copyright nor violate any proprietary rights and that any ideas, techniques, quotations, or any other material from the work of other people included in my thesis, published or otherwise, are fully acknowledged in accordance with the standard referencing practices. Furthermore, to the extent that I have included copyrighted material that surpasses the bounds of fair dealing within the

meaning of the Canada Copyright Act, I certify that I have obtained a written permission from the copyright owner(s) to include such material(s) in my thesis.

I declare that this is a true copy of my thesis, including any final revisions, as approved by my thesis committee and the Graduate Studies office, and that this thesis has not been submitted for a higher degree to any other University or Institution.

ABSTRACT

In the present times there is a progressive surge in the energy requirements for industrial and domestic purposes, hence it is imperative to harvest energy from renewable sources. In addition to serving as a sustainable source of energy, these energy sources prove to be indispensable in the mitigation of the greenhouse effects.

In the past several decades, various methods and processes for utilizing renewable energy sources have been developed and continue to be improved. Hydrogen holds the highest energy density compared to any common fuel. Along with its abundance and lightweight nature hydrogen is more eco-friendly during utilization and can be produced via sustainable methods that do not pollute our planet. Through extensive research, numerous methods for extracting hydrogen are identified. Among them, a promising one is the thermochemical copper-chlorine (Cu-Cl) cycle, which is a clean hydrogen production method. As the Cu-Cl cycle is a relatively novel concept, it has been found that it is not well-defined in thermophysical and material properties for its specific application and thus predisposing it to approximation and assumptions from published data.

In the Cu-Cl cycle, heat can be recovered from molten cuprous chloride (CuCl) and it is then reacted with aqueous hydrochloric acid (HCl) in stoichiometric proportions to produce the anolyte for the H₂ production step of the cycle. However, the lack of precise thermophysical properties on CuCl heavily hinders the detailed investigations of heat recovery from the molten salt as it cools from 450°C to 90°C. A new method is developed to determine the thermophysical property of CuCl and silver chloride (AgCl) as the molten salts are changing phases to solid. This is achieved by correlating electrochemistry data with thermal data. A model that predicts the specific heat capacity during phase change process is developed based on the existing electromotive force (EMF) and thermal data from literature. The developed model shows the EMF derived specific heat capacity values of AgCl and CuCl are similar with a slight offset since they have similar EMF's at higher temperatures. A numerical method is adopted for estimating the amount of heat that could be recovered during quenching process by analyzing the interactions between CuCl droplets with the nitrogen (N₂). These interactions are modeled numerically in COMSOL Multiphysics for various droplet sizes of CuCl and AgCl with the developed specific heat model. The heat recovery analysis shows that after quenching, the average internal temperature of the droplet does not change significantly with droplet diameter and quenching height.

ACKNOWLEDGEMENTS

First and foremost, I wish to express my sincere gratitude to my mentor and supervisor Dr. O. A. Jianu for the continuous support for my masters' study and research, for her patience, motivation, enthusiasm and immense knowledge. Her invaluable guidance and insight have helped me throughout the duration of this research and thesis writing. Without her help and guidance, the goal of my research would not have been realised.

I want to thank my committee members Dr. V. Roussinova and Dr. M. Azzouz for their valuable guidance and input throughout my research. I also want to thank the rest of the I-FuELs research group for their input and assistance during our weekly meetings.

A special thanks to my family. Words cannot express how grateful I am to my mother and father for all the sacrifices that they have made on my behalf. Their prayers for me was what sustained me thus far. I also like to thank Isha for her invaluable love and support.

I extend my sincere gratitude to all my friends who incited me to strive towards my goal. I would also like to thank my friends Madhan, Siddarth, Sarah, Rhea for their encouragement.

This accomplishment would not have been possible without them. Thank you.

TABLE OF CONTENTS

DECLARATION OF CO-AUTHORSHIP/ PREVIOUS PUBLICATION	iii
ABSTRACT	vi
ACKNOWLEDGEMENTS	vii
LIST OF FIGURES.....	xi
LIST OF TABLES.....	xiv
LIST OF APPENDICES.....	xv
LIST OF ABBREVIATIONS/SYMBOLS.....	xvi
NOMENCLATURE.....	xvii
Chapter 1 - Introduction	1
1.1 Background and Motivation	1
1.2 Objectives.....	2
1.3 Literature Review	2
1.3.1 Hydrogen production methods	6
1.3.2 Thermochemical Copper Chlorine cycle (Cu-Cl) cycle.....	9
1.3.3 Heat Recovery in the Copper-Chlorine Cycle	13
1.3.4 Heat Transfer and Solidification of Droplet	14
1.3.5 Description of Cuprous Chloride (CuCl)	18
1.3.6 Description of Silver Chloride (AgCl)	18

1.4	Thesis Outline.....	18
Chapter 2 - Methods to Determine Thermophysical Properties.....		20
2.1	Introduction.....	20
2.2	Methodology.....	20
2.2.1	Quantum Mechanics Approach.....	20
2.2.2	Thermal Measurements.....	25
2.2.3	Electro-Magnetic Force Method.....	26
2.2.4	Summary of Methodology.....	27
2.3	Literature of Thermophysical Properties of AgCl.....	28
2.3.1	Heat Capacity of AgCl.....	28
2.3.2	Other Properties: Thermal Conductivity, Density, Viscosity.....	31
2.4	Thermophysical Properties of CuCl.....	33
2.4.1	Heat Capacity of CuCl.....	33
2.4.2	Other Properties: Thermal Conductivity, Density, Viscosity.....	34
Chapter 3 - Heat Capacity Results of AgCl and CuCl.....		37
3.1	Modelling of Heat Capacity of AgCl.....	37
3.2	Modelling Specific Heat Capacity of CuCl.....	40
Chapter 4 - Heat Recovery Study.....		43
4.1	Introduction.....	43
4.2	Free Fall.....	44
4.3	Assumptions.....	44

4.4	Numerical model	45
4.4.1	Momentum Equation:	46
4.4.2	Energy Equation:	47
4.5	Results and Discussion	48
4.5.1	Free fall	48
4.5.2	Phase Change in AgCl and CuCl Droplet.....	49
4.6	Validation of Computational Results.....	53
4.7	Heat Recovery	55
Chapter 5 - Summary and Conclusion		57
5.1	Findings and Results	57
5.2	Recommendations and Future Work	57
BIBLIOGRAPHY		59
APPENDICES		73
VITA AUCTORIS.....		74

LIST OF FIGURES

Figure 1. U.S primary energy consumption by energy source, 2019 [2]	3
Figure 2. Schematic model of a working fuel cell [8]	4
Figure 3. Global demand of pure hydrogen from 1975 to 2018 [23].....	5
Figure 4. Current policy support for hydrogen deployment, 2018 [23].....	6
Figure 5. Sources of hydrogen production [32].....	7
Figure 6. Stoichiometric chart of Cu-Cl cycle.....	11
Figure 7. Solubility difference of CuCl in binary and ternary systems [75]	14
Figure 8. Droplet suspended on a thermocouple junction [88].	16
Figure 9. Levitation of droplet using magnetic field [94].....	16
Figure 10. Electrostatic levitation of a Titanium-Zirconium-Nickel alloy [95].....	17
Figure 11. Physics fields (adopted from [109])	21
Figure 12. Quantum leap of electrons due to excitation and emission of quanta [111]	22
Figure 13. Model of atomic structure [108]	22
Figure 14. Structure of Solids (a) Crystalline, (b) Amorphous [116].....	23
Figure 15. Temperature dependence on molar heat capacity for different solids [116]	24
Figure 16. Variation of specific heat capacity of Silver Chloride (AgCl) as a function of temperature. Data adopted from [131], [132], [134]–[138]	29
Figure 17. Electromotive force (EMF) of AgCl as function of temperature. Data extracted from literatures [142], [146], [147], [149]–[152]	30
Figure 18. Variation of Density of Silver Chloride (AgCl) as a function of temperature.....	31
Figure 19. Variation of thermal conductivity of Silver Chloride (AgCl) as a function of temperature	32
Figure 20. Variation of dynamic viscosity of Silver Chloride (AgCl) as a function of temperature...	32

Figure 21. Variation of specific heat capacity of Cuprous Chloride (CuCl) as a function of temperature. Data adopted from[161], [162], [164]–[166].....	33
Figure 22. Electromotive force (EMF) of CuCl as function of temperature. [167]–[169].....	34
Figure 23. Variation of density of Cuprous Chloride (CuCl) as a function of temperature[170].....	35
Figure 24. Variation of thermal conductivity of Cuprous Chloride (CuCl) as a function of temperature[170].....	35
Figure 25. Variation of dynamic viscosity of Cuprous Chloride (CuCl) as a function of temperature[170].....	36
Figure 26. Variation of specific heat capacity of AgCl and CuCl with temperature derived from EMF sources	37
Figure 27. Consolidated specific heat capacity of AgCl as function of temperatures from EMF and thermal sources[130]–[132], [134]–[138].....	39
Figure 28. Comparison of EMF between AgCl and CuCl as function of temperature. AgCl data adopted from [167].....	40
Figure 29. Consolidated specific heat capacity of CuCl as function of temperatures from EMF and thermal sources [161], [162], [164]–[166].....	41
Figure 30. 2D Model Geometry of the model with droplet and N ₂ domain with their inflow and outflow directions.	45
Figure 31. Velocity and distance travelled by the AgCl droplet with respect to time various radiuses, R (0.0025m, 0.005m, 0.01m)	48
Figure 32. Velocity and distance travelled by the CuCl droplet with respect to time for various radiuses, R (0.0025m, 0.005m, 0.01m)	49
Figure 33. Temperature distribution of N ₂ and droplet (AgCl) domain with droplet radius of 0.0025m	50
Figure 34. Temperature distribution of N ₂ and droplet (AgCl) domain with droplet radius of 0.005m	51

Figure 35. Temperature distribution of N ₂ and droplet (AgCl) domain with droplet radius of 0.01m	51
Figure 36. Temperature distribution of N ₂ and droplet (CuCl) domain with droplet radius of 0.0025m	52
Figure 37. Temperature distribution of N ₂ and droplet (CuCl) domain with droplet radius of 0.005m	52
Figure 38. Temperature distribution of N ₂ and droplet (CuCl) domain with droplet radius of 0.01m	53
Figure 39. Variation of average heat transfer coefficient with time	54
Figure 40. Temperature increase of water by CuCl droplets for the quenching height of 10cm.....	56

LIST OF TABLES

Table 1. Best suited specific heat estimation model for approximate temperature ranges. (* approximate temperature).....	28
Table 2. Thermal properties of AgCl	38
Table 3. Values of A, B, C, D, E and F in the AgCl specific heat capacity equation 16.....	39
Table 4. Values of A, B, C, D, E and F in the CuCl specific heat capacity equation 15.....	41
Table 5. Geometric dimensions and thermophysical properties of the model	46

LIST OF APPENDICES

Appendix 1. Temperature increase of water by CuCl droplets for the quenching height of 20cm 73

Appendix 2. Temperature increase of water by CuCl droplets for the quenching height of 30cm 73

LIST OF ABBREVIATIONS/SYMBOLS

BTU	British thermal units
SI	International System of Units
AgCl	Silver Chloride
CuCl	Cuprous Chloride / Copper (I) Chloride
SnO ₂	Tin (IV) Oxide
ZnO	Zinc Oxide
MgO	Magnesium Oxide
CeO ₂	Cerium (IV) Oxide
Ce ₂ O ₃	Cerium (III) Oxide
HCl	Hydrochloric acid
CNL	Canadian Nuclear Laboratories
EMF	Electro motive force
CAD	Computer Aided Design
FEA	Finite Element Analysis
ARC	Accelerating Rate Calorimetry
ADC	Adiabatic Pressure Dewar Calorimetry
DSC	Differential Scanning Calorimeter

NOMENCLATURE

c_p	Specific heat
g	Gravitational acceleration
H	Enthalpy
k	Thermal conductivity
L	Latent heat
V	Velocity
p	pressure
R_d	Radius of the droplet
t	Time
T	Temperature
q	Heat flux
F_g	Force due to gravity
F_z	Drag force
ρ	Density
μ	Dynamic viscosity
ν	Kinematic viscosity
α	Thermal diffusion coefficient
Nu	Nusselt number
Re	Reynolds number
Pr	Prandtl number
ω	Angular velocity

h	Planks constant
λ	Wavelength
m	Mass
R	Universal gas constant
E	Electro motive force
F	Faraday's constant
n	Number of free electrons
N	Number of droplets

Subscripts

i	Initial
m	Melting
c	Critical
d	Droplet
g	Gravity

Chapter 1 - Introduction

1.1 Background and Motivation

Energy is the fundamental driving force for all the living and the nonliving things. It can also be defined as the ability to do work. The energy is ubiquitous and is found in several forms such as light, heat, electrical and gravitational energy. After intense research scientists have concluded that energy could never be created nor destroyed, it can only be transformed from one form to another [1]. This is known as the law of conservation energy or the First Law of Thermodynamics. Energy can be grouped into two general types: the potential energy (stored energy) and the kinetic energy (working energy). The most common examples of stored energy are fossil fuels, batteries, biofuels, etc. Fossil fuels and batteries are good examples for energy in stored form that occurs naturally and artificially. Both potential and kinetic energy can be transformed into one another. For example, car uses gasoline, a type of fossil fuel, to run. Here, the car converts the energy from gasoline to mechanical form using engine.

Fossil fuels are crude oil or petroleum made of hydrocarbons, which are compounds of hydrogen and carbon. For centuries fossil fuels served as a primary source for energy. Even today, more than 80 percent of the energy needs are fulfilled by fossil fuels [2]. These stored energies are harvested using machineries for satisfying our energy consumption. The process of burning fossil fuels causes several grave issues such as toxic gas emissions, air pollution, acid rain, ozone depletion, climate change, global warming etc. Moreover, the fossil fuels being an exhaustible source of energy, the society face the impending scarcity of these energy sources in the next semi-centennial [3]. In speculating this scarceness, various countries have at present incentivised their scientists to improvise their technologies to utilise renewable sources of energy. Renewable sources of energy are those which can be replenished in a short span of time and thus do not deplete altogether. Sources of renewable energy are the sun, tides, wind and geothermal energy from which energy can be extracted directly or through indirect methods. The extracted energy needs to be stored in an easily accessible manner. Batteries are most common method of storing the extracted energy. Hydrogen is a promising alternative, which can be used as an energy carrier. Due to its abundance and eco friendly nature makes it a suitable energy carrier in the quest to create a sustainable world.

Our planet serves water as a rich source of hydrogen and the thermochemical copper-chlorine (Cu-Cl) cycle shows promising potential for large scale hydrogen production. The Cu-Cl cycle uses cuprous

chloride (CuCl) salt and hydrochloric acid (HCl) for hydrogen production. One of the step in that process involves, cooling of CuCl salt from around 530°C to 90°C. Many researchers are investigating different methods for recovering the energy released during the cooling process of CuCl [4].

Thermophysical properties such as specific heat, density, dynamic viscosity and thermal conductivity are prerequisite for any type of heat recovery study. But the thermophysical properties of CuCl are not well defined across the temperature range desired. So, the heat recovery analysis performed based on existing thermophysical properties would be inaccurate. Hence, the outcome of this thesis is to develop techniques to determine the thermophysical properties of CuCl. As specific heat plays a vital role in heat recovery study, the main focus is to model the specific heat capacity variation across a wide temperature range. After analyzing several heat recovery methods, a new method was developed to recover the energy effectively and it was analyzed numerically in COMSOL Multiphysics [5] using the developed specific heat model.

1.2 Objectives

This research is performed to analyze the thermal energy recovery within the thermochemical Cu-Cl cycle. Integration of the heat recovery with copper chlorine cycle is also investigated to further improve the overall efficiency of the cycle. The first objective is to determine the potential spots for excessive heat loss and analyze different methods to recover the heat. Upon studying the literature, it is revealed that the major part of the heat can be recovered during the solidification process of molten cuprous chloride (CuCl), hence this thesis is focused on recovering heat from molten CuCl.

The specific goals of this work include:

- To determine the stoichiometric proportions of CuCl, HCl and H₂O.
- To determine the thermophysical properties of CuCl.
- To analyze the effective heat recovery method for cooling of CuCl.
- To analyze the cooling process a CFD model, developed using the commercial software COMSOL Multiphysics.
- To investigate the effect of cooling by varying the diameter of the CuCl droplet.
- To investigate the amount of heat recovered by quenching the CuCl droplets.

1.3 Literature Review

The most common problems associated with the renewable energy is the availability of power, quality of power, resource locations, storage and cost issues. For example, though solar energy harvesting is the most popular method, it has the disadvantage that electricity can be generated only during the

daytime thus the energy output is also dependent on its location and climate conditions of that day. Each renewable method has its own set of shortages and all the different methods may not be applicable in every location.

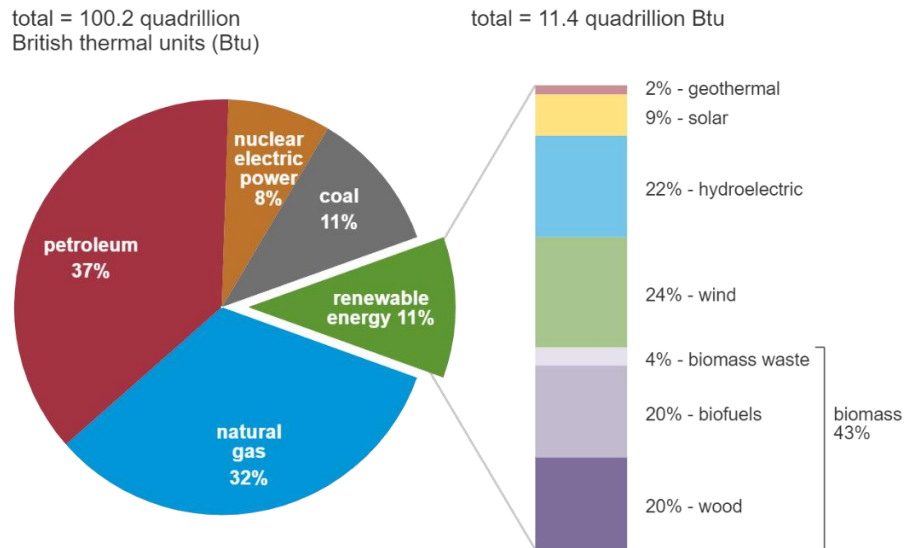


Figure 1. U.S primary energy consumption by energy source, 2019 [2]
 Note: Sum of components may not equal to 100% because of independent rounding

In contrast to fossil fuels, most of the renewable energies are not in a stored form hence, conversion and storage are necessary steps. Storing the energy is another significant challenge and batteries are primarily used for storing the electricity generated from the renewable sources. High capacity batteries are predominantly built from rare earth minerals and also possess the risk of potential toxicity when the emissions of battery chemicals are exposed into the aquatic ecosystem. So, the energy storage in batteries cannot be considered a long-term solution.

Another promising alternative fuel is hydrogen. Hydrogen is one of the most abundant element in this universe and one of the cleanest forms of fuel, as it produces water when it is consumed by fuel cell [6], [7], which is a device that converts chemical potential energy into electrical energy. In a fuel cell hydrogen is passed at the anode (negative terminal) where the catalysts splits hydrogen into protons (positively charged particles) and electrons (negatively charged particles), as shown in Figure 2 [8]. The separated protons are passed through a porous electrolytic membrane while the electrons are forced through a circuit generating heat and electricity. The electrons, protons and oxygen meet at the cathode (positive terminal) to produce water molecules. Since there are no moving parts, the fuel cells operate very silently and with high reliability. There are several different configurations in fuel cells, however, all fuel cells operate on the similar methodology.

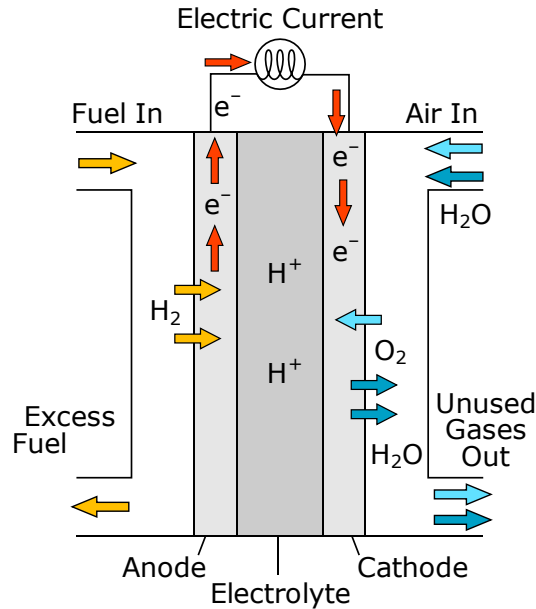


Figure 2. Schematic model of a working fuel cell [8]

Hydrogen's eco-friendliness, lightweight nature and high energy density (nearly 2.5 times higher than the any of the conventional fuels) makes it one of the best energy carriers of the future [9]–[12]. These attributes make hydrogen an alluring fuel option for applications like transportation and electricity generation. Adopting hydrogen as an energy carrier will be the crucial driving force for increased demand in the future. However, currently most of the world's hydrogen is produced from fossil fuels through some type of reforming process [13], [14]. A sustainable, low cost and large-scale method is essential to meet the future needs of hydrogen with lower carbon footprint. There are several eco-friendly methods to produce hydrogen, such as electrolysis, thermochemical water decomposition using renewable sources like solar energy, wind energy, nuclear energy and geothermal energy.

Though electrolysis of water is simpler and seems to be a compelling option, it may not be currently feasible as it needs higher energy input and the overall efficiency is typically about 24% while thermochemical water splitting cycle using nuclear heat can achieve upto about 50% on heat input to hydrogen efficiency [15], [16]. Due to higher overall efficiency many thermochemical water decomposition cycles exhibits significant potential for large scale hydrogen production [17]. Over the past few decades, several thermochemical cycles for hydrogen production were developed among those the copper-chlorine cycle is most promising method because of its lower temperature requirements (around 550°C) and higher efficiency of the cycle [15], [18], [19]. Different hydrogen production methods and their effectiveness are explored more in Section 1.3.1.

Hydrogen will play an important role as an energy carrier of the future. As the hydrogen has a wide variety of applications it may be used as a replacement for almost all the current fossil fuel applications with an added advantage of eco-friendly by-products. Several studies show that, hydrogen can be used as fuel in energy systems to obtain mechanical, thermal and electrical energy, more efficiently than fossil fuels [20].

Public perception of hydrogen is negatively influenced due to its history of bad incidents. A good example would be the Hindenburg disaster, a fatality occurred in 1937 wrongly attributed to hydrogen, that is still in the mind of the society [21]. Despite the public perception, hydrogen is as safe as any other fuel if handled properly [22]. However, hydrogen cannot be found in its elemental form in nature, so it must be extracted from hydrogen-rich compounds.

As of 2018, the global demand for pure hydrogen is about 74 megatons (Figure 3), of which it is primarily used for ammonia production and conversion of heavier crude oils to lighter liquid fuels [23], [24]. The rapid growth in demand is primarily due to decreased availability of lighter crude oils which do not require much hydrogen for the conversion of gasoline whereas heavier crude oils require substantial amounts of hydrogen for gasoline conversion.

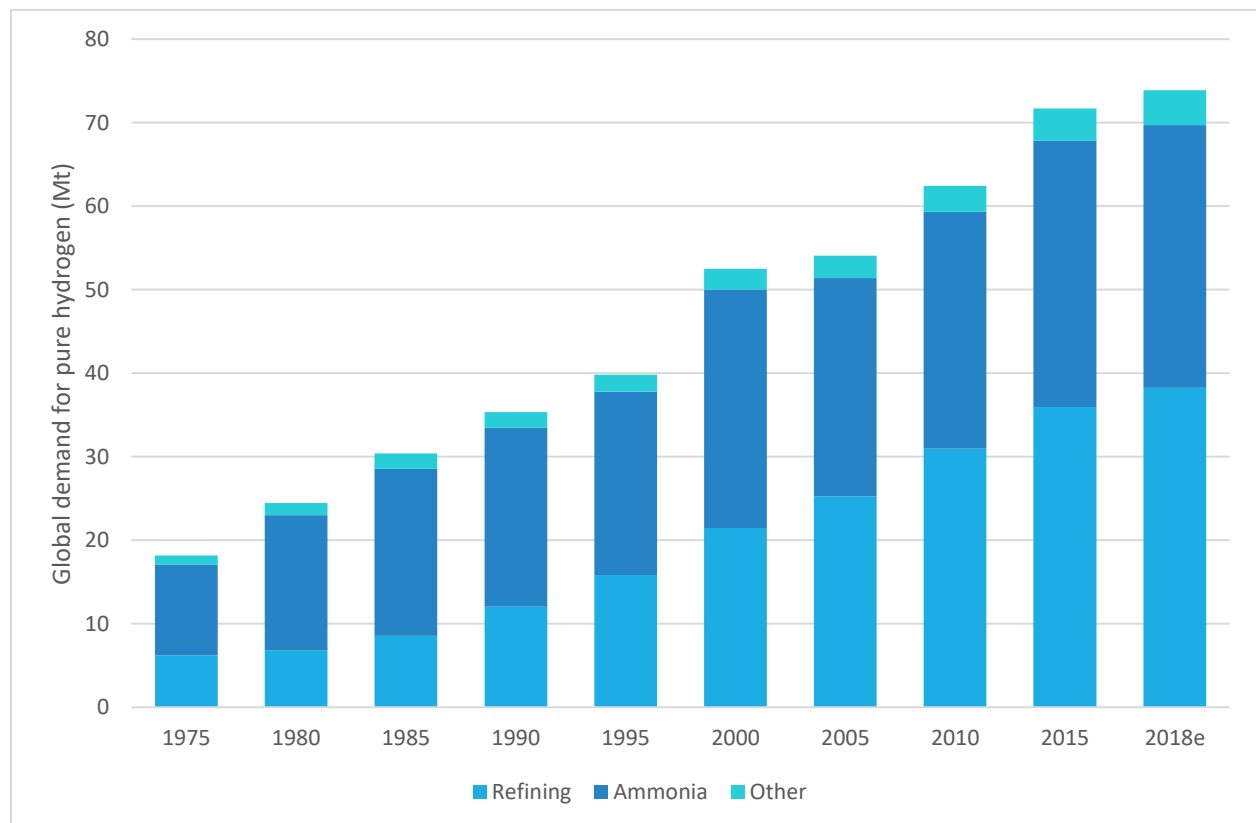


Figure 3. Global demand of pure hydrogen from 1975 to 2018 [23].

Another contributing factor for the hike in hydrogen fuel demand could be to the adaptation of the sustainable development goals by several countries set by the United Nations in 2015, where various novel policies and incentives that enhances hydrogen fuel technology is currently one of the top priorities [25].

Support from governments stimulates many companies to invest more on hydrogen technology. Several manufacturers are involved in the development of low-cost fuel cells which could result in hydrogen becoming a primary fuel for the entire transportation industry (Figure 4). This will result in excessive demand for hydrogen, nearly one to two orders of magnitude of current hydrogen demands within the next few decades [26].

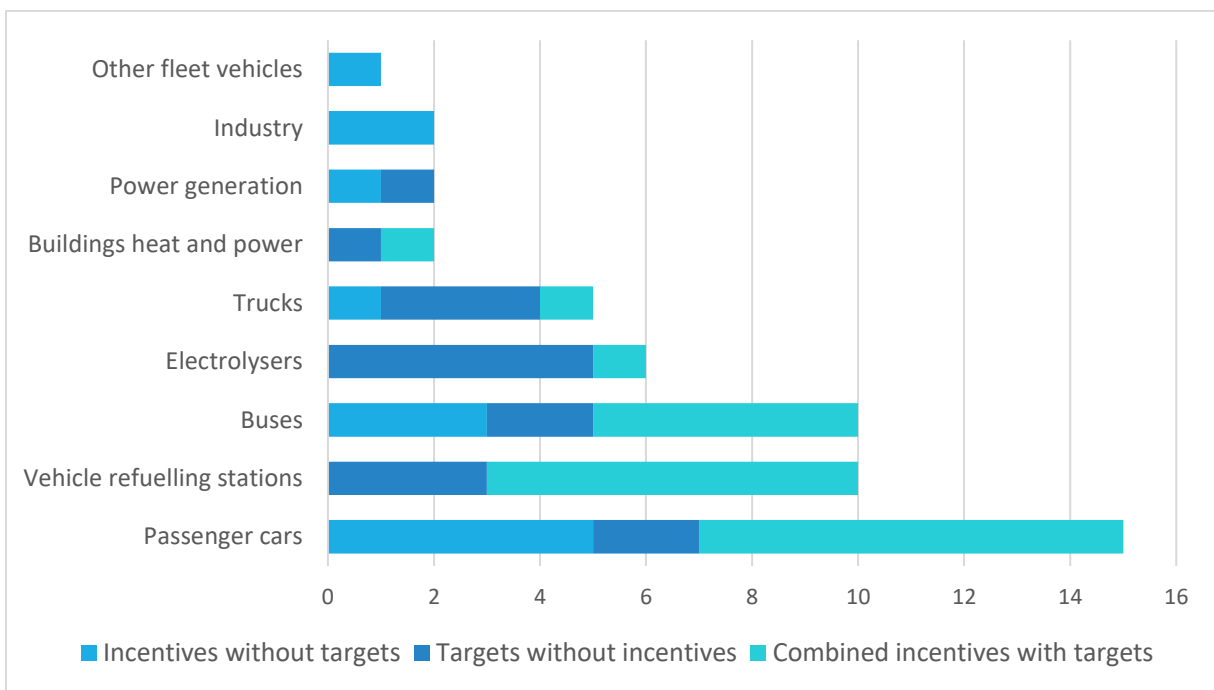


Figure 4. Current policy support for hydrogen deployment, 2018 [23]

1.3.1 Hydrogen production methods

Hydrogen can be extracted from diverse range of resources, such as biomass, natural gas, nuclear power, and renewable power like wind and solar. Nuclear energy provides a heat source which can be used for hydrogen production. Multiple methods for extracting hydrogen from water and heat are being studied. To be used for the production of hydrogen, the nuclear reactor must supply the heat

under conditions that satisfy the requirements of the hydrogen production cycle [24]. Newer technologies are being developed for converting and storing the renewable energy sources in the form of H_2 [27]. At present around 48% of hydrogen is produced by steam methane reforming of natural gas, 18% from coal gasification and 4% through electrolysis of water (Figure 5) [7], [13], [14], [28]–[31].

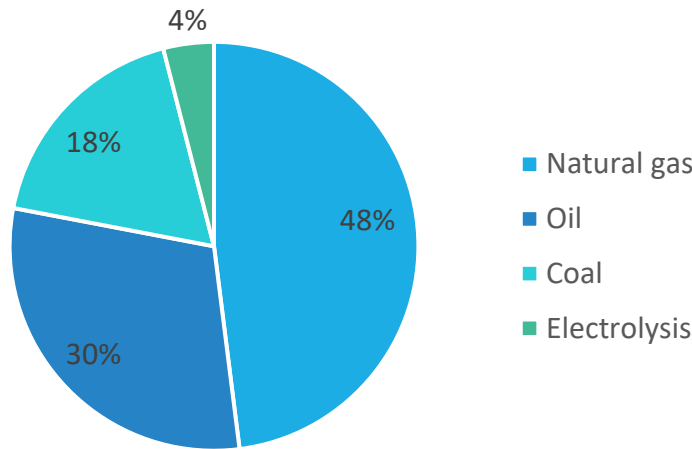


Figure 5. Sources of hydrogen production [32]

1.3.1.1 Steam reforming:

Today, hydrogen is derived mainly from the steam reforming of natural gas. Steam reforming is an energy-intensive low-pressure endothermic process requiring heat input at high temperature. The input of natural gas is used as a reduced chemical supply of hydrogen and burned to produce heat to drive the cycle at temperatures up to $900^{\circ}C$ [33]. Though steam reforming and coal gasification has high operational efficiency and low production costs, its by-products heavily contribute to the global warming other environmental problems. When a nuclear reactor provides the necessary heat, the amount of natural gas required for steam reform may be significantly reduced. The Japan Atomic Energy Research Institute is currently preparing to demonstrate hydrogen output by steam reforming the natural gas with the heat input provided by its HTTR (High-Temperature Engineering Test 9 Reactor) [33]. In Japan and other high-cost natural gas nations, economic analyzes show that hydrogen from nuclear-assisted steam reform of natural gas would cost less than natural gas alone [33].

1.3.1.2 Electrolysis:

Production of hydrogen using electrolysis is a mature technology. It is not currently competitive for the large-scale production of hydrogen, except in the regions with lower electricity costs. The long-term use of electrolysis for large-scale hydrogen output depends on the nature of the electrical grid, the capital cost of the electrolysis, and other factors [24]. Present capital costs are expected to be close to \$600 / kW, while others predict future capital costs may be close to \$300 / kW. The efficiencies of traditional alkaline electrolyzers are 70–85% and the efficiencies of proton-exchange-membrane electrolyzers are estimated to be 80–90% [24]. There is a significant trade-off between the cost of capital and output [26]. The peak electric demand in many developed countries is twice the minimum requirement. Consequently, low-cost, off-peak electricity in such jurisdictions is often available. Electrolysis can be feasible, provided that effective, low-cost electrolysis systems and local hydrogen storage and distribution systems are successfully developed.

1.3.1.3 Thermochemical cycle:

The thermochemical water decomposition cycle exhibits significant potential for alternative process for hydrogen extraction from water, as this is closed cyclic process with higher yields without any harmful effects to the environment [34]–[39]. In this cycle water is decomposed into hydrogen and oxygen using heat energy or combination of heat and electrical energy.



In the past various thermochemical water splitting cycles were investigated, using different energy sources. Abanades et al. [40] investigated the production of solar hydrogen from a two-step thermochemical cycle based on a redox reaction of SnO₂/SnO. Steinfeld [41] proposed a thermochemical cycle based on a Zn / ZnO redox reaction. Galvez et al. [42] investigated a two-step solar thermochemical process based on a redox reaction of MgO/Mg. Abanades and Flamant [43] demonstrated the feasibility of a solar thermochemical cycle, based on a CeO₂ / Ce₂O₃ cycle, at a laboratory scale. Huang and Raissi [44] examined the thermochemical process of sulfur-iodine, in which solar energy is used to decompose sulphuric acid.

Xinxin and Kaoru [45] researched the Sulfur-Iodine (S-I) cycle for nuclear-powered hydrogen production. Liberatore et al. [46] addressed the energy and economic evaluation of an industrial plant for hydrogen production through a thermochemical process of sulfur-iodine. The thermochemical cycle 's efficiency alone was around 34%, based on higher heat value. If this value is correlated with the output of electrical energy, including solar plant efficiency, the overall heat-to-hydrogen efficiency

was 21%. Graf et al. [47] explored the feasibility of sustainable development of hydrogen by solar energy and thermo-chemical cycles. The commercial electrolysis was compared with a metal oxide-based cycle and a hybrid sulfur cycle, and a sensitivity analysis was conducted for various cost scenarios.

Granovskii [48] presented a comparative performance assessment of the combined system by means of thermal and hydrogen production efficiencies including a supercritical water-cooled nuclear reactor and a chemical heat pump. The combined process can provide high temperature heat to a thermochemical water splitting cycle or hydrogen production. Lewis [15], [18], [19] examined alternate thermochemical cycles in hydrogen production. Their findings showed that with regard to energy-efficient engineering the copper-chlorine cycle is chemically viable and feasible. Dincer and Balta [49] discussed several possible hybrid cycles for the development of nuclear-based hydrogen production. The copper-chlorine cycle has proved to be a highly promising method for the production of hydrogen using nuclear energy.

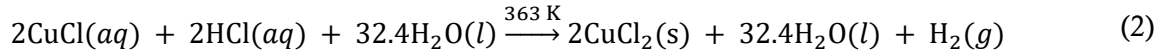
Rosen [16] has documented recent developments in the thermochemical cycles of hydrogen production, using non-fossil sources of energy such as nuclear or solar. Numerous developments have been made on the sulfur-iodine cycle, and it has been shown that the copper-chlorine cycle has considerable potential due to lower heat supply temperature requirements compared with most other thermochemical processes which leads to lesser material demands for construction. Moreover, the thermochemical copper chlorine (Cu-Cl) has good kinetics for hydrogen and oxygen generation reactions compared to other similar chemical cycles. This Cu-Cl cycle has been recognized as the most promising cycle for thermochemical hydrogen production by the Canadian Nuclear Laboratories (CNL) [50].

1.3.2 Thermochemical Copper Chlorine cycle (Cu-Cl) cycle

The thermochemical Cu-Cl cycle is identified as a promising clean hydrogen production method and a viable solution to producing fuel in large quantities. A sequence of reactions are performed in the thermochemical Cu-Cl cycle to achieve the overall splitting of water into H_2 and oxygen (O_2). This cycle typically forms a closed loop with water as the only input material and H_2 and O_2 as products. The cycle decomposes water into H_2 and O_2 using intermediate copper and chloride compounds, and all the intermediate chemicals produced are recycled in a closed internal loop on a continuous basis [4], [51]. The chemical reaction steps of thermochemical Cu-Cl cycle are detailed in Figure 6, where steps 7, 8, 9 are intermediate steps of the cycle.

The Cu-Cl cycle has three variants, depending on the number of key chemical reactions: three steps, four steps, and five steps. Naterer et al [17], [36]–[39], [50] and Lewis et al [15] have extensively researched on the working and feasibility of Cu-Cl cycle. The Cu-Cl cycle shown in Figure 6 is a four-step cycle adopted from Naterer’s work with a change in step 7 (intermediate step).

Step 1:



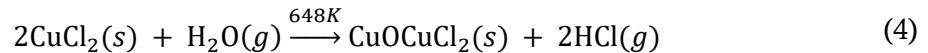
The electrolysis of CuCl / HCl is the first step in the four step Cu-Cl thermochemical cycle for hydrogen production. During the electrochemical reaction oxidation of copper(I) chloride (CuCl) occurs in the presence of hydrochloric acid (HCl) and water (H₂O) to produce hydrogen (H₂) and copper (II) chloride (CuCl₂). The Cu(I) ion at the anode is oxidized to Cu (II), and the hydrogen ion at the cathode is reduced.

Step 2:



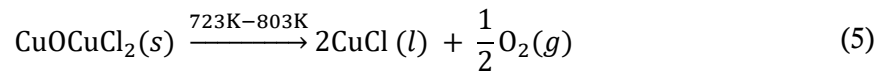
Second step of the cycle is drying. Aqueous CuCl₂ leaving the electrolysis cell is dried to create CuCl₂ particles, which are then transferred to the hydrolysis unit (Step 3) and reacted with superheated steam to produce solid copper oxychloride, CuO·CuCl₂ and hydrogen chloride gas.

Step 3:



At step 4 of this cycle the CuCl is regenerated by decomposition of CuO·CuCl₂ at 530°C in the decomposition reactor. The regenerated CuCl is in the molten state, which after being cooled to 90°C will be dissolved in aqueous HCl to form the anolyte solution of the electrolysis step 1 [3], [4]. The temperature of molten CuCl obtained from the decomposition reactor ranges from 430°C to 530°C.

Step 4:



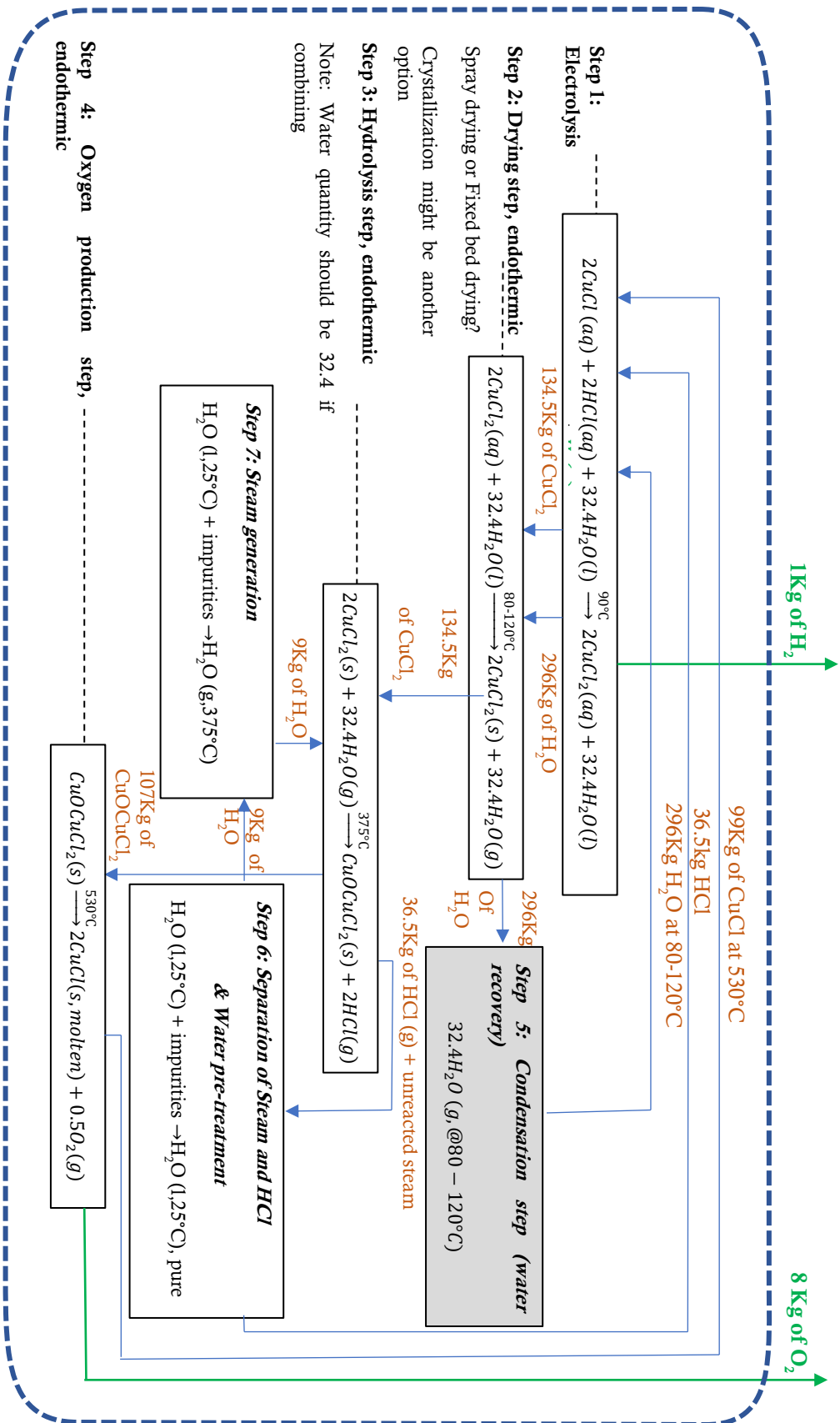


Figure 6. Stoichiometric chart of Cu-Cl cycle.

Several variants of copper-chlorine cycles were contrasted with different number of steps and grouping methods, and Wang et al [52] addressed major features of the cycles with different number of steps. Serban et al. [53] has provided a detailed kinetic analysis of the hydrogen and oxygen production reactions during the Cu-Cl process. Balta et al. [49] proposed a four-step Cu-Cl process of energy and exergy analysis, coupled with a geothermal source for hydrogen production. From the perspective of heat quantity, thermal efficiency and related engineering challenges, Wang et al. [54] compared the sulfur-iodine and copper-chlorine thermochemical cycles. Ghandehariun et al. [55] has analyzed a solar plant coupled with a Cu-Cl plant to produce hydrogen at three locations across Canada. The results demonstrated the feasibility of the solar thermochemical Cu-Cl cycle as a promising and efficient way to generate hydrogen on a large scale.

Naterer [17], [36], [39], [51] discussed Canadian developments in the nuclear-based processing of hydrogen via the Cu-Cl process. Orhan [56] researched the development of nuclear-based hydrogen using sea or brackish water using a hybrid cycle of Cu-Cl. Coupling of the Cu-Cl cycle with a desalination plant was analyzed in this study. Various desalination processes were examined to determine the most suitable option for the Cu-Cl cycle. Their tests are beneficial in developing and improving coupled systems. Orhan [57] has provided the cost analysis of a Cu-Cl thermochemical plant and the authors examined the cost sensitivity as a function of plant efficiency, capacity factor, and percentages of each cost variable. Zamfirescu [58] has studied the thermophysical properties of the copper compounds in the Cu-Cl cycle. Ozbilen [59] used life cycle assessment to present the environmental impacts of the Cu-Cl. Ferrandon [60] has studied the hydrolysis of CuCl_2 into $\text{CuO}\cdot\text{CuCl}_2$ and HCl using a spray reactor. It was shown that, due to improved mass transfer, a counter-current flow reactor results in a substantially higher yield of $\text{CuO}\cdot\text{CuCl}_2$ compared to a co-current flow. Naterer [61] analyzed the Cu-Cl cycle for the evaporative drying of aqueous copper (II) chloride (CuCl_2) droplets. Before entering a flash evaporator to generate solid CuCl_2 , an aqueous CuCl_2 stream leaving an electrochemical cell was preheated to 150°C . The results showed that, compared to evaporative drying in the spray drying process, the benefits of flashing the solution to improve drying were relatively small. Naterer [50] presented the thermal architecture of the oxygen-producing reactor for decomposing copper oxychloride into oxygen gas and molten cuprous chloride. Wang [62] examined the scale-up design problems in the copper-chlorine cycle for the hydrogen, oxygen, and hydrolysis reactors. In order to identify possible performance improvements in the cycle, Orhan [63] has researched various design schemes for the overall copper-chlorine cycle and its components.

1.3.3 Heat Recovery in the Copper-Chlorine Cycle

In the copper-chlorine cycle, heat recovery is crucial for the efficient performance and overall cycle viability [32], [44], [49]. Naterer [50] analyzed the heat requirements of different stages of the five-step copper-chlorine cycle. The authors analyzed the heat absorption and emission between the steps of the Cu-Cl cycle in order to recover as much heat as possible and to reduce the cycle's net heat supply. It has been shown that if all of the heat emitted is recovered within the cycle, the cycle output would increase significantly [50].

Jaber [64] studied heat recovery out of molten CuCl. A direct contact heat exchanger was proposed and the convective heat transfer in a counter-current spray flow between molten CuCl droplets was evaluated. The results showed that full heat recovery can be achieved with a diameter of the heat exchanger of 0.13 m and heights of 0.6 and 0.8 m for a droplet diameter of 1 and 0.5 mm respectively.

Zamfirescu explored the possibility of using copper(I) chloride as working fluid in a new vapor-compressed high-temperature heat pump. It has been shown that CuCl can be used as a working fluid in a vapor compression heat pump, and the copper-chlorine cycle oxygen reactor can be connected to the CuCl heat pump system.

Rabbani [65] presented a heat exchanger design which recovers heat from oxygen gas exiting the copper-chlorine cycle oxygen reactor. The best possible pathway for the recovering heat from oxygen was also investigated on the basis of energy and exergy. Most heat recovery inside the Cu-Cl cycle can be accomplished by cooling molten CuCl, exiting the cycle at around 530°C at the oxygen reactor. Since CuCl's melting point is around 430°C, the solidification takes place as molten CuCl cools. Ghandehariun [4] used pinch analysis to determine the maximum recoverable heat from CuCl. Based on existing industrial process on molten materials, Ghandehariun [4], [66]–[68] extensively studied heat recovery from molten salts for several configurations and found that direct contact using steam or air as coolant to be the most favorable method.

Manan et al [69] carried out an experiment on quenching CuCl directly into HCl at room temperature on different configurations and reported that quenching in HCl was not favorable due its vapor formation as it could enter the decomposition reactor, causing safety concerns. O'Connor [70], Linstrom and Mallard [71], Fritz and Konigsberger [72], Jianu et al. [73]–[75] comprehensively researched the dissolution of CuCl and developed correlations of ternary system in Cu-Cl cycle. The CuCl was found to be predominantly immiscible in water in the absence of HCl, as shown in Figure 7.

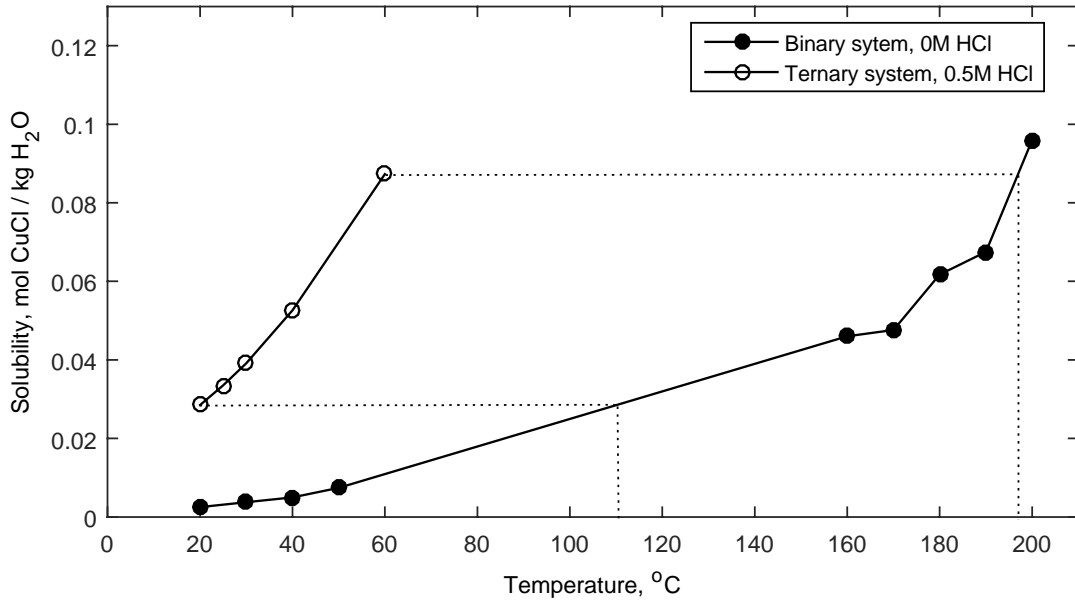


Figure 7. Solubility difference of CuCl in binary and ternary systems [75]

Based on Ghandehariun, Manan [69] and Jianu's findings, the best way to recover maximum heat is to quench CuCl directly in water with inert N₂ atmosphere. Quenching is a process where a hot material is soaked into a cold fluid and let the material cool rapidly, thus increasing the temperature of the cold fluid. Here water is used as a cold fluid and molten CuCl as hot material. Since the temperature of the step 1 (Figure 6) needs to be around 90°C. The molten CuCl is directly quenched into the water, obtained from step 7, and the quenched water is used in the electrolysis step as shown in Figure 6. The amount of water for quenching is calculated based on the stoichiometric proportion in step 3. The quenching process of molten CuCl involves liquid to solid phase change since the temperature of molten CuCl is close to its phase change temperature. The quenching in water is necessary as gaseous HCl from the hydrolysis reactor (step 3 in Figure 6) is added forming the aqueous HCl solution required for CuCl dissolution. By recovering heat during quenching of CuCl, the thermal efficiency of the cycle is increased making the cycle a suitable hydrogen production method [64], [66].

1.3.4 Heat Transfer and Solidification of Droplet

Determining the transition of temperature of a solidifying droplet is vital for the heat recovery process. Modelling solidification of a droplet by itself is a convoluted process and it becomes more complex with introduction of forced convection. In the past, the forced convection heat transfer rate has been studied for a number of process configurations. The Nusselt number for the sphere immersed in a

stationary infinite media in a steady state is 2 [76]. A functional dependency on Reynolds and Prandtl numbers were analyzed [76].

Richardson [77] proposed that the transfer of heat from the sphere can be seen as two parallel processes. The contribution to the Nusselt number should be of the form $Re^{1/2}Pr^{1/3}$ in the laminar boundary layer region, whereas in the wake region the contribution should be of the form $Re^{2/3}Pr^{1/3}$ [77]. The final form of equation for the Nusselt number was found with the work of Vliet and Leppert [78] and the supporting data of Kramers [79]:

$$Nu = 2 + \left(0.4Re^{\frac{1}{2}} + 0.06Re^{\frac{2}{3}}\right) Pr^{\frac{2}{5}} \left(\frac{\mu_{\infty}}{\mu_s}\right)^{1/4} \quad (6)$$

This correlation is valid for $3.5 < Re < 7.6 \cdot 10^4$, $0.71 < Pr < 380$ and $1 < \frac{\mu_{\infty}}{\mu_s} < 3.2$. In some special cases Ranz and Marshall [80] correlations were used for modelling the convective heat and mass transfer of spheres.

When a droplet breaks away from the feeding system, it may oscillate in shape, and the formation process may cause some internal motion. As the droplet accelerates, the shear stress on the surface generates internal circulation and the aerodynamic forces tend to distort the droplet's shape. In the Ranz-Marshall [80] correlation, Yao and Schrock [81] suggested a transient correction factor which is responsible for the effects of vibration and droplet shape distortion as it falls. Two different methods were proposed by the authors for modeling heat transfer inside a droplet, one by assuming a uniform temperature within the droplet and the other by solving the equation for internal heat conduction. Due to the internal mixing within the droplet results in a uniform temperature inside it. The contributions of drop distortion and internal resistance are difficult to account for precisely. However, Yao and Schrock's [81] estimated empirical method provides precise predictions for water droplets with diameters varying from 3 mm to 6 mm. A numerical model was developed by Argyropoulos and Melissari [82] to describe the transport phenomena involved when a melting sphere is immersed in a moving fluid. This model was used to estimate the melting times of different spheres submerged in fluids with different Prandtl numbers. A dimensionless heat transfer correlation was proposed over a sphere for forced convection, and the findings were compared with experimental data for liquid metals and water. Analysis of a droplet's solidification is of considerable significance in the spray crystallisation study. spray crystallisation is a process of solidification of liquid by atomization in relatively cold atmosphere [83]. This process is mainly used for powdering materials such as metals, pharmaceuticals, food products and artificial snow [84]–[87]. Free flight and levitation are the two

common techniques for studying single droplets. In the free flight study droplet is allowed to free fall and the observations are made at different droplet heights by measuring appropriate variables. In the case of levitation study, droplet remains constant as the fluid around it flows past it.

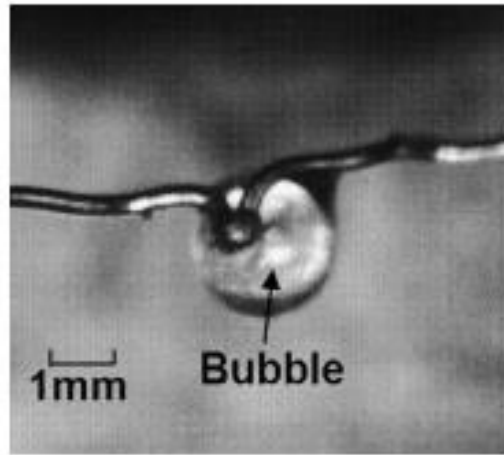


Figure 8. Droplet suspended on a thermocouple junction [88].

Techniques for levitation can be either non-intrusive or intrusive. Intrusive approaches include either hanging a droplet on a thin mesh or plate, or on a thermocouple junction. The suspension of droplets on the thermocouple junctions was widely used in earlier studies (Figure 8) [87], [89], [90]. In the non-intrusive technique droplets are levitated using electrostatic, electromagnetic or aerodynamic forces, as shown in Figure 9 and Figure 10 [91]–[93]. Unlike intrusive method, the non-intrusive method can replicate actual conditions since there is no interference in any form. Though non-intrusive technique has significant advantage over intrusive method, non-intrusive technique is not often preferred because of its limited application and expensive experimental setups.

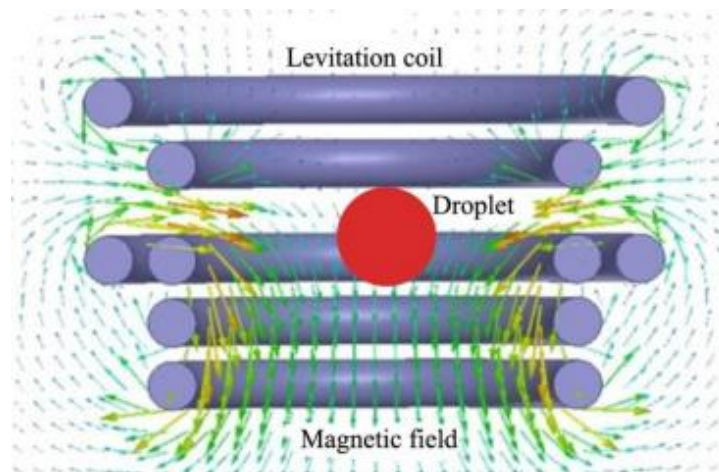


Figure 9. Levitation of droplet using magnetic field [94].

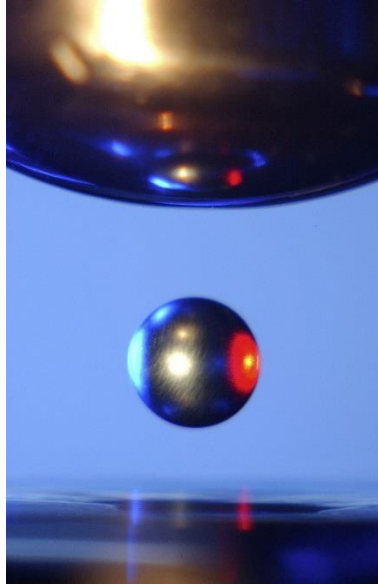


Figure 10. Electrostatic levitation of a Titanium-Zirconium-Nickel alloy [95].

Several investigations were carried out in the field of solidification in the processes of atomization [96], [97]. Liu et al. [98] investigated interactions between droplet and gas in spray atomization of tantalum-tungsten (Ta-2.5W) alloy with nitrogen as gas. To simulate the flow and heat transfer phenomena of the rapid solidification of droplets in the spray cone, a simple two-dimensional (2D) flow model and a lumped parameter formulation based on the modified Newton's cooling law was developed. The concentration of droplets in the atomization gas was presumed to be sufficiently diluted, so that interactions between droplets are ignored. The gas flow was not solved but the gas velocity distribution was assumed to have an exponential correlation.

In an atomization process for powder production, Zeoli et al [99], [100] developed a numerical model which combines both a cooling process and break-up in a single computation. FLUENT, a commercial software, was used for computing the gas flow. The evaluations showed that the droplets during the gas atomization have very similar profiles. It was found that the in-flight distance was a major factor affecting the atomization and solidification processes of droplets.

In another study, Li et al [101] developed a simulation method for predicting the solidification of gas-atomized droplets of Sn-5% Pb (on a mass basis). The model predicts the nucleation mode, the time and duration of recalescence (a temporary rise in temperature during cooling of a metal caused by a change in crystal structure), the undercooling, the duration of the post-recalescence plateau, and the solid fraction at the end of recalescence. During solidification they assumed a uniform droplet temperature and followed the model DiVenuti [102] suggested for droplet temperature variation. Unlike the current research, the aim of all these works was to solidify instead of heat recovery.

Several studies have been reported on spray tower heat exchangers, regarding heat and mass transfer characteristics between continuous and dispersed phases. Song et al. [92] developed an analytical solution for a simple model with direct contact heat transfer between two immiscible liquids. Jaber et al. [64], [103] developed a model with molten CuCl and analysed the droplet flow and heat transfer in a counter-current spray flow heat exchanger.

1.3.5 Description of Cuprous Chloride (CuCl)

The thermophysical properties of CuCl are essential for studying heat recovery methods to improve performance and efficiency of the thermochemical Cu-Cl cycle [104], [105]. The transition temperature of CuCl is reported as 703K [106]. The CuCl in the solid phase is in the form of γ -cubic structure until it reaches 683K, and as a β -hexagonal crystal from 683K to its melting point [50], [58]. These structures influence the specific heat capacity (c_p) of the molten salt, hence playing a crucial role in the heat transfer study. However, the lack of precise thermophysical properties on CuCl heavily hinders the detailed investigations of heat recovery from molten CuCl. In this thesis, a new method is developed to determine the thermophysical property of CuCl and silver chloride (AgCl) as the molten salts are changing phases to solid. This is achieved by correlating electrochemistry data with thermal data. A model that predicts the specific heat capacity during phase change process is developed in this thesis based on the existing electromotive force (EMF) and thermal data from literature.

1.3.6 Description of Silver Chloride (AgCl)

To develop new model EMF data is essential. Due to the lack of literature data on CuCl, an alternate material AgCl was chosen for this study since it exhibits similar structure to CuCl and thermophysical data is available in literature. Moreover, AgCl and CuCl both have the same face-centered cubic crystal (fcc) structure like NaCl and they also belong to the same group in the periodic table. The solid to liquid phase transition temperature of AgCl is 728K [106]. Even though the melting point temperature varies considerably with CuCl, for the purpose of validating the methodology AgCl is well suited.

1.4 Thesis Outline

The thesis is laid out in six chapters.

Chapter 2 contains the literature review of the thermophysical properties and discusses about different methods of determining the properties.

Chapter 3 details the results of the thermophysical properties obtained from different methods.

Chapter 4 is based on heat recovery study CuCl. It details about the numerical analysis and the CFD model developed in COMSOL Multiphysics and the overview of governing equations for the numerical study and discusses the simulated results in detail.

Chapter 5 presents the conclusion with the findings of the research summarized and provides recommendations for future work.

Chapter 2 - Methods to Determine Thermophysical Properties

2.1 Introduction

For any scientific analysis, material and thermophysical properties are mandatory. Thermophysical properties are strongly dependent on molecular and atomic structure. Thermophysical properties comprise of thermal conductivity, specific heat capacity, latent heat of fusion, viscosity and the coefficient of linear thermal expansion. Specifically, in the heat recovery study the specific heat capacity data plays a crucial role in determining the amount of energy that could be recovered. So, this chapter is mainly focused on methods of determining specific heat capacity and their existing literature data of AgCl and CuCl.

2.2 Methodology

Behaviour of materials varies drastically at different temperature ranges, therefore, it would be inaccurate to use a single method to determine the specific heat capacities at different temperatures. The variation in specific heat capacity with temperature has to be modelled using distinctive physical approaches at different temperatures. At very low temperatures specific heat capacity is modelled using Debye's model. For the temperatures beyond melting point, specific heat capacity is determined using Gibbs-Helmholtz relation. Mainly calorimetry data is used for the temperature range from 298K till the solid to liquid phase change temperatures.

2.2.1 Quantum Mechanics Approach

To understand quantum mechanics, it is necessary to grasp the fundamentals of classical mechanics and know how it differs from quantum mechanics. In the early twentieth century, the word classical mechanics was coined to describe the method of mathematical physics started by Isaac Newton and other contemporary seventeenth-century workers, building upon Johannes Kepler's earlier astronomical theories [107]. At initial stage of the development of classical mechanics, it was commonly referred as Newtonian mechanics since most of the physical concepts and mathematical methods were invented and employed by Newton himself [108]. Newton proposed three laws of motion, the law of inertia, law of acceleration and the rule of action and reaction, and thereby laid the foundations for classical mechanics. Both the second and third laws of Newton were given adequate scientific and mathematical treatment hence distinguishes them from earlier attempts to explain similar phenomena, which were either incomplete, incorrect, or given little accurate mathematical expression [107], [108]. Also, Newton was the first to formulate correct scientific and mathematical

relations for gravity in Newton's law of universal gravitation. The combination of Newton's laws of motion and gravitation offers the most comprehensive and accurate explanation of classical mechanics.

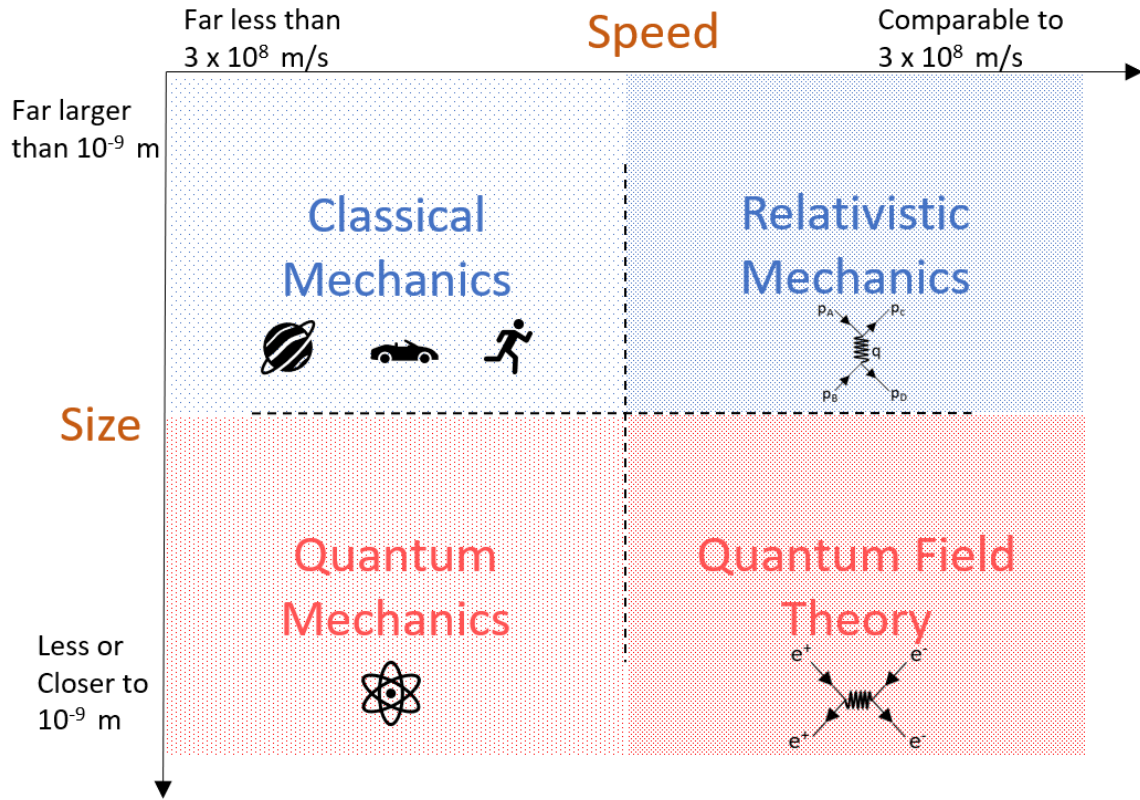


Figure 11. Physics fields (adopted from [109])

In general, classical mechanics is applicable to larger objects with lower velocity whereas in quantum mechanics describes the behaviour of subatomic particles at the nanoscopic level, as shown in Figure 11. It is theorised that at the subatomic level energy can only be released and absorbed in discrete indivisible units called quanta [110]. This means electrons have fixed orbits around the nucleus of the atom as their energy comes in discrete amounts. When the electron gets excited or de-excited they absorb or emit a specific quanta of energy which means they leap from one orbit to another without inhabiting the space in between - this is called the quantum leap, as shown in Figure 12. In essence there are places within the atom that the electron will likely be and other places where they will not since energy is being absorbed and released in discrete units.

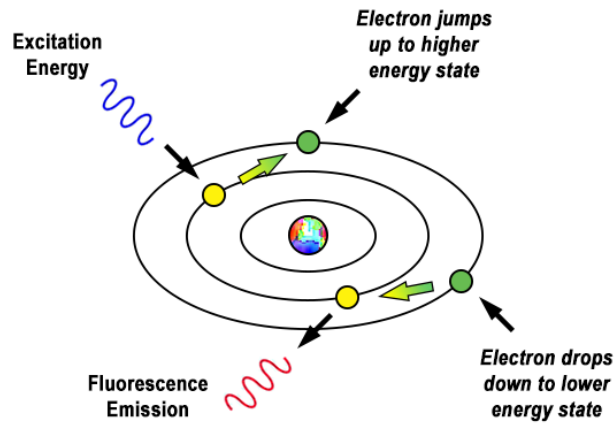


Figure 12. Quantum leap of electrons due to excitation and emission of quanta [111]

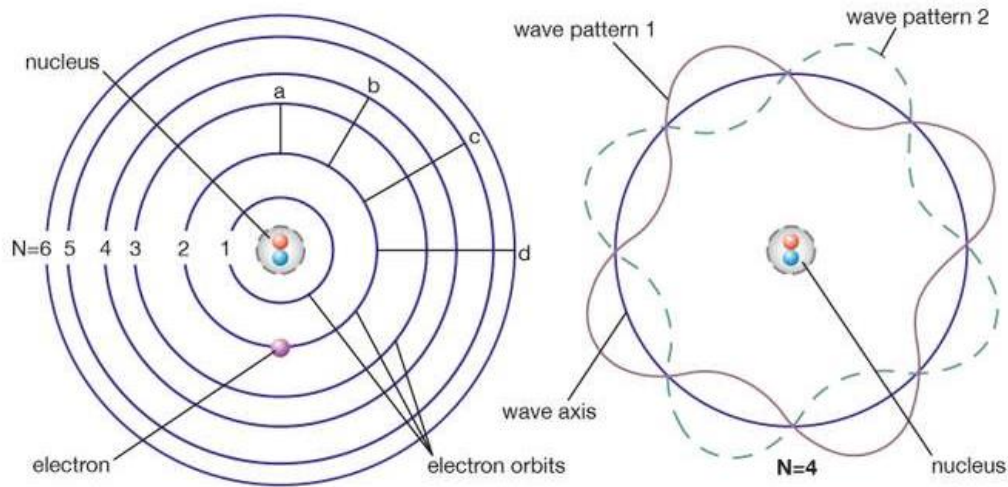


Figure 13. Model of atomic structure [108]

A famous experiment in quantum physics named the double slit experiment revealed that electrons display both particle and wave-like behaviour [113]. To get a perspective, sound is a good example of wave (a form of vibrations or oscillations). Similarly, an electron behaves like a wave in fixed orbits as shown in Figure 13.

Louis de Broglie hypothesized that all particles should also exhibit such a duality [114], as represented in Equation (7), which means every object in this world should possess wave nature. But in reality, we do not observe the wave nature in any of the objects, because wavelength is inversely proportional to the mass. The greater the mass, the shorter will be the wavelength, λ , which is given by Eq. 7:

$$\lambda = \frac{h}{mv} \quad (7)$$

where λ is the wavelength, h is planks constant, m is the mass of a particle, v is the velocity. Since electrons' mass is very small, its wavelength is in the order of 10^{-10}m , whereas larger objects such as a baseball will have a wavelength of around 10^{-36}m .

Erwin Schrodinger developed wave equation to describe the wave mechanics of the electron [115]. As a result. The model of an atom being comprised of electrons revolving around a nucleus similar to how planets revolve around a star is no longer valid. Instead an electron is modeled as a cloud of probability density that represents regions where the electron can be found.

Quantum mechanics serves as a foundation for the condensed matter physics (CMP). CMP explores the fundamental properties of matter in its condensed state at macroscopic and microscopic level, by analyzing the interactions of large number of atoms and electrons in both crystalline and amorphous materials. Crystalline materials have atoms positioned on a repeating three-dimensional lattice whereas the atoms in the amorphous materials are not arranged in regular fashion, as shown in Figure 14. Lattice vibrations are the vibrations of the atoms inside a crystal. The quantum mechanical treatment of lattice vibrations is called phonons i.e. energy in the lattice vibrations can be quantized and these packets of vibrational energy are called phonons.

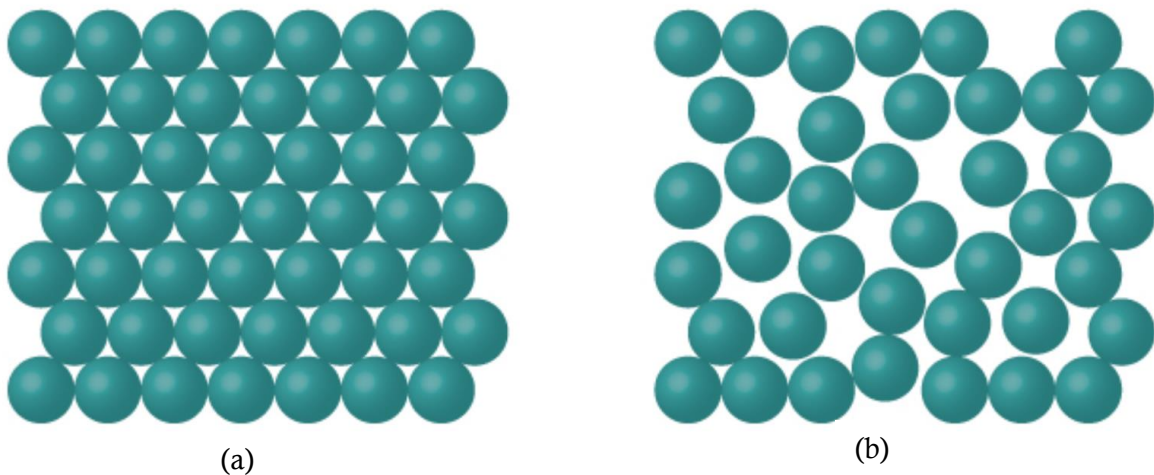


Figure 14. Structure of Solids (a) Crystalline, (b) Amorphous [116]

In 1819, Dulong and Petit [117] experimentally found that the heat capacities of many solids are around $3R$, where R is the universal gas constant. This was in agreement with classical statistical theory of Boltzman, where the specific heat capacity is measured with the modes of vibrations with quadratic potential and kinetic energy terms [118]. When Weber and Dewar [119] measured the heat capacities of diamond over a wide range of temperature, they found that at very high temperature the specific heat capacity reaches the Dulong and Petit limit but at low temperature specific heat

systematically drops to low values indicating that it may approach zero. This study helped them to conclude that specific heat capacity is a function of temperature. Boltzman theory was unable to explain the variation of specific heat capacity at low temperatures.

In 1906, Einstein attempted to solve this by considering these vibrations at the atomic lattice as phonons with plank's quantum theory which states that the energy of the oscillator is quantized which must be an integer multiple $\hbar\omega$ [120]. Where \hbar is $h/2\pi$, h is the planks constant and ω is angular frequency of oscillator. Einstein assumed that atoms in the solids are identical and are uncoupled oscillators vibrating at the same frequency. Even though Einstein's model could capture the essential physics of specific heat, due to his assumptions, it was unable to predict the accurate variations of specific heat at very low temperatures. In reality, oscillators were not vibrating at the same frequency instead they were vibrating at a spectrum of frequencies [121]. Debye [121] used this assumption to model the specific heat capacity and determined that specific heat capacity is proportional to T^3 . This model's limit is given by Debye's temperature (θ_D). Debye's model follows the Dulong-Petits [117] law at high temperatures. Debye's model only works for the materials at low temperature in their condensed state. As anharmonic vibrations start to appear, Debye's model becomes invalid.

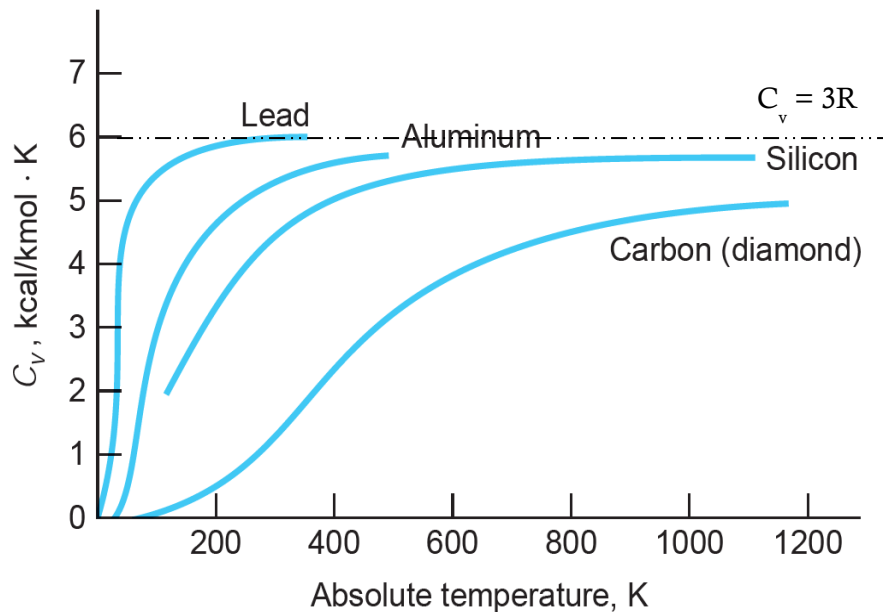


Figure 15. Temperature dependence on molar heat capacity for different solids [116]

During heat addition at very low temperature, the atoms in the crystals tend to vibrate harmonically. From the Dulong-Petits law at high temperatures, the specific heat capacity should remain constant (Figure 15). But due to the imperfections in the crystal, the atoms in the solid starts vibrating anharmonically, which leads to thermal expansion and increase in specific heat capacity. A profound

study on anharmonic vibrations within the solids may lead to accurate prediction of specific heat capacity and thermal expansion.

2.2.2 Thermal Measurements

The general method to measure specific heat capacity is using calorimetry. In this process the amount of heat absorbed or released is measured with calibrated object as reference. When two bodies at different temperatures are placed in physical contact, the heat is transferred from high to low temperature body. By law of conservation of energy, heat lost by hot body is gained by the cold body. Specific heat capacity of the hot body is calculated based on the known calibrated cold body.

There are several types of calorimeters namely, adiabatic calorimeter, reaction calorimeter, bomb calorimeter, calvet-type calorimeter, constant-pressure calorimeter, differential scanning calorimeter (DSCs), and isothermal titration calorimeter [122].

An adiabatic calorimeter [122] does not release heat to surroundings, and it works under zero heat exchange conditions. This is mainly used to measure the enthalpy change in the system during crystallization, mixing, dilution, or some other form of energy changing process. Since enthalpy calculation in a system involves consideration of both the kinetic and thermodynamic loss of heat measurements, adiabatic calorimeters are usually more robust than many other types and can be used in explosion-prone systems. There are two common forms of adiabatic calorimeters: adiabatic pressure dewar calorimeter (ADC) and accelerating rate calorimeter (ARC). ADC calorimeters can operate at lower pressures and are scalable up to one liter [122].

Reaction calorimeters [122] can be used to capture both endothermic and exothermic changes occurring during the reaction. Common types of reaction calorimeters are heat balance, constant flux, heat flow, and power compensation calorimeters [122]. It is a real-time non-destructive and non-invasive technique that is safe for scaling up and for the hazardous process.

Bomb calorimeters [122] are robust and are generally made out of steel. This type of calorimeter is used for estimating enthalpy of combustion in a reaction. During the reaction phase, these calorimeters can withstand the explosive effects of both the induced pressure and the exothermic release. These calorimeters operate by using a substitution method to calculate the enthalpy of combustion, where the heat extracted from the sample is assessed against the heat release of a known norm. Inside the calorimeter, the heat emitted is absorbed and the temperature change is measured [122].

Calvet-type calorimeters [122] are commonly used to calculate the changes in enthalpy during sublimation reactions and to evaluate material behavior. Constant pressure calorimeters are one of the

simplest forms and it measures the enthalpy change of a solution reaction while maintaining constant pressure [122].

DSCs [122] are a common class of calorimeters and used both in industrial and academic applications. By calculating the heat emitted from a sample, DSCs measure the enthalpy change in the endothermic and exothermic process. DSCs are widely used for measuring latent heat of melting, the heat of fusion, reaction energy, reaction temperature of polymeric materials [122].

In calorimetry it is very difficult to study the specific heat capacity beyond materials solid-liquid phase change. Since the phase change process has significant influence on the specific heat capacity determinations, a different approach has to be used in which effect of the phase change is minimal. The science of electrochemistry can be used for exploring the specific heat capacity in the phase change.

2.2.3 Electro-Magnetic Force Method

Electrochemistry mainly focuses on the chemical reactions that involves the movement of electrons. These electron movements are otherwise called electricity, that can be produced by the transfer of electrons from one element to another in a reaction known as the redox (reduction and oxidation) reaction. These redox reactions can be either endothermic (heat absorption) or exothermic (heat rejection) Robert Mayer [123] was the first to point out that there is a relation between chemical and electrical energy. Helmholtz [124], [125] speculated that the all the chemical energy lost reappeared in the electrical form. Later investigations by Raoult [124], Thomsen [124] and Braun [124] showed experimentally that the electrical energy may be either greater or less than the heat of chemical reaction. Gibbs and Helmholtz [124], [125] theoretically came to the same conclusion. Helmholtz called that portion of whole heat energy which can be transformed into electrical energy as free energy and the portion which cannot be transformed as bound energy. Total energy is the sum of free energy and bound energy. Gibbs-Helmholtz relation is represented in Equation (8):

$$E = \frac{H}{nF} + T \frac{dE}{dt} \quad (8)$$

where E is the emf (mV), F is the Faraday's constant (C/mol), H is the heat of reaction (J, amount of heat added or removed during a chemical reaction), n is the valance ion and T is the absolute temperature. It is observed that if $\frac{dE}{dt} = 0$ or $T = 0$, then $nfE = H$ in other words electrical energy

produced is equal to the heat energy absorbed from the surroundings. If $\frac{dE}{dt} > 0$ or the temperature coefficient is positive, then the electrical energy is greater than the heat of reaction. If $\frac{dE}{dt} < 0$ or temperature coefficient is negative, then heat of reaction is greater than electrical energy.

$$H = nF \left(E - T \frac{dE}{dt} \right) \quad (9)$$

Mellenchamp [124] experimented with simple concentration cells, made up of various solutions for which the heats of dilution (enthalpy change) was determined, and were investigated with reference to the application of the Gibbs-Helmholtz equation.

Barieau [126] details some misconceptions on Gibbs-Helmholtz relation was caused due to incorrect cell reactions by Lewis and Randall [127]. According to Lewis and Randall [127], Gibbs-Helmholtz relation was not applicable for the electromotive cells with concentration changing with temperature. Barieau [126] states with confidence that Gibbs-Helmholtz relation is directly applicable for any reversible galvanic cells as the Gibbs-Helmholtz equation is derived from very general principles involving the relationship between isothermal entropy change and corresponding temperature coefficient of reversible work. Gibbs Helmholtz relation is used for determining the emf, and since it is related to heat of reaction it can be used to determine H when emf and temperature are known. The other forms of Gibbs-Helmholtz equation and the relation between H and specific heat capacity are given by Equation (9), (10) and (11) [128]:

$$\left[\frac{\partial \left(\frac{\Delta G}{T} \right)}{\partial T} \right]_p = \frac{-\Delta H}{T^2} \quad (10)$$

$$\left[\frac{\partial \Delta H}{\partial T} \right]_p = \Delta C_p \quad (11)$$

Estimating specific heat capacity using this method is best suited for the temperatures from the solid to liquid phase transition point. This technique fails below the solid to liquid phase transition temperature as the mobility of ions is heavily hindered as it changes its phase from liquid to solid.

2.2.4 Summary of Methodology

Each of the above methodologies has its own set of limitations and they are well suited at specific temperature ranges. As discussed earlier, determining specific heat using Debye's model is well suited at lower temperatures, and it fails as soon as the anharmonic vibrations starts to appear. Debye's model limit is given by Debye's temperature and it varies with material to material.

Calorimetry method can be applied for a wide temperature range as it just involves heat exchange between two bodies. Though several new types of calorimetry and data analysis techniques are developed estimating specific heats using calorimetry at phase transition is extremely difficult and it bound have more errors [129].

In the case of EMF method, due to hindrance of mobility of ions in the solid state calculating specific heat in the solid state is not possible. This Gibbs-Helmholtz relation works well on and above solid to liquid phase transition temperature. Approximate temperature range and best suited model for estimating specific heat is listed in the Table 1.

Table 1. Best suited method to estimate specific heat at approximate temperature ranges. (* approximate temperature)

Temperature (K)	Best suited model for estimating c_p
0 – 298*	Debye's model
298* – Phase transition temperature	Calorimetry
On and above phase transition temperature	Calorimetry and emf method

2.3 Literature of Thermophysical Properties of AgCl

2.3.1 Heat Capacity of AgCl

In the case of AgCl, Berg [130] used calorimetry to determine the c_p up to 20 K, which agrees well with Eastman and Milner's [131] data as a function of temperature to 292 K. Harteck and Clusius [132] also reported on c_p under 20 K. The Debye's temperature of AgCl is 280 K [133]. Maqsood [134] concluded that at below 5 K, c_p follows the Debye's T^3 law and flattens out as it reaches near room temperature. Akdere [135] performed classical molecular dynamics simulation for calculating the temperature dependence of molar heat capacities on AgCl by using constant volume-energy (NVE) and constant pressure-temperature (NPT) models at both solid and liquid phases. NVE estimates are in accord with Rycerz's [136] differential calorimetry data. Kubashewski [137] and Pankratz [138] heat capacities data have some discrepancies near the melting point region as shown in Figure 16. Reynolds and Laskar [139] speculated that the excess increase of specific heat capacity in silver halides at high temperatures is due to the defects in the crystal structure. Laskar [140], [141] extensively studied the enthalpies and diffusivity of silver halides and compared them with Kobayashi's [141] experimental work. The author also studied how the defects in the crystal structure affects the Gibbs free energy.

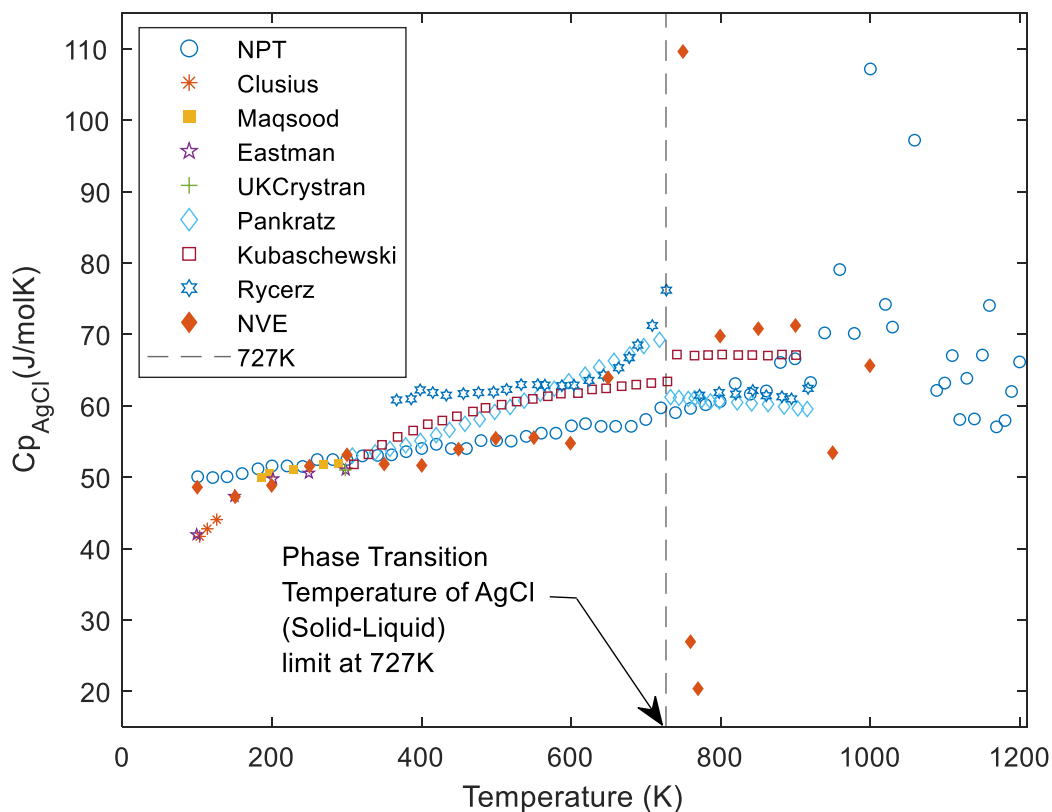


Figure 16. Variation of specific heat capacity of Silver Chloride (AgCl) as a function of temperature. Data adopted from [131], [132], [134]–[138]

Figure 16 illustrates the specific heat data at different temperatures collected from various literature sources. Though literature data are pretty much consistent both before and after the solid to liquid phase transition temperature, including additional data sets to the exiting will result in accurate model of c_p . As discussed in previous section, Gibbs-Helmholtz relation can be implemented to acquire more data sets on c_p , specifically beyond the solid to liquid phase transition temperature. Variation of EMF with temperature is necessary for applying Gibbs-Helmholtz relation.

2.3.1.1 Literature study of EMF variation of AgCl

Initial literature study for extracting EMF variation data set showed that most of the EMF studies related to AgCl are performed on binary or ternary solutions of AgCl. Only those studies which had the results with AgCl mole fraction as one was only considered and they are listed below.

Wilde [142] used the electronic commutator technique, for accurate EMF prediction, and developed a relation between the enthalpy and temperature for fused halides. Metz [143] measured the EMF of the halides in non-isothermal conditions and combined them with the isothermal data to derive the EMF values of the silver halides. Mari and Terzaghi [144] studied the EMF variations of the halides

in a mixture of nitrogen, chlorine atmosphere at different pressures. Pelton [145] and Panish [146], [147] conducted several experiments with various mixtures of alkali chlorides and silver chloride at different mole fractions and studied the effect of composition on EMF at different temperatures. Pelton [145] developed a semiquantitative method for the dual bonding model in which ionic and covalent silver coexist. Guion [148] conducted similar experiments like Panish but with ternary solutions and developed a relation between EMF and temperature.

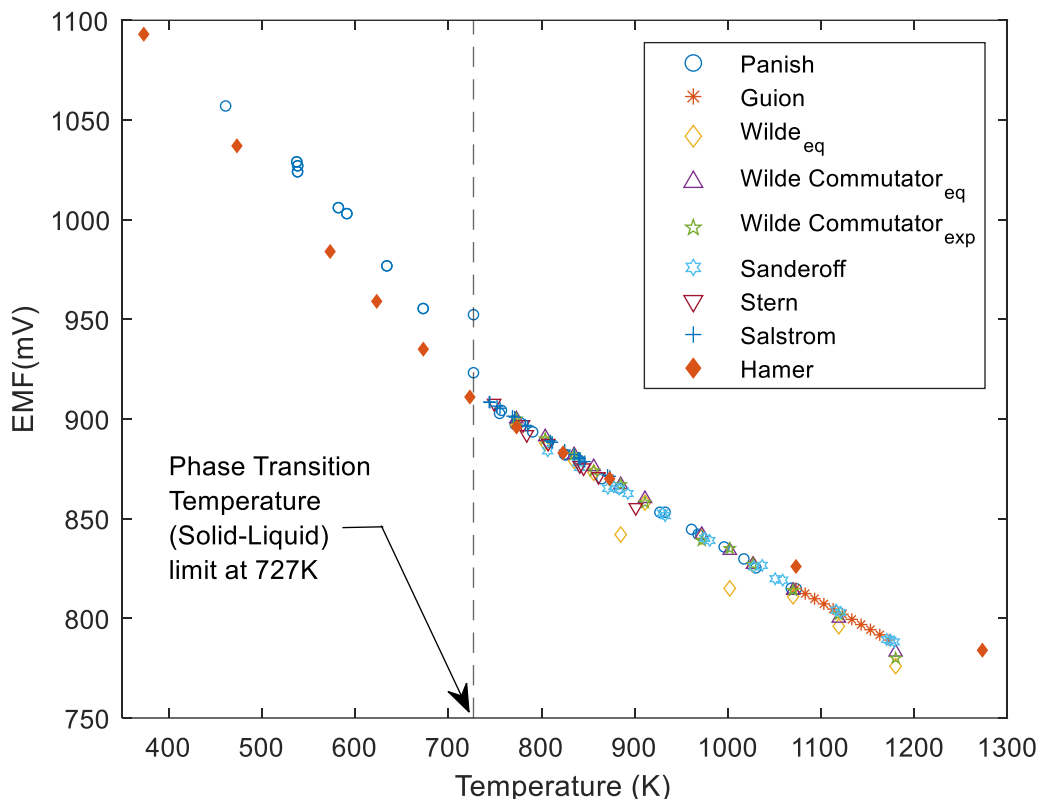


Figure 17. Electromotive force (EMF) of AgCl as function of temperature. Data extracted from literatures [142], [146], [147], [149]–[152]

Pelloux [153] also followed a similar approach in which a completely oxygen-free environment was maintained by using a chlorine atmosphere. Markov and Kuzyakin [154] studied the temperature dependence of the thermopotential of the cell for different silver halides. Sanderoff and Mellors [155], [156] experimental EMF data agrees well with Salstrom [151], Sterns [150] and Janz [157] data which led him to believe that data calculated by Hamer [152] from Brewer's [158] data were similar at low temperatures (773K) but at very high temperatures (1173K) it was off by 15mV. Based on the work presented in the literature review section, the EMF data has been extracted across these studies and plotted against the temperature as shown in Figure 17. In the solid state there are only two data sets reported from Panish [146], [147] and Hamer [152] and the EMF increases rapidly as the temperatures

fall below the phase transition temperature 727 K. The data sets from Figure 17 are curve fitted and used for modelling the variation of specific heat with temperature, explored in detail in Section 3.1.

2.3.2 Other Properties: Thermal Conductivity, Density, Viscosity

The solid to liquid phase transition temperature of AgCl is 727 K. For AgCl, the thermal conductivity (k) is given by Equation (12) and (13) for the temperature ranges $77 \text{ K} < T < 727 \text{ K}$ and $727 \text{ K} < T < 900 \text{ K}$ respectively [134].

$$k_{AgCl} = 296T^{-1} \quad (12)$$

$$k_{AgCl} = ((2.7187e - 08)T^2) - 0.00011153T + 0.24499 \quad (13)$$

The dynamic viscosity (μ) of AgCl is given by Equation (14) [157], [159], [160].

$$\mu_{AgCl} = A + BT + CT^2 + DT^3 \quad (14)$$

where $A = 6.91305$, $B = -0.447411E-02$, $C = -6.49368E-06$, $D = 5.41584E-09$. The variation of density, thermal conductivity and viscosity with temperature are plotted in Figure 18, 19 and 20 for AgCl.

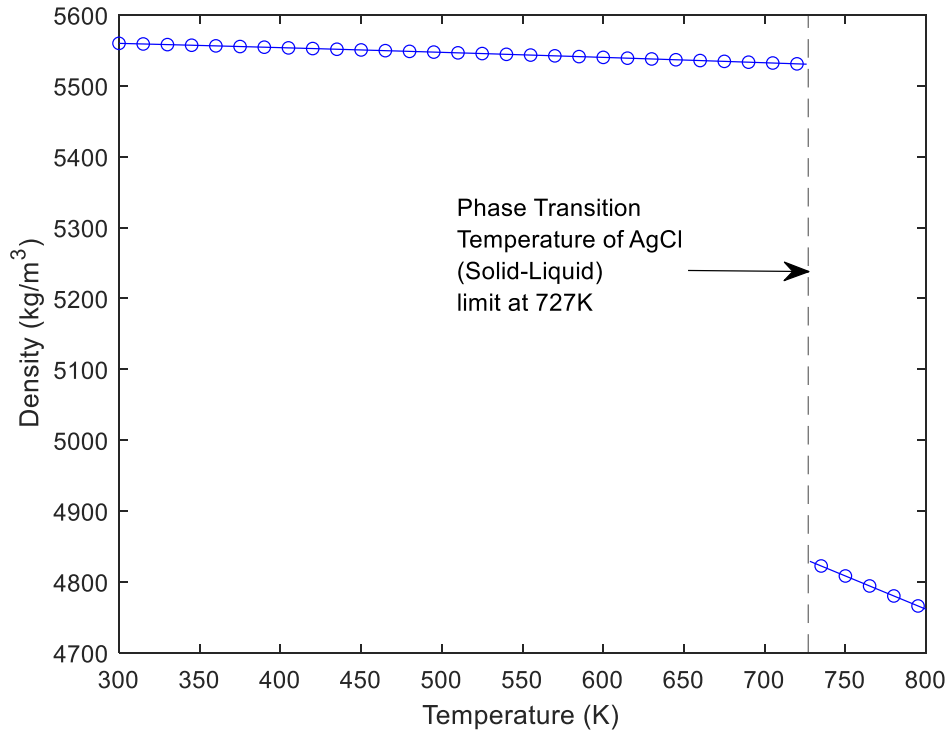


Figure 18. Variation of Density of Silver Chloride (AgCl) as a function of temperature

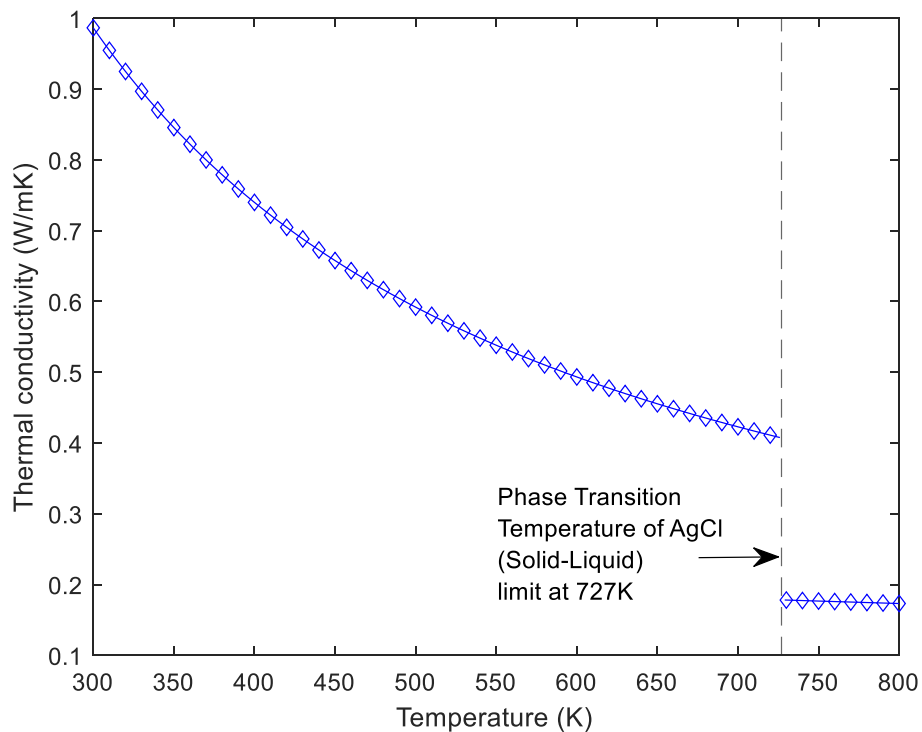


Figure 19. Variation of thermal conductivity of Silver Chloride (AgCl) as a function of temperature

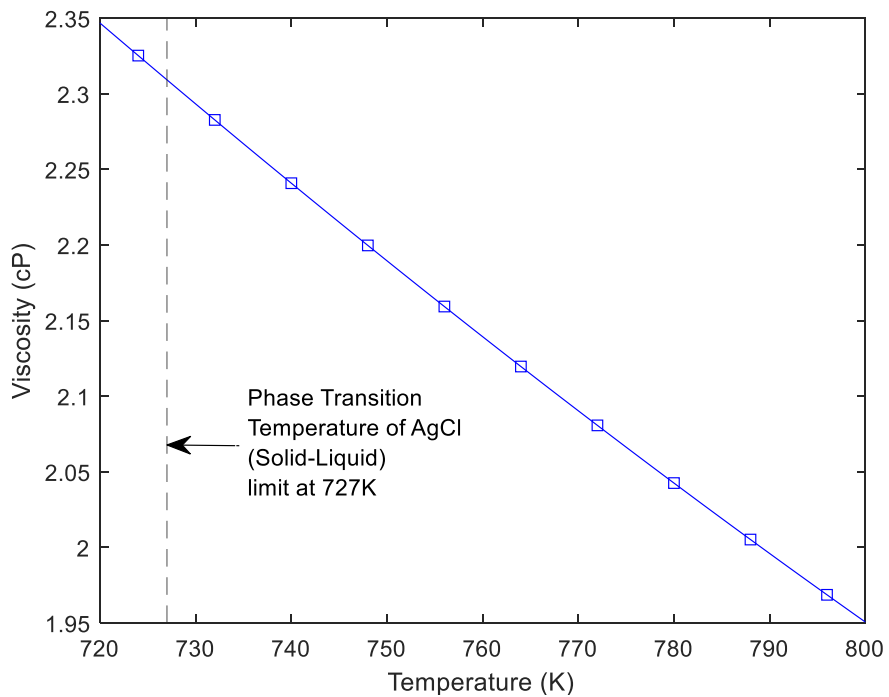


Figure 20. Variation of dynamic viscosity of Silver Chloride (AgCl) as a function of temperature

2.4 Thermophysical Properties of CuCl

2.4.1 Heat Capacity of CuCl

The CuCl exhibits γ -cubic structure and β -hexagonal crystal for the temperatures below and above 683 K. Influence of these structures on c_p of the molten salt plays a crucial role in the heat transfer study. At very low-temperature specific heat variation was studied by Vardeny [161] using the quantum mechanics model. Chase [162] used Shomate's equation to describe the specific heat capacity, but it does not show c_p variation during the γ - β transition. Further studies by Chase [162] give the enthalpy change of CuCl, which is comparable to the values stated by Zamfirescu [58] and Avsec et al [163]. Data reported by Knacke [164] and Avsec [163] falls close in regard to the enthalpy and γ - β transition but they have a discrepancy in specific heats in the β and liquid phase of CuCl, as in Figure 21. Zamfirescu [58] discussed the thermophysical properties of CuCl in detail and developed an equation for specific heat capacity however, the results were concluded only from Knacke's [164] hence results and are not validated.

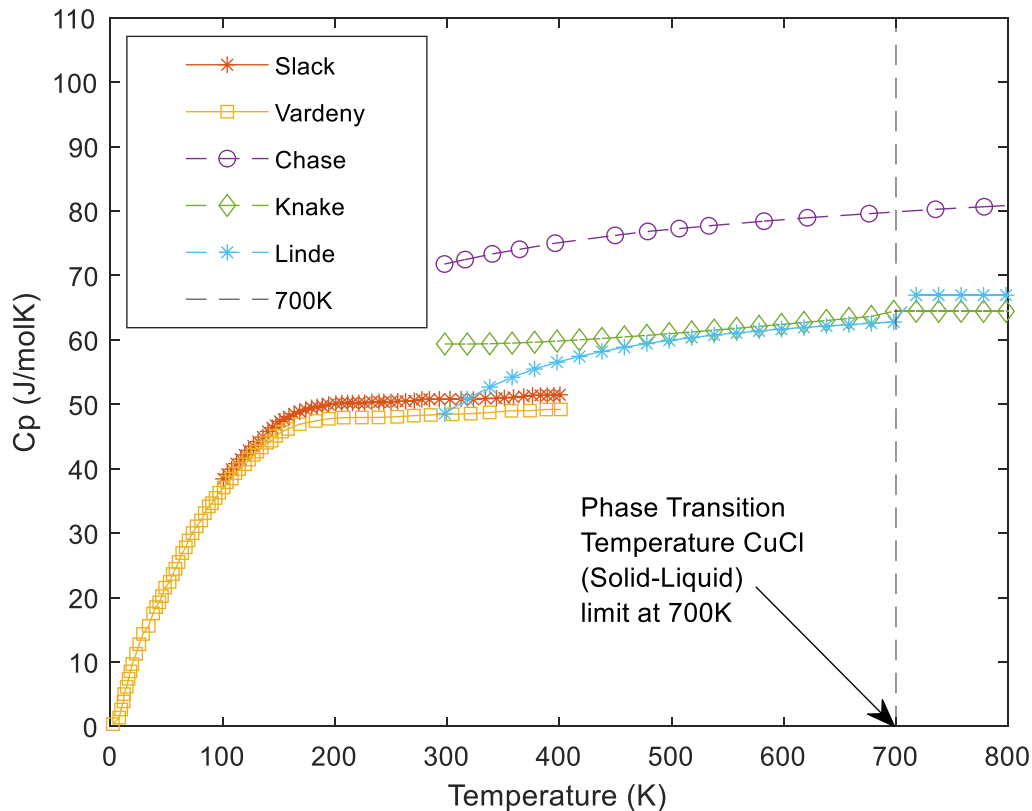


Figure 21. Variation of specific heat capacity of Cuprous Chloride (CuCl) as a function of temperature. Data adopted from [161], [162], [164]–[166]

2.4.1.1 Literature study of EMF variation of CuCl

Similar to AgCl, most of the EMF literature studies on CuCl are with binary or ternary solutions of CuCl. Unlike AgCl, most of those studies did not include the EMF findings with mole fraction of CuCl as 1. A study conducted by Glaztzoglou [167] [168] included the EMF variation for pure CuCl, as shown in Figure 22. During the experimentation of high temperature batteries, Sudworth [169] experimentally measured the EMF variation with temperature for CuCl.

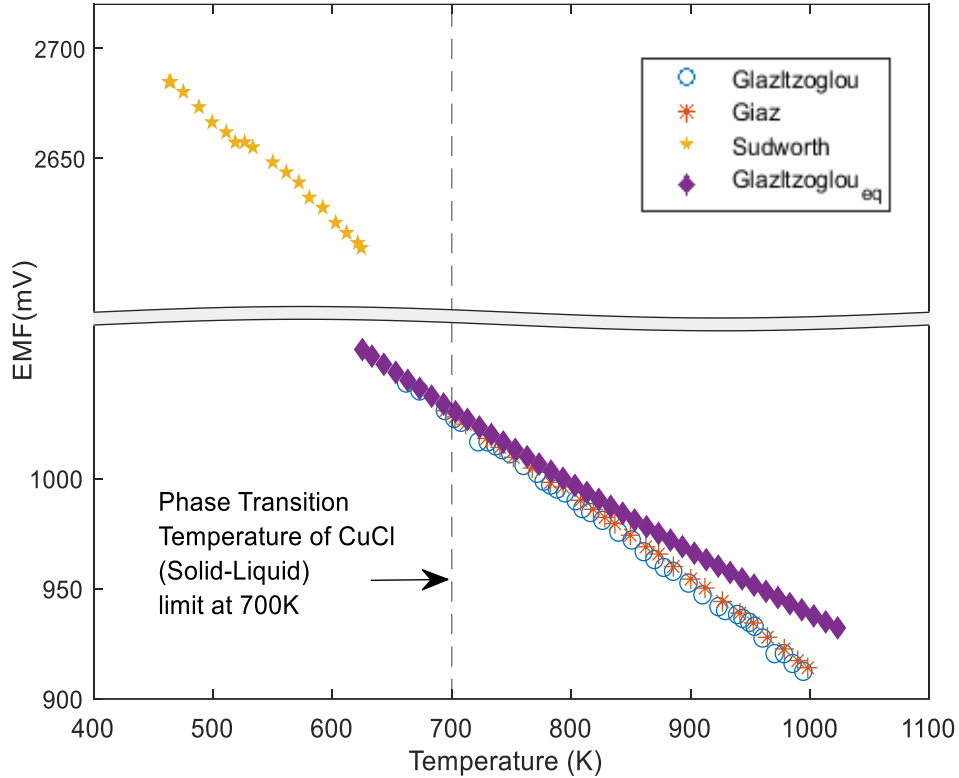


Figure 22. Electromotive force (EMF) of CuCl as function of temperature. [167]–[169]

2.4.2 Other Properties: Thermal Conductivity, Density, Viscosity

Zamfirescu [58] reported that CuCl is considered a molecular liquid above its melting point. Due to the absence of experimental data, the low temperature molecular liquid's empirical relations are used for both dynamic viscosity and thermal conductivity for CuCl as given in Equation (15) and (16):

$$\mu_{CuCl} = 0.365 \exp\left(-6.95 + \frac{1418}{T}\right) \quad (15)$$

$$k_{CuCl} = \frac{0.19(1 - T_r)^{0.38}}{T_r^{1/6}} \quad (16)$$

where T_r is the reduced temperature ($T_r = T/T_c$) and T_c is the critical temperature. The variation of density, thermal conductivity and viscosity with temperature are plotted in Figure 23, 24 and 25 for CuCl.

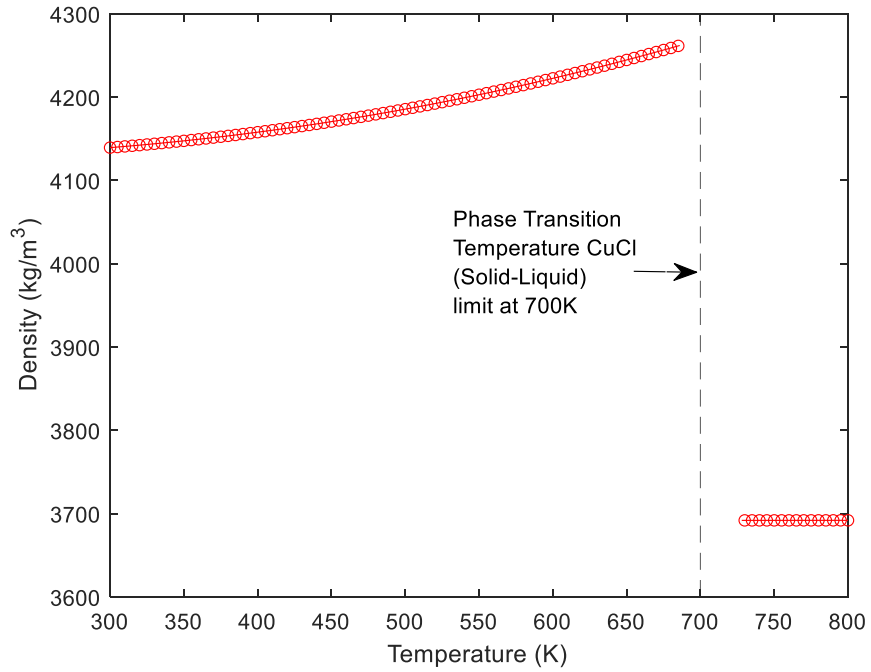


Figure 23. Variation of density of Cuprous Chloride (CuCl) as a function of temperature[170]

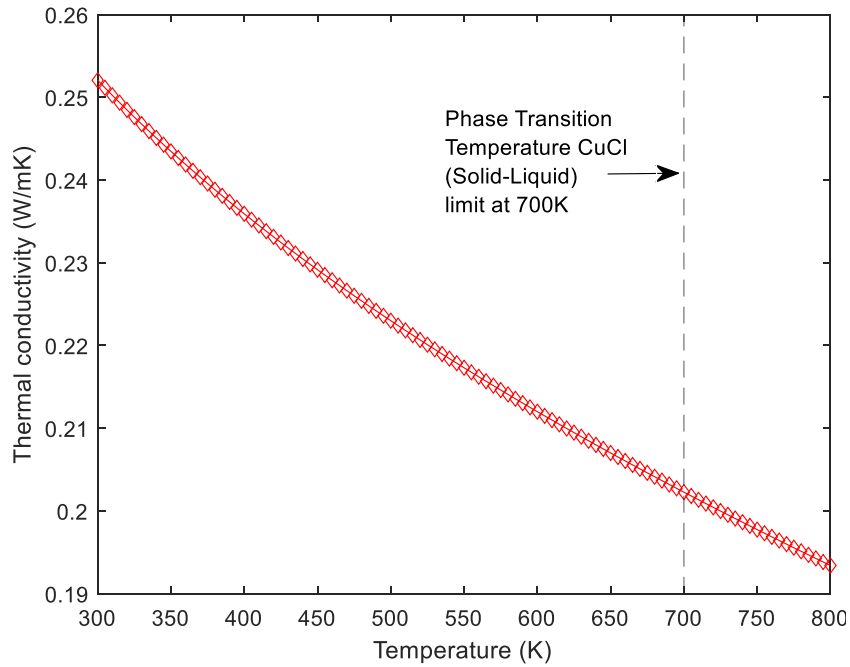


Figure 24. Variation of thermal conductivity of Cuprous Chloride (CuCl) as a function of temperature[170]

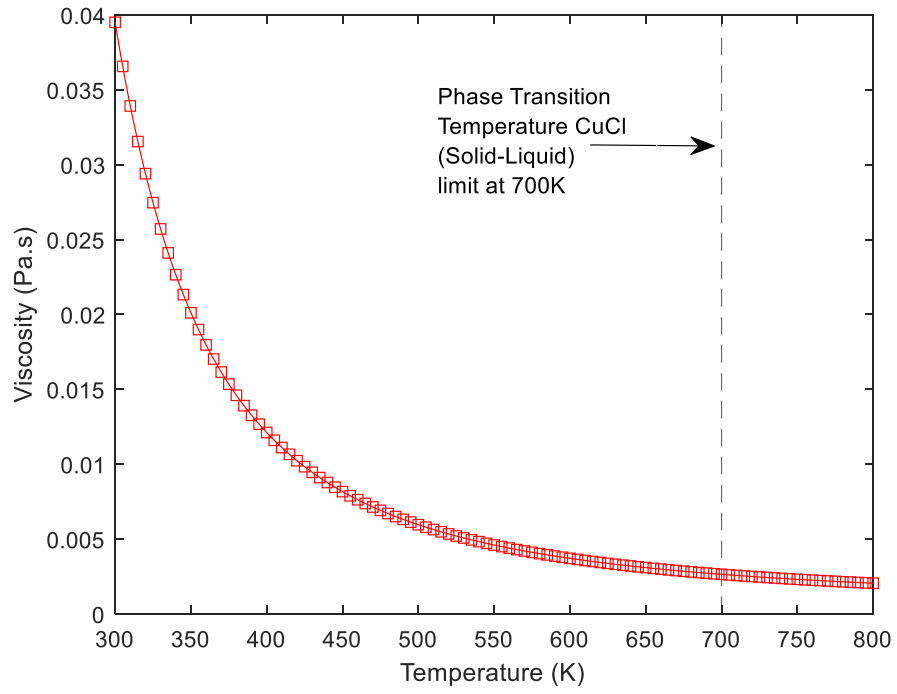


Figure 25. Variation of dynamic viscosity of Cuprous Chloride (CuCl) as a function of temperature[170]

Chapter 3 - Heat Capacity Results of AgCl and CuCl

3.1 Modelling of Heat Capacity of AgCl

The EMF values in Figure 17 was curve fitted using least square method and the curve is used to determine the enthalpy using Equation (9), (10) and (11). The calculated enthalpy values agree well with the values reported by Janz [157]. The c_p is calculated from the evaluated enthalpy values using Equation (9) and with the reference data from Table 2. The computed specific heat capacity data has been plotted against temperature as shown in Figure 26. There is a steep increase in specific heat below the melting point. This is due to the hindrance in mobility of ions in the solid state.

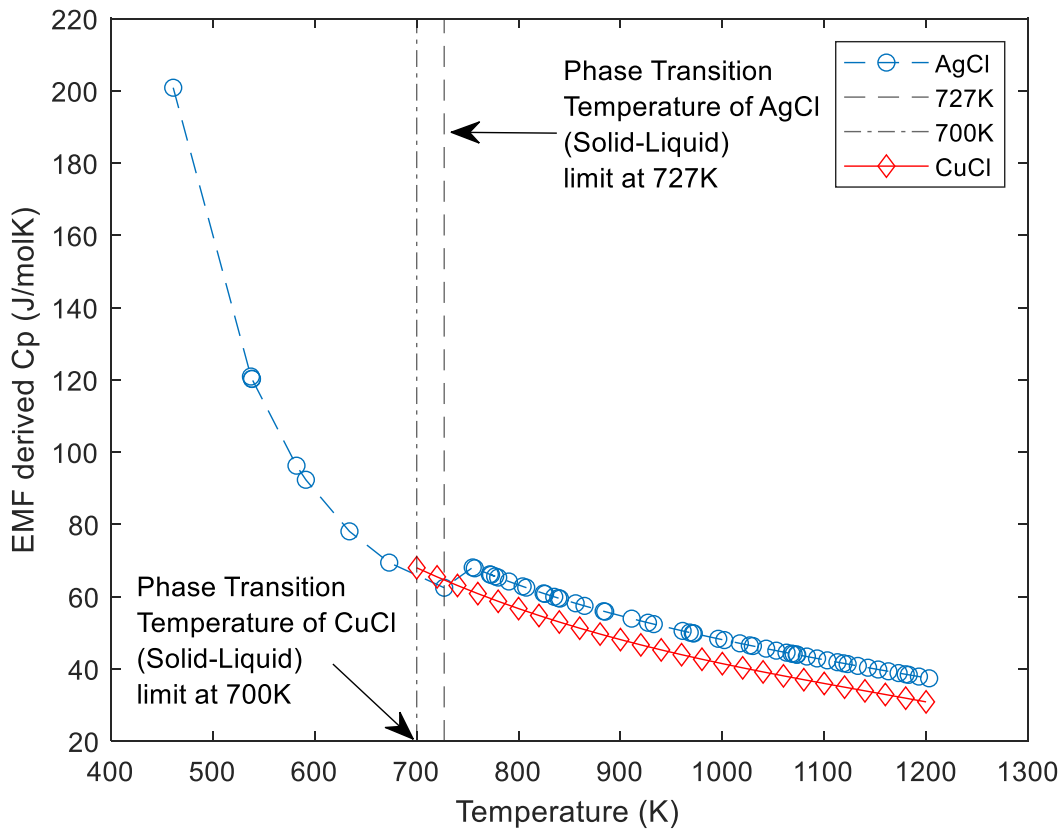


Figure 26. Variation of specific heat capacity of AgCl and CuCl with temperature derived from EMF sources

Table 2. Thermal properties of AgCl

Description	Values
Melting point	727 [K]
Heat capacity at 298 [K][171]	50.8 [J/molK]
ΔH at 728 [K] (Form thermal sources)[157]	25.55 [kcal/mole]
EMF at 728 [K][157]	0.9132 [V]
ΔH_{EMF} at 728 [K] (Derived from EMF)[157]	25.98 [kcal/mole]

During an electrochemical process, silver ions and chlorine ions migrate and get deposited on the respective electrodes. The mobility of the ions rely upon the material properties and temperature of the material [172], [173]. As the AgCl changes its phase from liquid to solid, the ionic mobility is heavily hindered. The effect of this phenomenon is reflected well, in Figure 26, in the form of uncharacteristic behavior of c_p as the temperature goes low. A similar effect can be observed where the EMF increases rapidly as the temperature abates below the melting point. So, the EMF derived c_p values have been neglected due to erratic behavior of c_p in the solid-state. The c_p values beyond the melting point show a downtrend and slowly stabilizes to a constant value. Though the values reported in other literature and this study vary around 5 J/molK the trend is analogous to the literature where values remain almost constant after the melting point [136], [138], [164]. This variation could be due to the errors involved in the EMF measurement in the literature that ranges from 0.5mV to 3mV, which translates to approximately 1 to 4J/molK in c_p . Moreover, the EMF data extracted from the literature uses different techniques for experiments.

The data from Figure 16 has been combined with the EMF derived c_p values of AgCl from Figure 26 and shown in Figure 27 with error bounds. Along with the calculated values of c_p in solid-state from Figure 26, some values from the simulated data sets of NPT and NVE were also neglected due to drastic variations, especially near the melting point regions. The compiled data has been curve fitted using the least square method, and the curve is defined using Equation (17) and the corresponding coefficients are tabulated in Table 3.

In Matlab, the norm of residuals represents the goodness of the fit, where a smaller value indicates a better fit than a larger value. The residual values of the developed heat capacity model for AgCl varies from 0 to 40 at different temperatures, which is an acceptable considering the inconsistency between various literature sources.

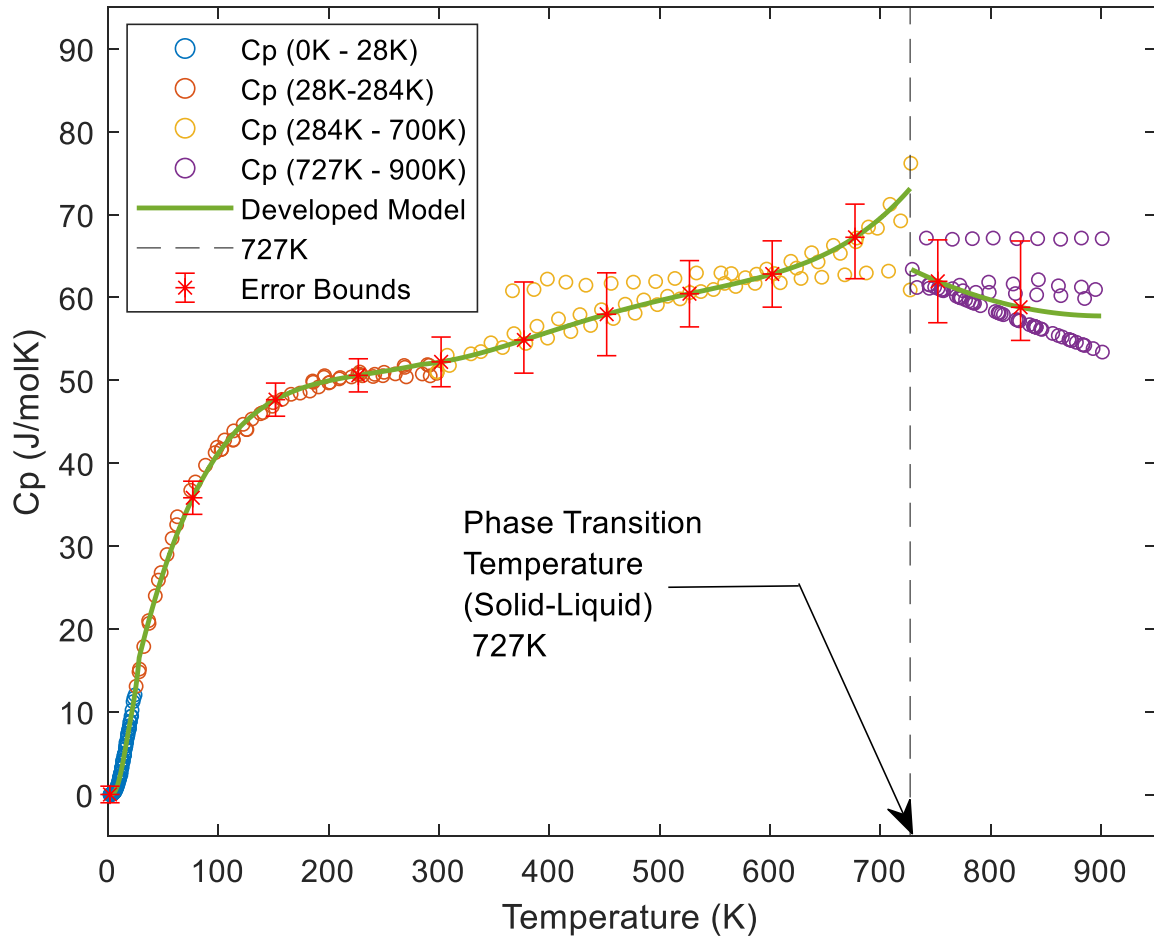


Figure 27. Consolidated specific heat capacity of AgCl as function of temperatures from EMF and thermal sources[130]–[132], [134]–[138]

$$c_p = AT^5 + BT^4 + CT^3 + DT^2 + ET + F \quad (17)$$

Table 3. Values of A, B, C, D, E and F in the AgCl specific heat capacity equation (17)

Temperature[K]	Coefficient					
	A	B	C	D	E	F
T < 28.39	5.9E-06	-3.9E-04	8.4E-03	-4.2E-02	7.4E-02	-1.6E-02
28.39 < T < 284.4	7.7E-12	-1.6E-08	1.2E-05	-4.4E-03	7.6E-01	-1.8E+00
284.4 < T < 727		2.1E-09	-4.0E-06	2.7E-03	-7.6E-01	1.3E+02
727 < T < 900				1.9E-04	-3.3E-01	2.1E+02

3.2 Modelling Specific Heat Capacity of CuCl

The EMF data for CuCl is presented by Glazltzoglou [167]. On comparing the EMF values of AgCl and CuCl, the slopes of the lines defined by the data look nearly parallel with some offset as shown in Figure 28. The angle between the curve fitted line of AgCl and CuCl is 1.96° . Since the angle between the curve fitted lines is relatively small, both the lines are assumed to be parallel to each other. As CuCl and AgCl EMF values follow a linear trend, their c_p values will also follow a similar trend and their offset is determined using the reference from Linde [166], as shown in Figure 26. Linde's [166] specific heat data is used for reference as it is the only data set that is comparable with specific heat values calculated using Debye's model by Slack [165] and Vardney [161], as shown in Figure 29.

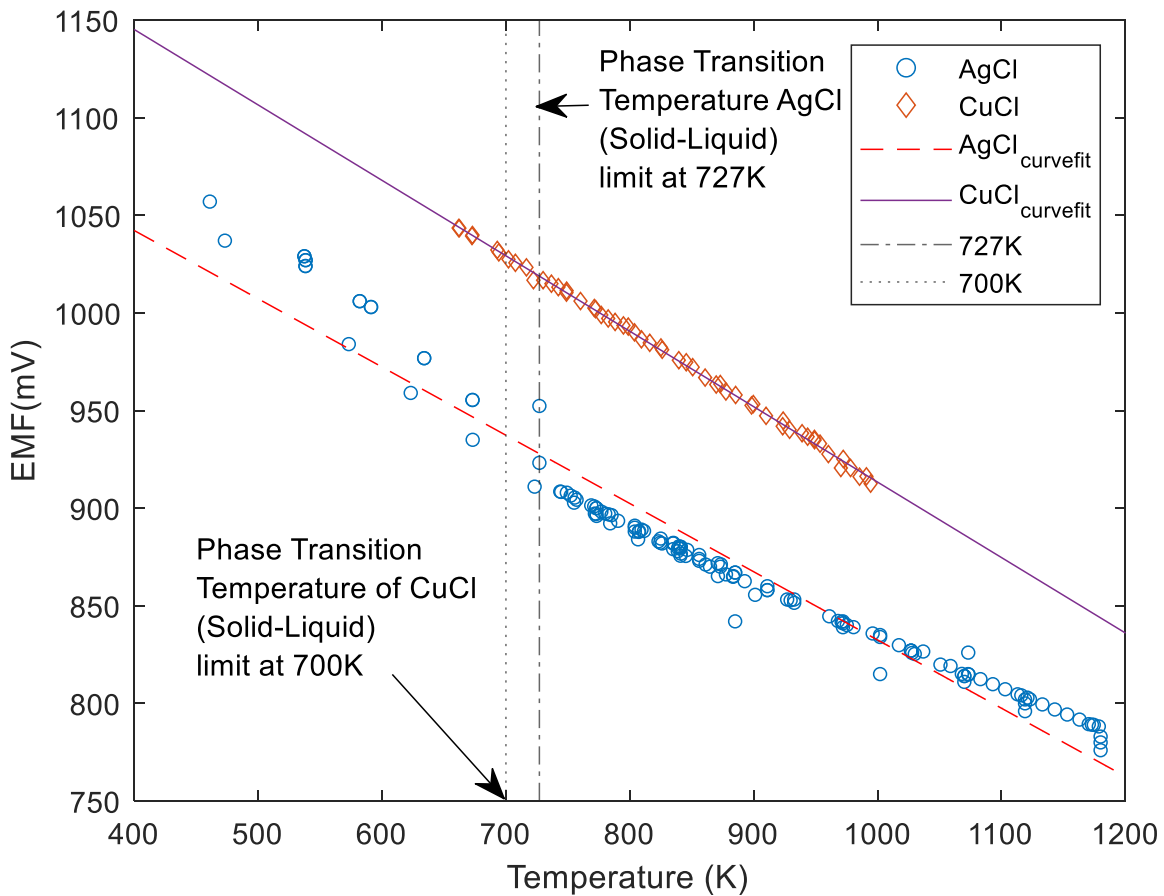


Figure 28. Comparison of EMF between AgCl and CuCl as function of temperature. AgCl data adopted from [167]

Similarly to AgCl, the EMF derived c_p values beyond the solid to liquid phase transition point is considered for CuCl. This EMF derived c_p data set is combined with the c_p values determined using thermal sources and Debye's model to form a hybrid model, as shown in Figure 29. This data set has been curve fitted using least square method and characterized using Equation (18) and their respective

coefficients are given in Table 4. The residual values of the heat capacity model developed for CuCl range from 0 to 60 at different temperatures, which is appropriate despite the discrepancies between different sources in the literature.

$$c_p = AT^6 + BT^5 + CT^4 + DT^3 + ET^2 + FT + G \quad (18)$$

Table 4. Values of A, B, C, D, E and F in the CuCl specific heat capacity Equation (18)

Temperature [K]	Coefficient						
	A	B	C	D	E	F	G
1 < T < 20	-6.4E-06	1.5E-02	-1.1E+01	2.9E+03			
20 < T < 135.4	4.9E-09	-1.8E-06	-1.1E-03	4.9E-01	3.0E-01		
135.4 < T < 700	-1.1E-14	3.0E-11	-3.8E-08	1.7E-05	-4.9E-03	7.8E-01	3.8E+00
700 < T < 850	-6.4E-06	1.5E-02	-1.1E+01	2.9E+03			

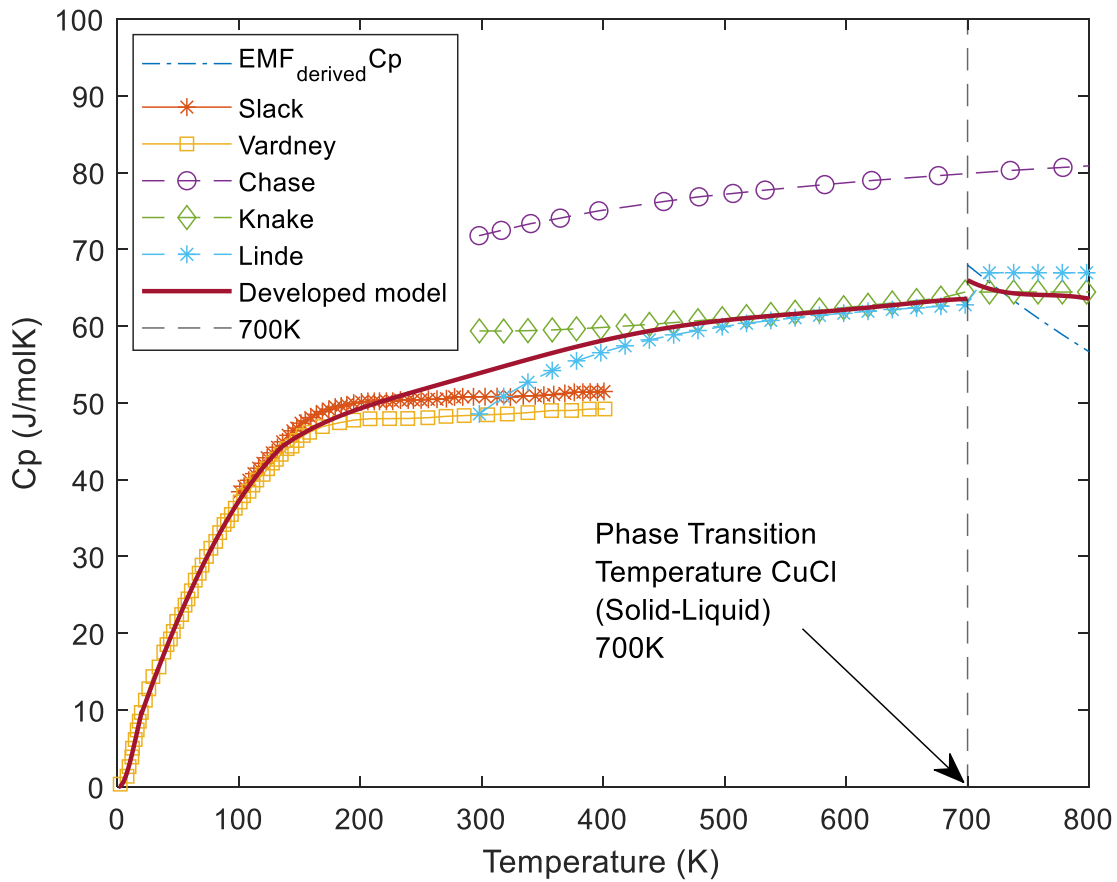


Figure 29. Consolidated specific heat capacity of CuCl as function of temperatures from EMF and thermal sources [161], [162], [164]–[166]

Since the Equation (17) and (18) consists of higher-order terms, it is strongly suggested to use the appropriate coefficients for the respective temperature bounds. The data should not be extrapolated beyond $\pm 5\text{K}$. In Figure 29, there is a discrepancy between thermally determined and Debye's model in the temperature range of 285K to 400K. Similarly, the EMF derived c_p values show a significant downtrend when compared to the thermally determined c_p , which is constant beyond the melting point of CuCl. This could be due to the usage of imprecise reference for the EMF derived specific heat capacity offset. These anomalies are difficult to analyze due to the lack of sufficient consistent data.

Chapter 4 - Heat Recovery Study

4.1 Introduction

The heat recovery is process of retrieving the energy that was spent on some object or material or on a process. In most cases only a part of the energy can be recovered, as it is practically impossible to retrieve all the energy spent. Here, as in Figure 6, the temperature of the first reaction step must be around 90°C. The temperature of the CuCl produced by decomposing the CuO·CuCl₂, at step 4, is at 530°C which is cooled by quenching in a water bath. As CuCl is being highly reactive in the presence of oxygen, forming more stable complexes, the quench cell is purged with an inert N₂ atmosphere to ensure an oxygen-free environment. As the molten CuCl enters the quench cell, it thermally interacts with N₂. These interactions between N₂ and the droplet is modelled numerically using COMSOL Multiphysics. The main objective of this model is to estimate the amount of energy in the form of heat that can be recovered from the droplet by analyzing the amount of heat lost by droplet to its surroundings during a free-fall.

The FEA process begins with a computer-aided design (CAD). In this, a model/geometry (1D,2D, or 3D) is developed along with the knowledge of material properties and the applied loads and constraints. In FEA a larger system/model is subdivided into smaller finite elements and a set of governing partial differential equations are solved in two or three space variables. The process of subdividing the model into smaller domains is called meshing. The accuracy of the FEA results is directly related to the mesh size used in the model. As the mesh is refined, ie. as the elements are made smaller and smaller, the FEA solution of the model will approach a true solution.

Calvet [174] numerically studied the phase change process of a PCM by intensifying the effective thermal conductivity of the PCM using COMSOL Multiphysics [5]. Jalal [175] used COMSOL Multiphysics to study the forced convection cooling on packaged vents. Mayank [176] examined the effect of conduction on a PCM in a spherical and cylindrical vessel during a phase change process using COMSOL Multiphysics with a fixed temperature boundary. Azad [177] performed both numerical and experimental studies to investigate the effects of heating temperature on phase change of a PCM with natural convection. Eduard [178] analysed the temperature gradients inside a the PCM capsules using energy equation model and their results were validated with the experimental results. Nabeel [179] performed analytical, numerical and experimental investigations for thermal energy storage by melting and ensuing convection of PCM in various shaped enclosures. After profound

analysis of above studies, a new numerical model is developed to examine the CuCl and N₂ interactions.

4.2 Free Fall

From Newtonian physics, any object that moves under the sole force of gravity is called free fall. Generally, the term free fall is used more loosely for example ball falling due to gravity is called as a free-falling ball. But in reality, the air acts a resistance and creating an opposing drag force which means that ball is not in free fall. For the sake of simplicity, here the droplets are termed as free-falling droplet even though droplet experiences the opposing drag force caused by N₂. Any object that accelerates only due to gravity reaches a maximum velocity called terminal velocity ($V_{terminal}$) and the velocity remains constant thereafter. The object reaches its maximum velocity when the objects drag force (D) equals to its weight (W) ie. net force (F) becomes zero.

$$F = D - W \quad (19)$$

$$D = \frac{C_d \rho v^2 A}{2} \quad (20)$$

$$W = mg \quad (21)$$

$$v_{terminal} = \sqrt{\frac{2mg}{C_d \rho A}} \quad (22)$$

where m is mass of the object (kg), g is the gravitational acceleration (m/s²), C_d is the coefficient of drag, ρ is the density of the medium through it falls (kg/m³) and A is the frontal area (m²).

4.3 Assumptions

The following assumptions are made to simplify the numerical model and reduce computation time:

1. N₂ is considered to be an ideal incompressible fluid, as the numerical simulation is primarily focused on evaluating heat interactions between N₂ and the droplet.
2. To reduce the complexity the shape of the droplet is assumed to be spherical and its shape does not change with time. Also, it is assumed that the bubble retains its spherical shape and any forces acting on the bubble will not deform it since the outer layer solidifies swiftly.
3. To have consistent thermophysical properties throughout the simulation, the droplet is presumed to be homogeneous and will be a function of temperature both in its molten and solid-state.
4. A preliminary study with varying density and constant volume revealed that approximate change in mass is less than 2% for the desired time range. The volume change will be the same as mass

change, as the volume is proportional to the mass. As the volume change is negligible, moving mesh method in COMSOL Multiphysics is not applied here which could lead to undesired results and it is computationally expensive. Abiding by the law of mass conservation, the density is taken as an average value between solid and liquid phases.

5. According to the conservation of mass as in Equation (23), mixing within the droplet is caused by density changes with respect to time.

$$\frac{\partial \rho}{\partial t} + \nabla \cdot (\rho u) = 0 \quad (23)$$

However, since the density is taken as constant due to insignificant volume change in the droplet the internal velocity (u) becomes zero as in Equation (23), thereby no mixing within the droplet.

4.4 Numerical model

A 2D axisymmetric geometry is adopted to model the interactions between droplet and N_2 , as shown in Figure 30. An axisymmetric approach was selected to reduce the finite element calculations during simulation. The droplet is placed in the center of the N_2 domain where N_2 enters at the bottom and exits at the top of the domain. The basic measurements of the domain are tabulated in Table 5.

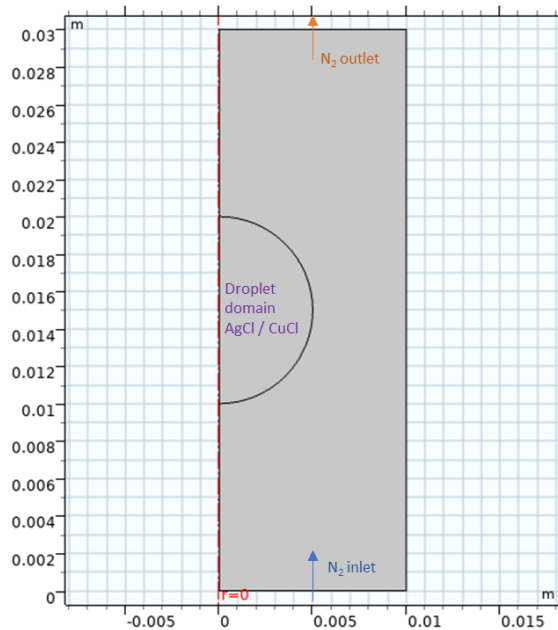


Figure 30. 2D Model Geometry of the model with droplet and N_2 domain with their inflow and outflow directions.

To simulate a free-falling droplet, N_2 is made to flow relative to the fixed droplet. The relative acceleration of N_2 is calculated using Equation (16).

$$a_d - \frac{F_z + F_g}{m_d} = 0 \quad (24)$$

where a_d is the acceleration of the droplet as it is free-falling through the N_2 atmosphere in m/s^2 , F_g is the force due to gravity on the droplet in Newtons, F_z is the net drag force caused by N_2 on the droplet which is calculated computationally. Drag force is a resistive force caused by the motion of droplet in N_2 . This drag force acts in the opposite direction of the upstream fluid. During the run time of the simulation, at every time step, the resistive force experienced by the droplet on its surface is calculated on each node of the model and then aggregated to form the net drag force (F_z).

Table 5. Geometric dimensions and thermophysical properties of the model

Description	Name	Value
Radius of droplet	R_d	0.005 [m]
Width of the domain	width	0.01 [m]
Height of the domain	height	0.03 [m]
Initial temperature of the droplet (AgCl)	$T_{i,d}$	740 [K]
Temperature of the N_2	T_f	298.15 [K]
Density of CuCl	ρ_{CuCl}	4038.075 [kg/m ³]
Melting point of CuCl	$T_{m,CuCl}$	700 [K]
Latent heat of CuCl	$L_{m,CuCl}$	71.51587[J/g]
Density of AgCl	ρ_{AgCl}	5179[kg/m ³]
Melting point of AgCl	$T_{m,AgCl}$	727 [K]
Latent heat of AgCl	$L_{m,AgCl}$	92105 J/kg

4.4.1 Momentum Equation:

The Nitrogen is treated as Newtonian fluid, then the incompressible form of Navier-Stokes equation in a coordinate free representation, is expressed as in Equation (25).

$$\frac{D\vec{V}}{Dt} = \vec{g} - \frac{\nabla P}{\rho} + \nu \nabla^2 \vec{V} \quad (25)$$

\vec{V} is the velocity of the N_2 in (m/s), \vec{g} represents the gravitational acceleration (m/s^2), ν represents the kinematic viscosity (m^2/s), ρ is the density of the N_2 (kg/m^3), P represents the pressure and V_∞ is the free stream velocity (close to the terminal velocity of the droplet). The walls of the droplet are taken as a no slip boundary. For a stationary wall that means that $V = 0$ and $V = V_\infty$ at infinity. As there is no mixing inside the droplet, Navier-Stokes equation is applied only for N_2 domain.

4.4.2 Energy Equation:

For modelling the interactions between the droplet and the N₂, the energy equation is applied for both the droplet and N₂ domain. The conservation of energy is expressed as

$$\rho C_p \frac{\partial T}{\partial t} + \rho C_p u \cdot \nabla T + \nabla \cdot q = 0 \quad (26)$$

$$q = -k \nabla T \quad (27)$$

where ρ is the density and C_p is the thermal capacity. The thermal conductivity k describes the relationship between the heat flux vector q and the temperature gradient ∇T in $q = -k \nabla T$, which is Fourier's Law of heat conduction. As it was determined that there is no mixing inside the droplet, energy change due to the viscous dissipation can be neglected. As the droplet does not react with N₂, for the numerical simulation, the boundaries of the droplet can be treated as a wall, which implies that only heat transfer occurs across the boundaries of the droplet and there is no mass transfer across it. Rate of conduction in the droplet and the rate of convection by the N₂ are equal at the boundaries of the droplet.

$$\dot{Q}_{Conduction} = \dot{Q}_{Convection} \quad (28)$$

$$-k(T) \frac{\partial T}{\partial r} = h(T_s - T_\infty) \quad (29)$$

Reynolds number is a non-dimensional number, and it is used to categorize the fluids flow pattern-based viscosity and velocity and it is given by Equation (30):

$$Re = \frac{\rho d V}{\mu} \quad (30)$$

where ρ is the density of the nitrogen, d is the diameter of the droplet, V is the velocity and μ is the viscosity of the fluid. If the $Re < 2300$ then the fluid flow is considered to be laminar, in which the fluid particles travel in parallel layers, each of which has a constant velocity but is in motion relative to its neighboring layers [180].

Since this analysis is for a lab scale quench cell model, the total height of the quench cell is less than 50m. Based on the initial analysis, the Reynolds number was found be well below 2300 for the lab scale model. Hence, the flow of nitrogen is taken as laminar.

The thermophysical properties are essential for any numerical analysis. Since the droplets are made of AgCl or CuCl, its thermophysical properties such as specific heat, thermal conductivity, dynamic

viscosity explored in the chapter 2.3 and 2.4 can be utilised. The initial conditions and the constant density of CuCl, AgCl are presented in Table 5.

4.5 Results and Discussion

4.5.1 Free fall

Initially, the droplet's acceleration is equal to the gravitational acceleration. The acceleration of the droplet affected due to the buoyant and drag force. The buoyant forces are neglected since the volume of the droplet is small hence the buoyant force is negligible compared to the drag force and force of gravity. The coefficient of drag (C_D) being a function of velocity, the drag force initially decreases and remains constant after the terminal velocity. Ghandehariun [66]–[68] evaluated the drag force by assuming C_d to be a constant, whereas the drag force calculated computationally in this manuscript is a function of velocity, thereby increasing the accuracy of the computation.

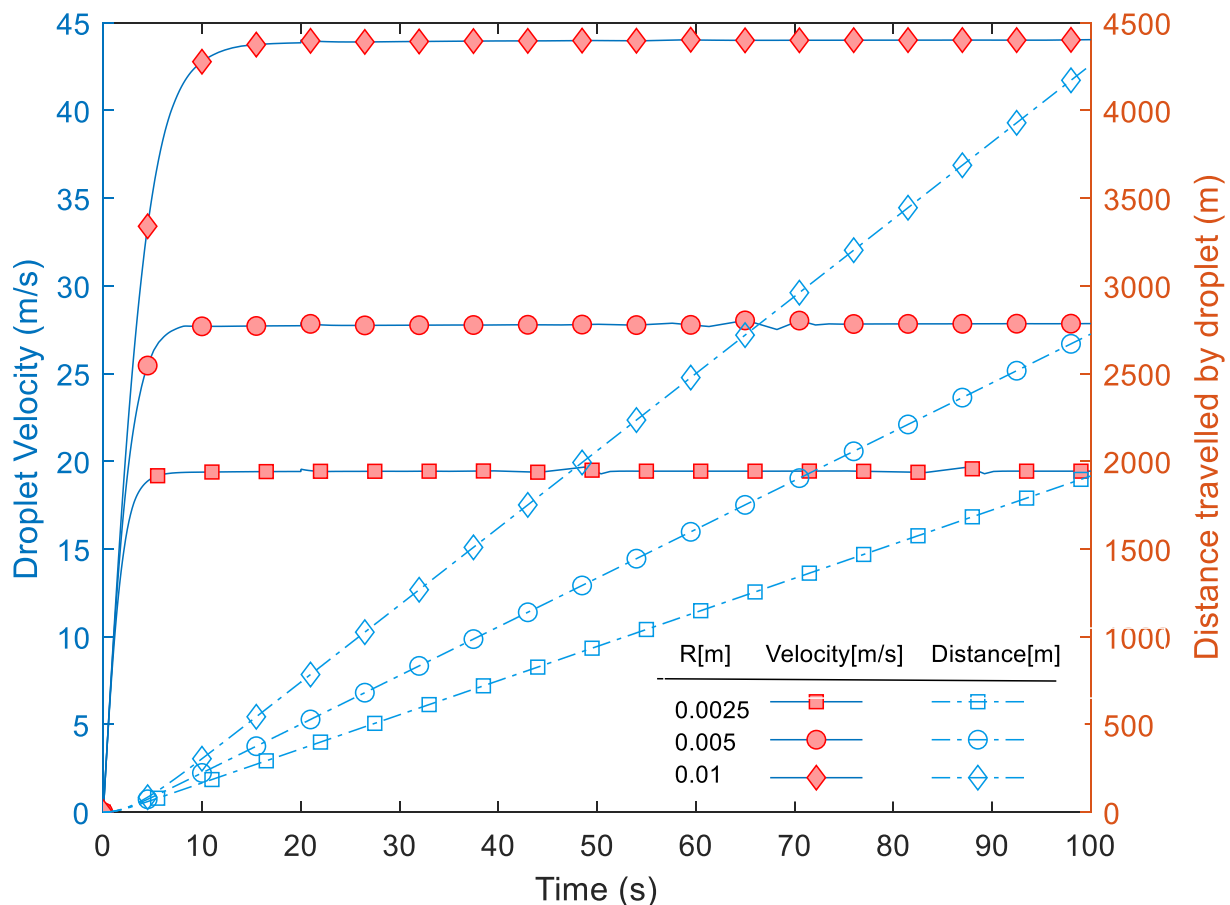


Figure 31. Velocity and distance travelled by the AgCl droplet with respect to time various radiuses, R (0.0025m, 0.005m, 0.01m)

The droplet velocity and the distance travelled by the droplet are determined using Equation (24) and the results are shown in Figure 32. As illustrated in Figure 32, the terminal velocity and the distance travelled by the droplet increases considerably for both AgCl and CuCl as the velocity is proportional to the mass of the droplet. Slight deviation in the terminal velocity of the droplets in Figure 31 and 32 is effectuated by numerical instabilities. Since the variations is less than 2% these deviations are neglected.

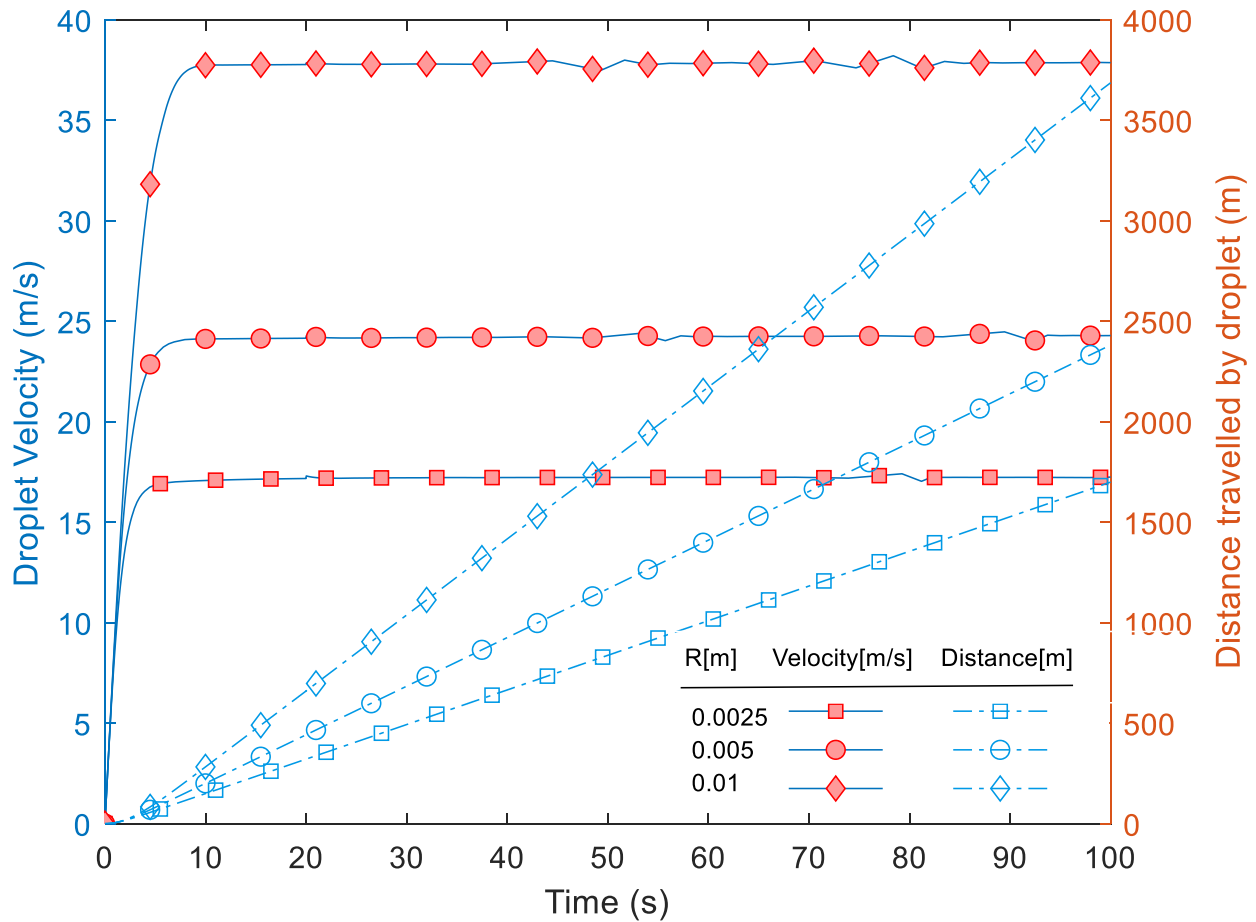


Figure 32. Velocity and distance travelled by the CuCl droplet with respect to time for various radiuses, R (0.0025m, 0.005m, 0.01m)

4.5.2 Phase Change in AgCl and CuCl Droplet

Figure 33 – 38 illustrate the temperature distribution of the droplet and the N₂ domain. The color spectrum for the legends for each figure is given on the right-hand side. (Note: The maximum and minimum values of the color spectrum for the legends varies for each figure).

From the below figures, it is obvious that the temperature distribution inside the droplet are not radially symmetric for both AgCl and CuCl. As the droplet free falls, the outer most layer of the droplet starts to solidify as soon as it reaches its liquid to solid phase change temperature. The interface that

separates the solid and liquid propagates radially inwards as the solidification occurs. The asymmetric nature of the temperature distribution in the droplet is due to the varying heat transfer rates within the droplet. The heat transfer rates are higher at the lower end of the droplet due to higher velocity of N_2 whereas at the upper end of the droplet the heat transfer rates are slower due to the reduced velocity and recirculation of N_2 above the droplet. Because of this, lower end of the droplet is has lower temperature compared to the upper end. The heat transfer rates between N_2 and the droplet steadily increases until the droplet reaches its terminal velocity after which it remains almost constant.

The initial temperature of the AgCl and CuCl droplets are 740K and 723K respectively. When comparing the AgCl and CuCl droplets of identical diameter, say Figure 33 and 36, it is evident that the change from liquid to solid phase occurs much faster in AgCl compared to CuCl. The AgCl's higher thermal conductivity, almost double compared to CuCl at their respective phase change temperatures, increases the thermal diffusivity of AgCl significantly which in turn increases the heat transfer rates of AgCl. The lower thermal diffusivity of CuCl facilitates energy retention which can be used for heat recovery.

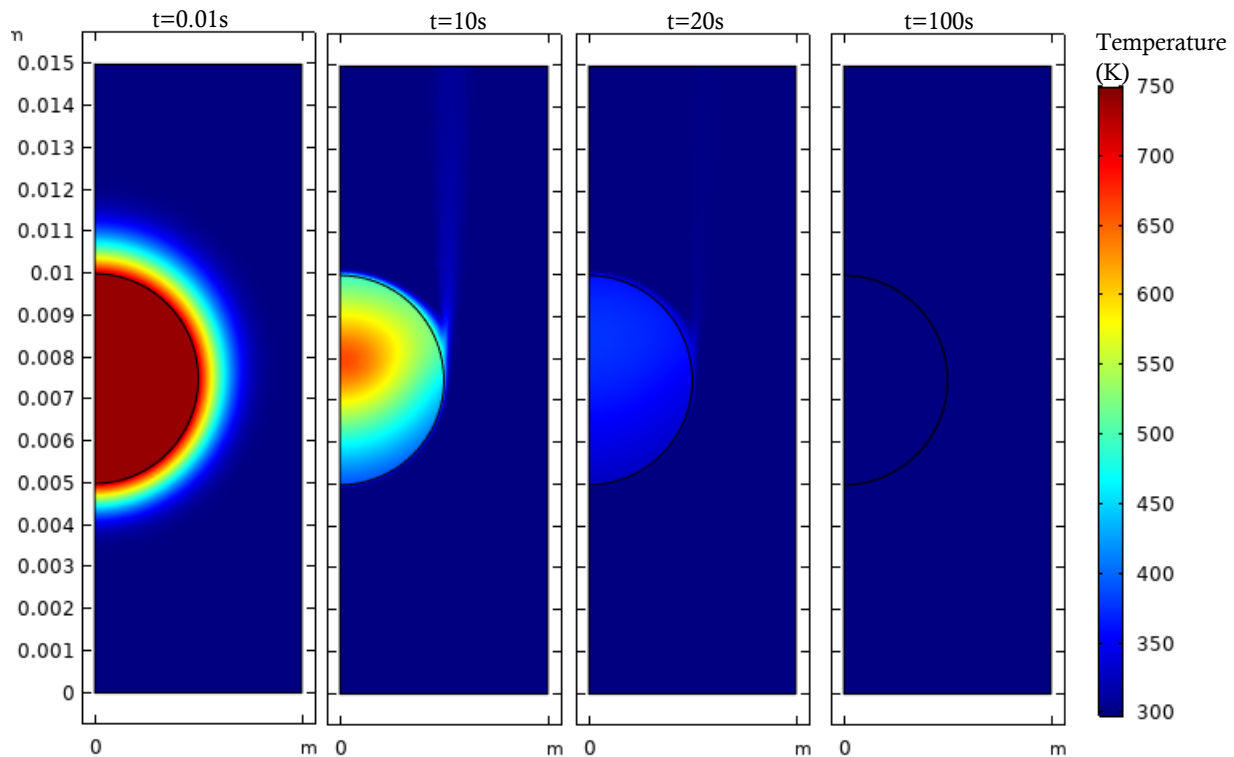


Figure 33. Temperature distribution of N_2 and droplet (AgCl) domain with droplet radius of 0.0025m

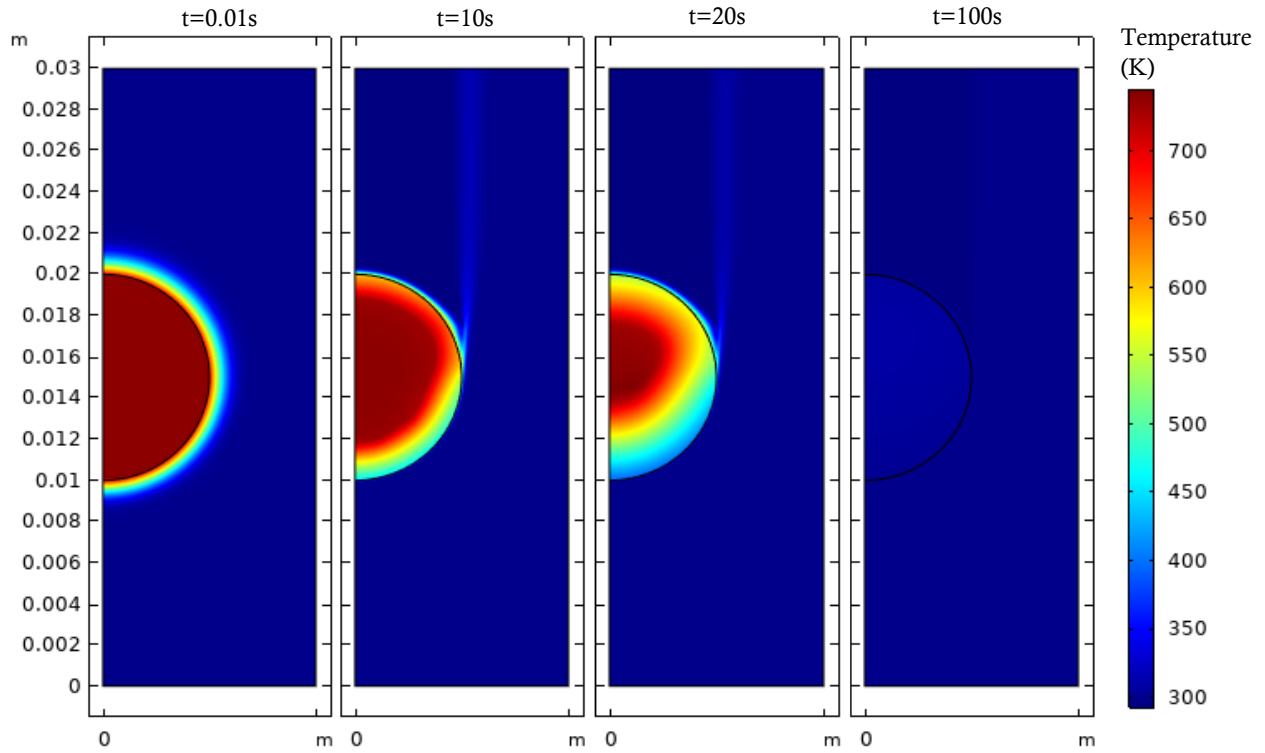


Figure 35. Temperature distribution of N_2 and droplet (AgCl) domain with droplet radius of 0.005m

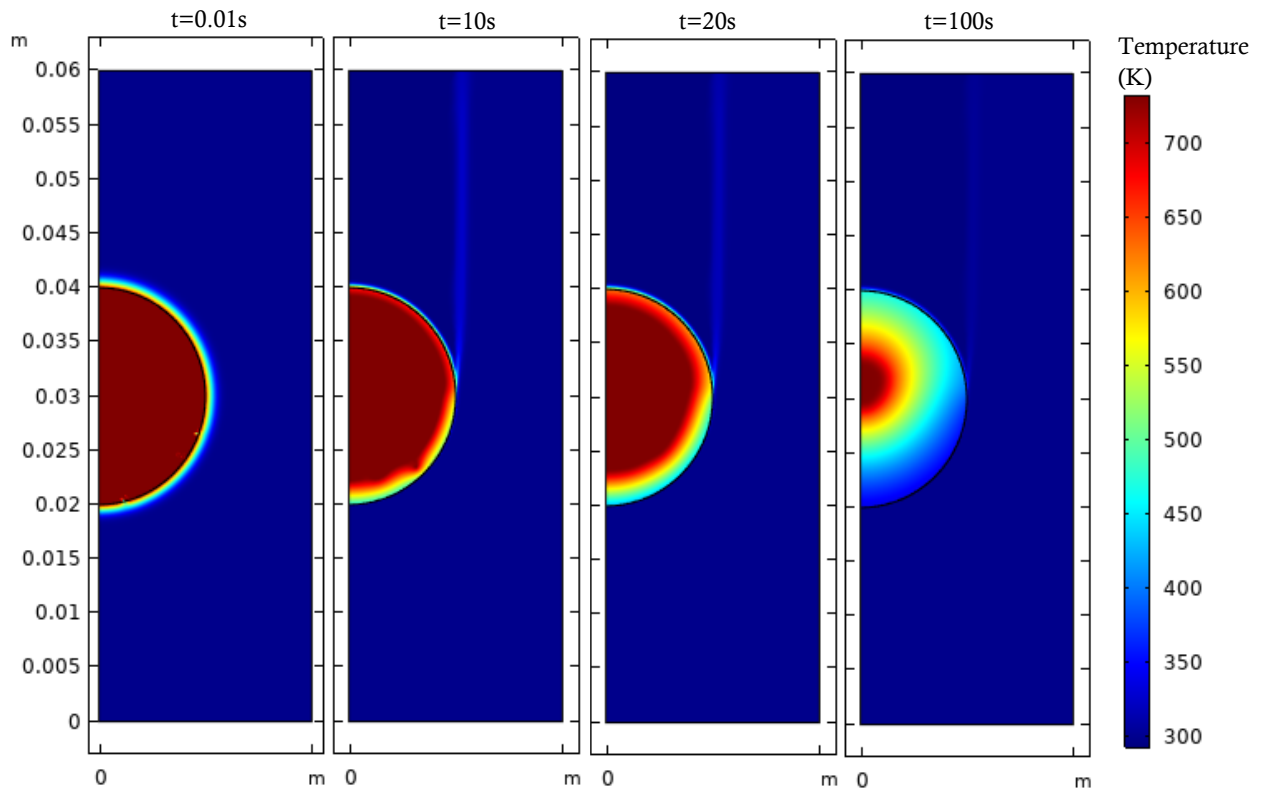


Figure 34. Temperature distribution of N_2 and droplet (AgCl) domain with droplet radius of 0.01m

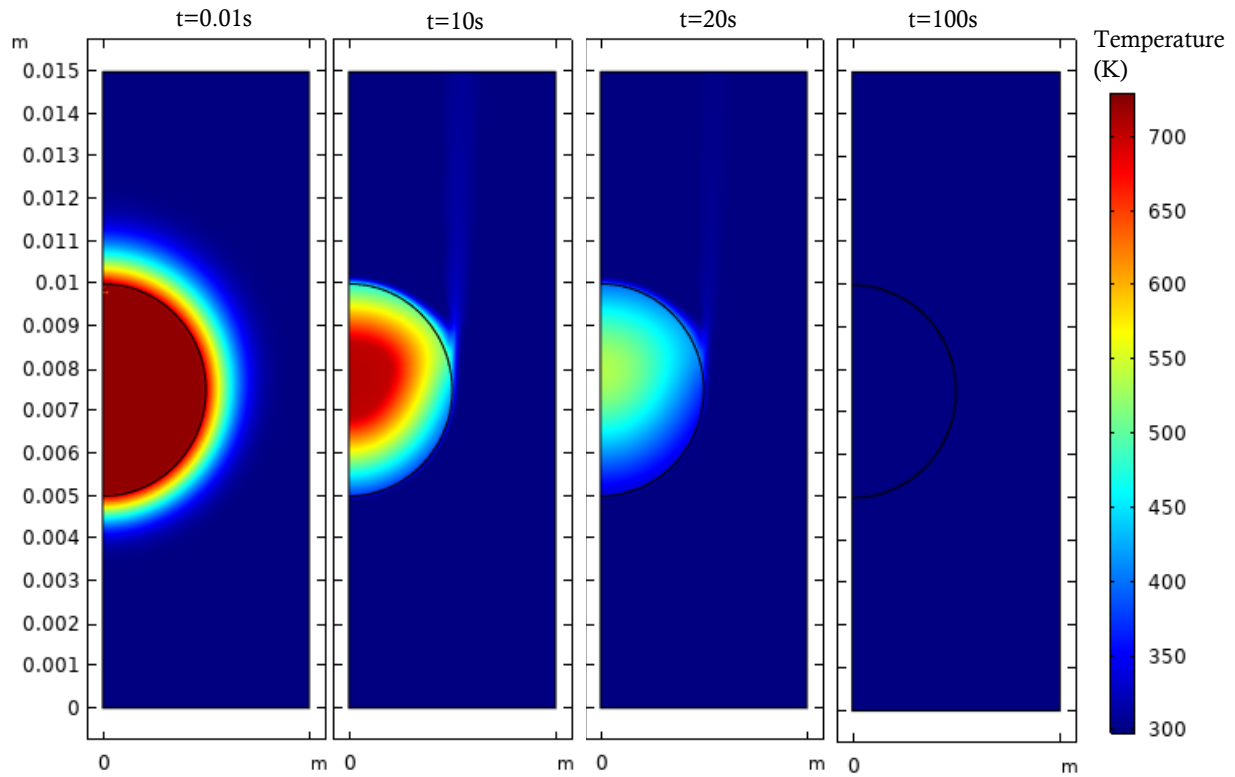


Figure 36. Temperature distribution of N_2 and droplet (CuCl) domain with droplet radius of 0.0025m

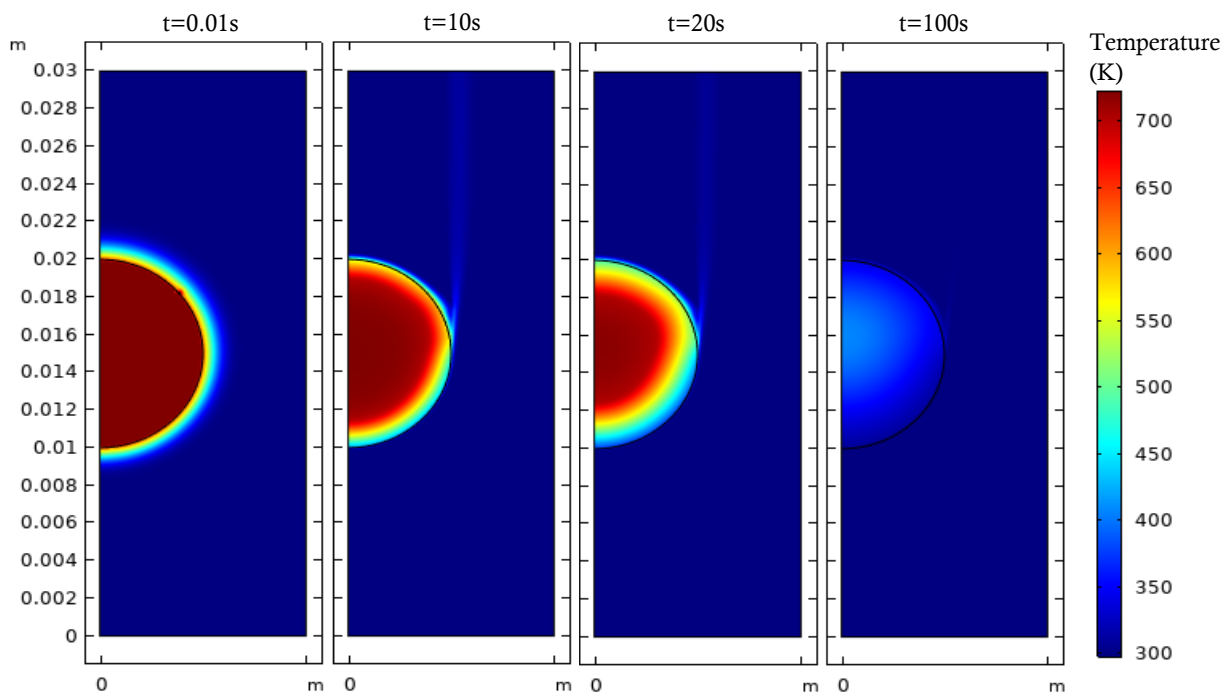


Figure 37. Temperature distribution of N_2 and droplet (CuCl) domain with droplet radius of 0.005m

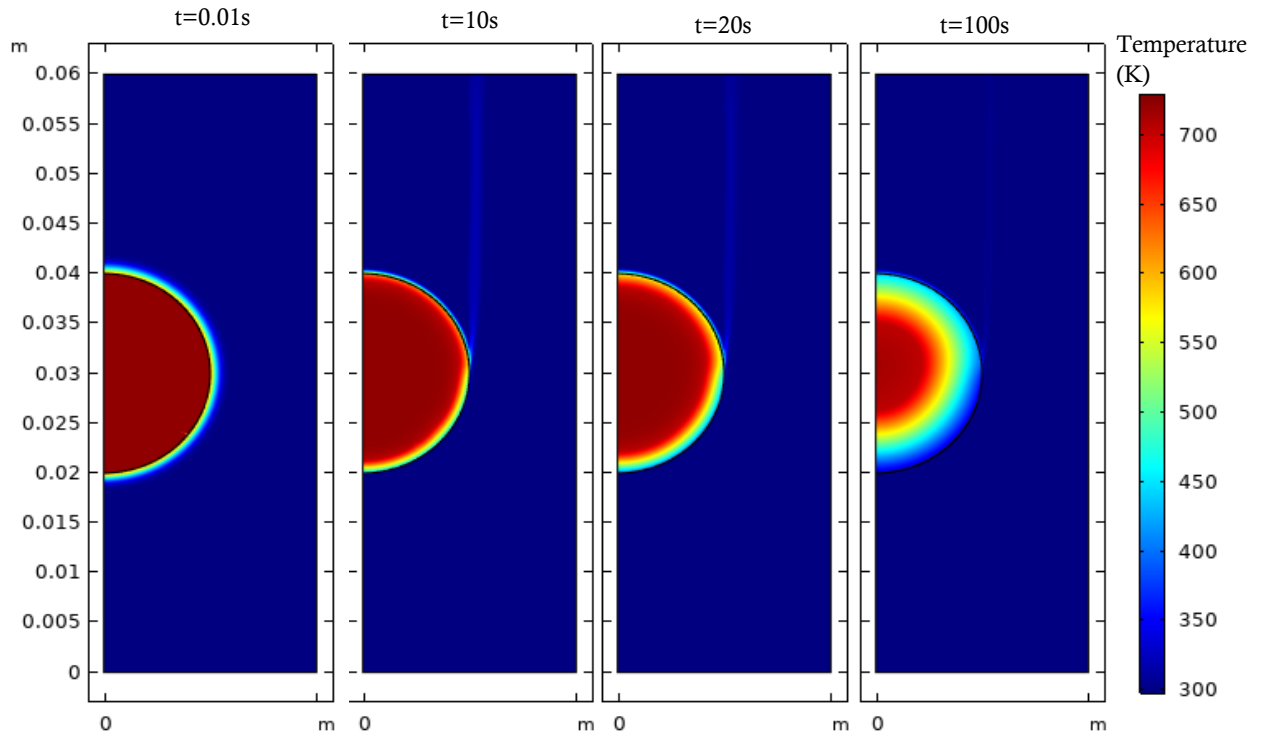


Figure 38. Temperature distribution of N₂ and droplet (CuCl) domain with droplet radius of 0.01m

Thermal diffusivity is the measure of heat transfer rate within a body. It describes how heat disperses throughout an object or a body. It is given by

$$\alpha = \frac{k}{\rho c_p} \quad (31)$$

Where k is the thermal conductivity, ρ is the density and c_p is the specific heat capacity of the material. From the above figures, for the same material, it is apparent that the phase change process is much slower as the diameter of the droplet increases. Since the heat transfer rate is proportional to the radius of the droplet, larger droplets will have higher heat transfer rates. Though the heat transfer rates are greater for larger droplets it takes longer to cool due to the higher energy content in large droplets compared to smaller ones.

4.6 Validation of Computational Results

The convection coefficient of heat transfer, h (W/m²K), is a quantitative characteristic of convective heat transfer between a fluid medium and the surface (wall) of a solid object [181], and it is given by Equation (32):

$$h = \frac{\dot{q}}{(T_s - T_f)} \quad (32)$$

where \dot{q} is the heat flux (W/m^2), T_s is the temperature at the outer surface of the droplet, T_f is the temperature of the nitrogen. Since the velocity of the nitrogen varies continuously the heat transfer coefficient (h) is a function of time and position. So, the variation of average heat transfer coefficient with time, is computed along the droplet's surface from the simulated results in COMSOL and that is illustrated in .

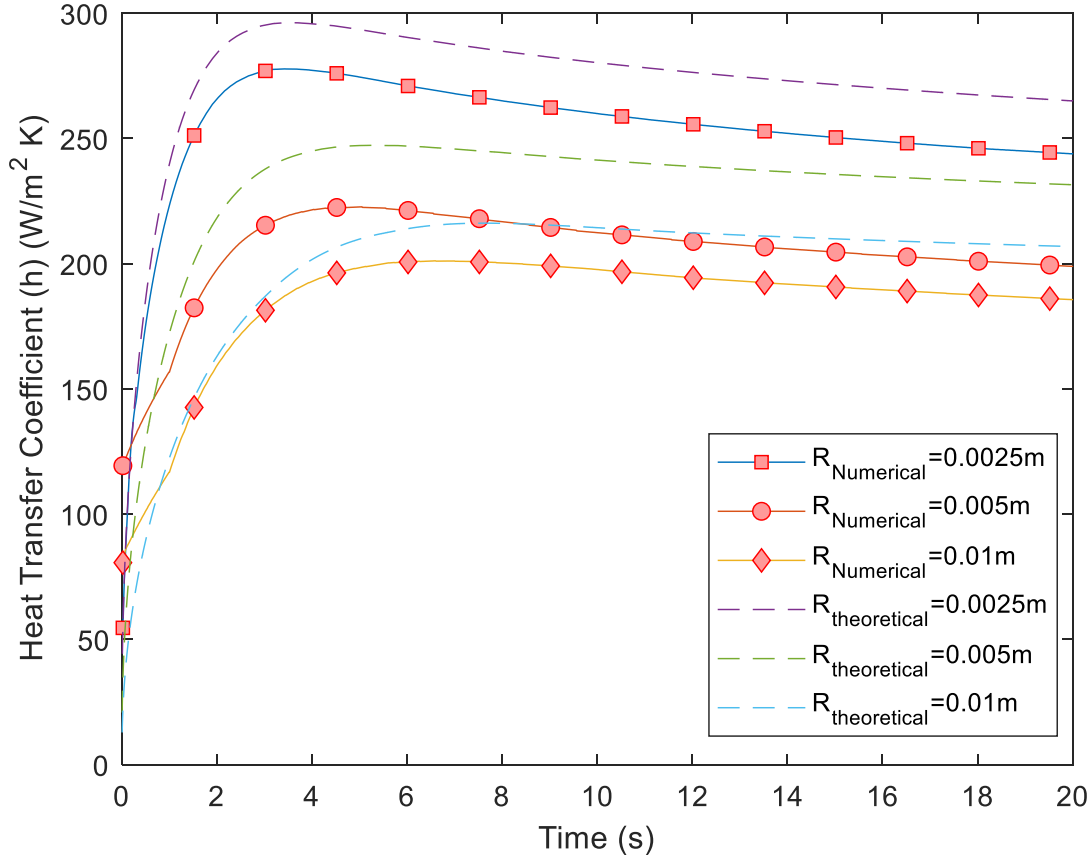


Figure 39. Variation of average heat transfer coefficient with time

The heat transfer coefficient can also be estimated using empirical Nusselt number relations. As discussed earlier in Section 1.3.4, there are different forms of Nusselt number relations. Though Equation (6) is a more accurate form Nusselt number relation for flow over a sphere, that cannot be applied for this model as $\frac{\mu_\infty}{\mu_s}$ is less than 1. So, the Ranz Marshal [80] Nusselt number relation given in Equation (33) is adopted:

$$Nu = 2 + 0.6Re^{0.5}Pr^{0.33} \quad (33)$$

where Re is the Reynolds number and Pr is the Prandtl number. This correlation is valid for $1 < Re < 10^4$ and $0.6 < Pr < 380$.

$$Nu = \frac{hl}{k} \quad (34)$$

where l is the characteristic length (for sphere $l = \text{diameter}$), k is the thermal conductivity of the fluid in the boundary layer, (W/mK). The heat transfer coefficient calculated using empirical relation is compared, with the numerically computed h in Figure 39. Both the numerical and theoretical model follow same trend across the temperatures. As heat transfer coefficient is inversely proportional to the diameter, smaller droplets have larger heat transfer coefficient. This trend can be seen both in theoretical and numerical model.

4.7 Heat Recovery

The error between the numerical model and theoretical model varies considerably across temperature range. The errors are very significant for the time steps between 0 to 1s, especially for the larger droplets in the numerical model. This could be because, initially for the larger droplets the velocity of the N₂ varies significantly between the lower and top end of the droplet, which directly influences the heat transfer rate and in turn the heat transfer coefficient. Since the variation of h is significant, it heavily influences the average heat transfer coefficient at the initial time steps.

The quenching height in a quench cell is defined as the distance between the droplet's contact with the water surface and the droplet's origin, distance which the droplet will travel in free-fall. The quenching process will increase the temperature of the water as the required temperature for the step 1 (Figure 6) is around 90°C. The rise in temperature of the water, from 80°C, is determined using the Equation (35). The effective temperature of the droplet is evaluated from the simulated results at the droplets contact point with the water surface. The effective temperature is taken as constant for all the droplets for the specific quenching height. The number of droplets (N) is calculated based on the stoichiometric proportions and droplet volume. By maintaining stoichiometric proportions of CuCl, the number of droplets (N) will be a rational number in most cases. To determine the accurate final temperature of the water, the decimal part in the N is converted as a whole droplet with the decimal fraction of the volume. For example, the N for the droplet with a radius of 0.0025m is 370.8740. The volume of the last droplet is taken as 0.8740 of the other droplets. The specific heat capacity and effective temperature of that droplet is assumed to be the same as the other droplets for the diameter considered. Figure 40 illustrates the raise in temperature of the water from 353K, quenching height of

10cm, for three different droplet diameters. Appendix 1 & 2 show the temperature rise in water for the quenching height of 20cm and 30cm respectively.

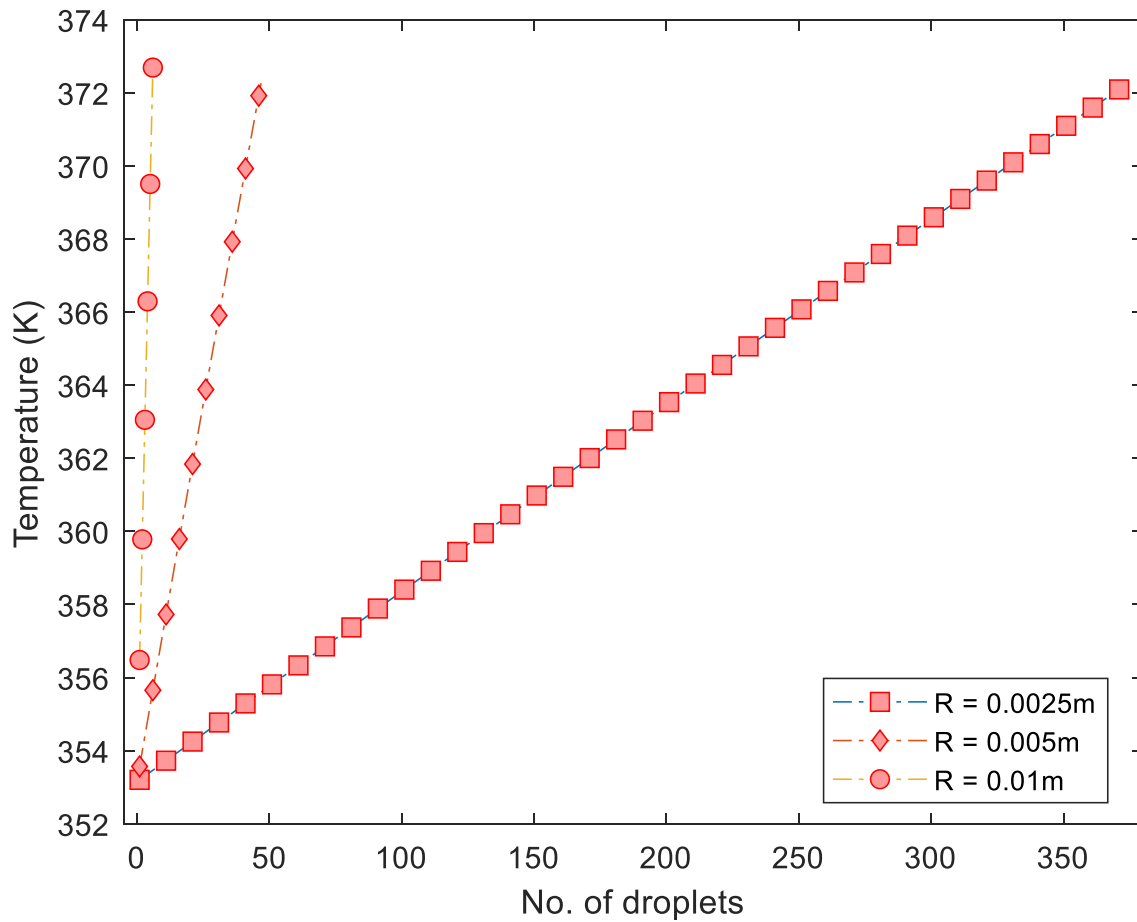


Figure 40. Temperature increase of water by CuCl droplets for the quenching height of 10cm

$$m_w C_{p,w} \Delta T = m_d C_{p,d} \Delta T \quad (35)$$

From Figure 40, it is apparent that the final temperature of the droplet is increasing with the increase in droplet diameters, but the variation is not significant. This is mainly due to the smaller quenching height and the phase change process. Generally, on increasing the quenching height should lower the final temperature of the droplet, but this is not true in this case because as the droplet cools it enters the phase change process and the temperature of the droplet will remain almost constant during the phase change process. So, the average temperature of the droplet will drop initially and will remain almost the same up to 2m of quenching height. Hence, the final temperature of the water does not vary considerably between different quenching heights.

Chapter 5 - Summary and Conclusion

5.1 Findings and Results

The specific heat capacity of monocrystalline AgCl and CuCl as a function of temperature has been determined using different physical approach at different temperature range. For the temperatures ranging from 0- 280K (θ_D), c_p values were calculated using Debye's model, which treats the vibrations in the atomic lattice as phonons. From 280K to the melting point, c_p data was extracted from the thermal experiments and simulations from the literature. For the temperatures beyond the melting point, the c_p is calculated from EMF values using Gibbs-Helmholtz relation which then combined with the thermal experimental values to form a hybrid data set. The EMF values of AgCl and CuCl were very similar, hence their EMF derived specific heat capacity values are also similar with a slight offset. This method of extracting thermophysical data from electrochemistry can be extended to other salts. This study shows that salts with similar EMF values can be grouped together, and a single specific heat capacity model can be developed.

Quenching the molten CuCl in water was identified to be best method for recovering heat. For both AgCl and CuCl, the terminal velocity and the distance traveled by the droplets during the quenching process is significantly greater for the droplets with larger diameter.

The AgCl and CuCl droplets of three different diameters were numerically modeled in COMSOL Multiphysics and their thermal interactions with N_2 were studied. It was determined that for AgCl the heat transfer rates are significantly higher compared to CuCl for the identical droplet diameters, since AgCl has higher thermal diffusivity.

Based on the simulated numerical model, heat recovery analysis on quenched CuCl droplets shows the final temperature of the water increases from 353K to 372K. The water's final temperature does not change significantly with droplet diameter and the quenching height, due to the salt's phase change from liquid to solid.

5.2 Recommendations and Future Work

As the thermophysical properties is the fundamental of heat recovery study, it becomes essential to have accurate variation of thermophysical properties with temperature. Though the specific heat capacity model developed here for CuCl provides a better representation of c_p compared with the

current literature, its accuracy can be improved with more consistent specific heat capacity and EMF data sets.

As explored in the thesis, specific heat capacity can be determined using various techniques such as Debye's model, calorimetry study and Gibbs Helmholtz relation. Since the heat recovery is primarily occurs during the liquid to solid phase transition of the CuCl, it is recommended to explore the thermophysical properties at the phase transition temperatures. As the specific heat variation plays a vital role on the heat recovery study, exploring specific heat variation with temperature takes higher precedence compared to other thermophysical properties.

Most effective way for estimating the specific heat variation with temperature in the liquid to solid phase transition temperature is by employing Gibbs Helmholtz relation. EMF data sets are necessary for this method. Conducting electrochemical experiments on CuCl to determine EMF will help in modelling the specific heat. Moreover, electrochemical experiments are relatively easier than other high temperature calorimetry experiments. Study of anharmonic vibrations can help us explore the specific heats at lower temperatures and around room temperatures.

Experiments on free falling molten CuCl droplets with high speed shadow imager might help us to get a better understanding on phase change process of CuCl along with accurate droplets shapes. A numerical model, similar to the one discussed in this thesis, can be developed to study the intricate details involved and can be validated with the experimental study.

BIBLIOGRAPHY

- [1] Y. Cengel, *Heat and mass transfer: fundamentals and applications*. McGraw-Hill Higher Education, 2014.
- [2] “U.S. energy facts explained - consumption and production - U.S. Energy Information Administration (EIA).” <https://www.eia.gov/energyexplained/us-energy-facts/> (accessed Jul. 12, 2020).
- [3] G. C. Watkins, “Oil scarcity: What have the past three decades revealed?,” *Energy Policy*, vol. 34, no. 5, pp. 508–514, 2006.
- [4] S. Ghandehariun, M. A. Rosen, G. F. Naterer, and Z. Wang, “Comparison of molten salt heat recovery options in the Cu–Cl cycle of hydrogen production,” *International Journal of Hydrogen Energy*, vol. 36, no. 17, pp. 11328–11337, Aug. 2011, doi: 10.1016/j.ijhydene.2010.11.093.
- [5] A. COMSOL, “Comsol multiphysics® v. 5.4 www.comsol.com. Stockholm, Sweden,” *COMSOL AB*, 2018.
- [6] K. Alanne and S. Cao, “Zero-energy hydrogen economy (ZEH2E) for buildings and communities including personal mobility,” *Renewable and Sustainable Energy Reviews*, vol. 71, pp. 697–711, 2017.
- [7] W. McDowall, “Technology roadmaps for transition management: The case of hydrogen energy,” *Technological forecasting and social change*, vol. 79, no. 3, pp. 530–542, 2012.
- [8] “File:Solid oxide fuel cell protonic.svg,” *Wikipedia*. Accessed: Jul. 13, 2020. [Online]. Available: https://en.wikipedia.org/wiki/File:Solid_oxide_fuel_cell_protonic.svg.
- [9] L. Das, “On-board hydrogen storage systems for automotive application,” *International Journal of Hydrogen Energy*, vol. 21, no. 9, pp. 789–800, 1996.
- [10] P. Ekins, *Hydrogen energy: economic and social challenges / edited by Paul Ekins*. 2010.
- [11] P. Ekins, *Hydrogen energy: economic and social challenges*. Earthscan, 2010.
- [12] A. F. Ghoniem, “Needs, resources and climate change: clean and efficient conversion technologies,” *Progress in energy and combustion science*, vol. 37, no. 1, pp. 15–51, 2011.
- [13] R. Kothari, D. Buddhi, and R. Sawhney, “Comparison of environmental and economic aspects of various hydrogen production methods,” *Renewable and Sustainable Energy Reviews*, vol. 12, no. 2, pp. 553–563, 2008.
- [14] R. Dell and D. A. J. Rand, *Clean energy*, vol. 5. Royal Society of Chemistry, 2004.
- [15] M. A. Lewis, M. S. Ferrandon, D. F. Tatterson, and P. Mathias, “Evaluation of alternative thermochemical cycles – Part III further development of the Cu–Cl cycle,” *International Journal*

- of *Hydrogen Energy*, vol. 34, no. 9, pp. 4136–4145, May 2009, doi: 10.1016/j.ijhydene.2008.09.025.
- [16] M. A. Rosen, “Advances in hydrogen production by thermochemical water decomposition: a review,” *Energy*, vol. 35, no. 2, pp. 1068–1076, 2010.
- [17] G. F. Naterer *et al.*, “Clean hydrogen production with the Cu–Cl cycle – Progress of international consortium, I: Experimental unit operations,” *International Journal of Hydrogen Energy*, vol. 36, no. 24, pp. 15472–15485, Dec. 2011, doi: 10.1016/j.ijhydene.2011.08.012.
- [18] M. A. Lewis, J. G. Masin, and P. A. O’Hare, “Evaluation of alternative thermochemical cycles, Part I: The methodology,” *International journal of hydrogen energy*, vol. 34, no. 9, pp. 4115–4124, 2009.
- [19] M. A. Lewis and J. G. Masin, “The evaluation of alternative thermochemical cycles–Part II: The down-selection process,” *International Journal of Hydrogen Energy*, vol. 34, no. 9, pp. 4125–4135, 2009.
- [20] S. Terol, *Proceedings of the 1986 International Congress on Renewable Energy Sources, Madrid, Spain, 18-23 May 1986*. Consejo Superior de Investigaciones Cientificas, 1987.
- [21] “Eyewitness.” <https://www.archives.gov/exhibits/eyewitness/html.php?section=5> (accessed Jul. 25, 2020).
- [22] F. Barbir, “PEM electrolysis for production of hydrogen from renewable energy sources,” *Solar energy*, vol. 78, no. 5, pp. 661–669, 2005.
- [23] “Global demand for pure hydrogen, 1975-2018 – Charts – Data & Statistics,” *IEA*. <https://www.iea.org/data-and-statistics/charts/global-demand-for-pure-hydrogen-1975-2018> (accessed Jul. 14, 2020).
- [24] C. W. Forsberg, “Hydrogen, nuclear energy, and the advanced high-temperature reactor,” *International Journal of Hydrogen Energy*, vol. 28, no. 10, pp. 1073–1081, 2003.
- [25] Martin, “Energy,” *United Nations Sustainable Development*. <https://www.un.org/sustainabledevelopment/energy/> (accessed Jul. 25, 2020).
- [26] J. M. Ogden, “Prospects for building a hydrogen energy infrastructure,” *Annual Review of Energy and the Environment*, vol. 24, no. 1, pp. 227–279, 1999.
- [27] A. C. Marques, J. A. Fuinhas, and D. A. Pereira, “Have fossil fuels been substituted by renewables? An empirical assessment for 10 European countries,” *Energy Policy*, vol. 116, pp. 257–265, 2018.
- [28] W. McDowall and M. Eames, “Forecasts, scenarios, visions, backcasts and roadmaps to the hydrogen economy: A review of the hydrogen futures literature,” *Energy policy*, vol. 34, no. 11, pp. 1236–1250, 2006.

- [29] I. E. Agency, "The Future of Hydrogen: Seizing Today's Opportunities," 2019.
- [30] B. Decourt, B. Lajoie, R. Debarre, O. Soupa, and H.-B. E. Conversion, "More Than Storage: System Flexibility," *SBC Energy Institute, Paria*, 2014.
- [31] K. Zeng and D. Zhang, "Recent progress in alkaline water electrolysis for hydrogen production and applications," *Progress in energy and combustion science*, vol. 36, no. 3, pp. 307–326, 2010.
- [32] "Hydrogen from renewable power: Technology outlook for the energy transition," p. 52.
- [33] S. Saito, "Nuclear Energy and Hydrogen Production—The Japanese Situation," *Policy Debate on The Potential Contribution of Nuclear Energy to Production of Hydrogen, OECD/NEA*, vol. 15, 2004.
- [34] A. Ozbilen, I. Dincer, and M. A. Rosen, "A comparative life cycle analysis of hydrogen production via thermochemical water splitting using a Cu–Cl cycle," *International Journal of Hydrogen Energy*, vol. 36, no. 17, pp. 11321–11327, Aug. 2011, doi: 10.1016/j.ijhydene.2010.12.035.
- [35] A. Ozbilen, I. Dincer, and M. A. Rosen, "Life cycle assessment of hydrogen production via thermochemical water splitting using multi-step Cu–Cl cycles," *Journal of Cleaner Production*, vol. 33, pp. 202–216, 2012.
- [36] G. Naterer *et al.*, "Recent Canadian advances in nuclear-based hydrogen production and the thermochemical Cu–Cl cycle," *International Journal of Hydrogen Energy*, vol. 34, no. 7, pp. 2901–2917, Apr. 2009, doi: 10.1016/j.ijhydene.2009.01.090.
- [37] G. F. Naterer *et al.*, "Progress of international hydrogen production network for the thermochemical Cu–Cl cycle," *International Journal of Hydrogen Energy*, vol. 38, no. 2, pp. 740–759, Jan. 2013, doi: 10.1016/j.ijhydene.2012.10.023.
- [38] V. N. Daggupati, G. F. Naterer, K. S. Gabriel, R. J. Gravelins, and Z. L. Wang, "Equilibrium conversion in Cu–Cl cycle multiphase processes of hydrogen production," *Thermochimica Acta*, vol. 496, no. 1–2, pp. 117–123, Dec. 2009, doi: 10.1016/j.tca.2009.07.009.
- [39] G. F. Naterer *et al.*, "Canada's program on nuclear hydrogen production and the thermochemical Cu–Cl cycle," *International Journal of Hydrogen Energy*, vol. 35, no. 20, pp. 10905–10926, Oct. 2010, doi: 10.1016/j.ijhydene.2010.07.087.
- [40] S. Abanades, P. Charvin, F. Lemont, and G. Flamant, "Novel two-step SnO₂/SnO water-splitting cycle for solar thermochemical production of hydrogen," *International Journal of Hydrogen Energy*, vol. 33, no. 21, pp. 6021–6030, 2008.
- [41] A. Steinfeld, "Solar hydrogen production via a two-step water-splitting thermochemical cycle based on Zn/ZnO redox reactions," *International journal of hydrogen energy*, vol. 27, no. 6, pp. 611–619, 2002.

- [42] M. Galvez, A. Frei, G. Albigsetti, G. Lunardi, and A. Steinfeld, "Solar hydrogen production via a two-step thermochemical process based on MgO/Mg redox reactions—thermodynamic and kinetic analyses," *International Journal of Hydrogen Energy*, vol. 33, no. 12, pp. 2880–2890, 2008.
- [43] S. Abanades and G. Flamant, "Thermochemical hydrogen production from a two-step solar-driven water-splitting cycle based on cerium oxides," *Solar energy*, vol. 80, no. 12, pp. 1611–1623, 2006.
- [44] C. Huang, T. Ali, and others, "Analysis of sulfur–iodine thermochemical cycle for solar hydrogen production. Part I: decomposition of sulfuric acid," *Solar Energy*, vol. 78, no. 5, pp. 632–646, 2005.
- [45] X. Wu and K. Onuki, "Thermochemical water splitting for hydrogen production utilizing nuclear heat from an HTGR," *Tsinghua Science and Technology*, vol. 10, no. 2, pp. 270–276, 2005.
- [46] R. Liberatore, M. Lanchi, A. Giaconia, and P. Tarquini, "Energy and economic assessment of an industrial plant for the hydrogen production by water-splitting through the sulfur-iodine thermochemical cycle powered by concentrated solar energy," *International journal of hydrogen energy*, vol. 37, no. 12, pp. 9550–9565, 2012.
- [47] D. Graf, N. Monnerie, M. Roeb, M. Schmitz, and C. Sattler, "Economic comparison of solar hydrogen generation by means of thermochemical cycles and electrolysis," *International journal of hydrogen energy*, vol. 33, no. 17, pp. 4511–4519, 2008.
- [48] M. Granovskii, I. Dincer, M. A. Rosen, and I. Piore, "Performance assessment of a combined system to link a supercritical water-cooled nuclear reactor and a thermochemical water splitting cycle for hydrogen production," *Energy Conversion and Management*, vol. 49, no. 7, pp. 1873–1881, 2008.
- [49] I. Dincer and M. T. Balta, "Potential thermochemical and hybrid cycles for nuclear-based hydrogen production," *International Journal of Energy Research*, vol. 35, no. 2, pp. 123–137, 2011.
- [50] G. Naterer, K. Gabriel, Z. Wang, V. Daggupati, and R. Gravelins, "Thermochemical hydrogen production with a copper–chlorine cycle. I: oxygen release from copper oxychloride decomposition," *International Journal of Hydrogen Energy*, vol. 33, no. 20, pp. 5439–5450, Oct. 2008, doi: 10.1016/j.ijhydene.2008.05.035.
- [51] G. Naterer *et al.*, "Clean hydrogen production with the Cu–Cl cycle—progress of international consortium, II: simulations, thermochemical data and materials," *International Journal of Hydrogen Energy*, vol. 36, no. 24, pp. 15486–15501, 2011.
- [52] Z. Wang, G. Naterer, K. Gabriel, R. Gravelins, and V. Daggupati, "Comparison of different copper–chlorine thermochemical cycles for hydrogen production," *International Journal of Hydrogen Energy*, vol. 34, no. 8, pp. 3267–3276, 2009.

- [53] M. Serban, M. Lewis, and J. Basco, "Kinetic study of the hydrogen and oxygen production reactions in the copper-chloride thermochemical cycle," in *AIChE 2004 spring national meeting, New Orleans, LA*, 2004, pp. 25–9.
- [54] Z. Wang, G. Naterer, K. Gabriel, R. Gravelins, and V. Daggupati, "Comparison of sulfur-iodine and copper-chlorine thermochemical hydrogen production cycles," *International Journal of Hydrogen Energy*, vol. 35, no. 10, pp. 4820–4830, 2010.
- [55] S. Ghandehariun, G. Naterer, I. Dincer, and M. Rosen, "Solar thermochemical plant analysis for hydrogen production with the copper-chlorine cycle," *International Journal of Hydrogen Energy*, vol. 35, no. 16, pp. 8511–8520, 2010.
- [56] M. F. Orhan, I. Dincer, G. F. Naterer, and M. A. Rosen, "Coupling of copper-chloride hybrid thermochemical water splitting cycle with a desalination plant for hydrogen production from nuclear energy," *International Journal of Hydrogen Energy*, vol. 35, no. 4, pp. 1560–1574, 2010.
- [57] M. Orhan, I. Dincer, and G. Naterer, "Cost analysis of a thermochemical Cu-Cl pilot plant for nuclear-based hydrogen production," *International journal of hydrogen energy*, vol. 33, no. 21, pp. 6006–6020, 2008.
- [58] C. Zamfirescu, I. Dincer, and G. F. Naterer, "Thermophysical properties of copper compounds in copper-chlorine thermochemical water splitting cycles," *International Journal of Hydrogen Energy*, vol. 35, no. 10, pp. 4839–4852, May 2010, doi: 10.1016/j.ijhydene.2009.08.101.
- [59] A. Ozbilen, I. Dincer, and M. A. Rosen, "Environmental evaluation of hydrogen production via thermochemical water splitting using the Cu-Cl Cycle: A parametric study," *International journal of hydrogen energy*, vol. 36, no. 16, pp. 9514–9528, 2011.
- [60] M. S. Ferrandon *et al.*, "Hydrogen production by the Cu-Cl thermochemical cycle: Investigation of the key step of hydrolysing CuCl₂ to Cu₂OCl₂ and HCl using a spray reactor," *International Journal of Hydrogen Energy*, vol. 35, no. 3, pp. 992–1000, 2010.
- [61] G. Naterer, V. Daggupati, G. Marin, K. Gabriel, and Z. Wang, "Thermochemical hydrogen production with a copper-chlorine cycle, II: flashing and drying of aqueous cupric chloride," *international journal of hydrogen energy*, vol. 33, no. 20, pp. 5451–5459, 2008.
- [62] Z. Wang, G. Naterer, and K. Gabriel, "Multiphase reactor scale-up for Cu-Cl thermochemical hydrogen production," *International Journal of Hydrogen Energy*, vol. 33, no. 23, pp. 6934–6946, 2008.
- [63] M. F. Orhan, I. Dincer, and M. A. Rosen, "Design of systems for hydrogen production based on the Cu-Cl thermochemical water decomposition cycle: configurations and performance," *international journal of hydrogen energy*, vol. 36, no. 17, pp. 11309–11320, 2011.

- [64] O. Jaber, G. F. Naterer, and I. Dincer, "Heat recovery from molten CuCl in the Cu–Cl cycle of hydrogen production," *International Journal of Hydrogen Energy*, vol. 35, no. 12, pp. 6140–6151, Jun. 2010, doi: 10.1016/j.ijhydene.2010.03.041.
- [65] M. Rabbani, I. Dincer, G. Naterer, and M. Aydin, "Determining parameters of heat exchangers for heat recovery in a Cu–Cl thermochemical hydrogen production cycle," *International journal of hydrogen energy*, vol. 37, no. 15, pp. 11021–11034, 2012.
- [66] S. Ghandehariun, M. A. Rosen, and G. F. Naterer, "Direct contact heat transfer from molten salt droplets in a thermochemical water splitting process of hydrogen production," *International Journal of Heat and Mass Transfer*, vol. 96, pp. 125–131, May 2016, doi: 10.1016/j.ijheatmasstransfer.2015.12.063.
- [67] S. Ghandehariun, Z. Wang, G. F. Naterer, and M. A. Rosen, "Experimental investigation of molten salt droplet quenching and solidification processes of heat recovery in thermochemical hydrogen production," *Applied Energy*, vol. 157, pp. 267–275, Nov. 2015, doi: 10.1016/j.apenergy.2015.08.002.
- [68] S. Ghandehariun, M. A. Rosen, M. Agelin-Chaab, and G. F. Naterer, "Heat transfer from molten salt droplets in various gases," *International Journal of Heat and Mass Transfer*, vol. 105, pp. 140–146, Feb. 2017, doi: 10.1016/j.ijheatmasstransfer.2016.08.108.
- [69] S. S. Manan, O. A. Jianu, and M. A. Rosen, "Investigation of Heat Extraction Methods from Cuprous Chloride for Improving the Efficiency of the Thermochemical Copper-Chlorine Cycle," *European Journal of Sustainable Development Research*, vol. 3, no. 1, Feb. 2019, doi: 10.20897/ejosdr/3976.
- [70] J. J. O'Connor, A. Thomasian, and A. F. Armington, "The analysis and solubility of cuprous chloride in hydrochloric acid solutions," *Journal of The Electrochemical Society*, vol. 115, no. 9, pp. 931–932, 1968.
- [71] P. J. Linstrom and W. G. Mallard, "The NIST Chemistry WebBook: A chemical data resource on the internet," *Journal of Chemical & Engineering Data*, vol. 46, no. 5, pp. 1059–1063, 2001.
- [72] J. J. Fritz, "Solubility of cuprous chloride in various soluble aqueous chlorides," *Journal of chemical and engineering data*, vol. 27, no. 2, pp. 188–193, 1982.
- [73] O. A. Jianu, Z. Wang, M. A. Rosen, and G. F. Naterer, "Shadow imaging of particle dynamics and dissolution rates in aqueous solutions for hydrogen production," *Experimental Thermal and Fluid Science*, vol. 51, pp. 297–301, Nov. 2013, doi: 10.1016/j.expthermflusci.2013.08.012.
- [74] O. A. Jianu, Z. Wang, M. A. Rosen, and G. F. Naterer, "Experimental investigation of particle dissolution rates in aqueous solutions for hydrogen production," *Heat and Mass Transfer*, vol. 52, no. 10, pp. 2067–2073, Oct. 2016, doi: 10.1007/s00231-015-1724-y.

- [75] O. A. Jianu, Z. Wang, G. F. Naterer, and M. A. Rosen, "Constituent solubility and dissolution in a CuCl-HCl-H₂O ternary system," *Chemical Engineering Science*, vol. 184, pp. 209–215, Jul. 2018, doi: 10.1016/j.ces.2018.03.004.
- [76] R. B. Bird, W. E. Stewart, and E. N. Lightfoot, "Transport Phenomena John Wiley & Sons," *New York*, vol. 413, 1960.
- [77] P. D. Richardson, "Estimation of the heat transfer from the rear of an immersed body to the region of separated flow," BROWN UNIV PROVIDENCE RI, 1962.
- [78] G. Vliet and G. Leppert, "Forced convection heat transfer from an isothermal sphere to water," 1961.
- [79] H. Kramers, "Heat transfer from spheres to flowing media," *physica*, vol. 12, no. 2–3, pp. 61–80, 1946.
- [80] W. Ranz, W. R. Marshall, and others, "Evaporation from drops," *Chem. eng. prog*, vol. 48, no. 3, pp. 141–146, 1952.
- [81] S.-C. Yao and V. Schrock, "Heat and mass transfer from freely falling drops," 1976.
- [82] B. Melissari and S. A. Argyropoulos, "Development of a heat transfer dimensionless correlation for spheres immersed in a wide range of Prandtl number fluids," *International journal of heat and mass transfer*, vol. 48, no. 21–22, pp. 4333–4341, 2005.
- [83] E. Windhab, "New developments in crystallization processing," *Journal of Thermal Analysis and Calorimetry*, vol. 57, no. 1, pp. 171–180, 1999.
- [84] J. C. Liao and K. C. Ng, "Effect of ice nucleators on snow making and spray freezing," *Industrial & engineering chemistry research*, vol. 29, no. 3, pp. 361–366, 1990.
- [85] M. Flemings, "Solidification Processing McGraw-Hill," *New York*, p. 416, 1974.
- [86] H. Leuenberger, "New Technologies for the Manufacture of Nanostructured Drug Carriers," *London: World Markets Research Centre*, 2001.
- [87] J. Hindmarsh, A. Russell, and X. Chen, "Experimental and numerical analysis of the temperature transition of a freezing food solution droplet," *Chemical engineering science*, vol. 59, no. 12, pp. 2503–2515, 2004.
- [88] L. Liu, W. Ma, and L. Zong, "EXPERIMENTAL AND NUMERICAL STUDY OF BUBBLE GROWTH PROCESS WITHIN A SUPERHEATED WATER DROPLET," *Atomization and Sprays*, vol. 27, no. 9, 2017.
- [89] J. Hallett, "Experimental studies of the crystallization of supercooled water," *Journal of the Atmospheric Sciences*, vol. 21, no. 6, pp. 671–682, 1964.
- [90] A. Trommelen and E. Crosby, "Evaporation and drying of drops in superheated vapors," *AICHE Journal*, vol. 16, no. 5, pp. 857–867, 1970.

- [91] N. El-Kaddah and J. Szekely, "The electromagnetic force field, fluid flow field, and temperature profiles in levitated metal droplets," *Metallurgical Transactions B*, vol. 14, no. 3, pp. 401–410, 1983.
- [92] S. Song and B. Li, "Free surface profiles and thermal convection in electrostatically levitated droplets," *International journal of heat and mass transfer*, vol. 43, no. 19, pp. 3589–3606, 2000.
- [93] B. Adhikari, T. Howes, B. Bhandari, and V. Truong, "Experimental studies and kinetics of single drop drying and their relevance in drying of sugar-rich foods: A review," *International Journal of Food Properties*, vol. 3, no. 3, pp. 323–351, 2000.
- [94] B. Yi *et al.*, "Effects of Applied Power on Temperature of Electromagnetic Levitation of Silicon and Silicon-Iron Droplets," *E&ES*, vol. 128, no. 1, p. 012144, 2018.
- [95] "NASA - NASA experiments validate 50-year-old hypothesis - Marshall Space Flight Center Photo Release 03-104 (06-30-03)." <https://www.nasa.gov/centers/marshall/multimedia/photos/2003/photos03-104.html> (accessed Aug. 03, 2020).
- [96] S. Tabakova, F. Feuillebois, and S. Radev, "Freezing of a supercooled spherical droplet with mixed boundary conditions," *Proceedings of the Royal Society A: Mathematical, Physical and Engineering Sciences*, vol. 466, no. 2116, pp. 1117–1134, 2010.
- [97] J. H. Hattel, N. H. Pryds, J. Thorborg, and P. Ottosen, "A quasi-stationary numerical model of atomized metal droplets. I: Model formulation," *Modelling and Simulation in Materials Science and Engineering*, vol. 7, no. 3, p. 413, 1999.
- [98] H. Liu, R. H. Rangel, and E. J. Lavernie, "Modeling of droplet-gas interactions in spray atomization of Ta-2.5 W alloy," *Materials Science and Engineering: A*, vol. 191, no. 1–2, pp. 171–184, 1995.
- [99] N. Zeoli and S. Gu, "Computational simulation of metal droplet break-up, cooling and solidification during gas atomisation," *Computational materials science*, vol. 43, no. 2, pp. 268–278, 2008.
- [100] N. Zeoli, S. Gu, and S. Kamnis, *RETRACTED: Numerical modelling of metal droplet cooling and solidification*. Elsevier, 2008.
- [101] S. Li, P. Wu, H. Fukuda, and T. Ando, "Simulation of the solidification of gas-atomized Sn-5mass% Pb droplets," *Materials Science and Engineering: A*, vol. 499, no. 1–2, pp. 396–403, 2009.
- [102] A. G. DiVenuti, "Modeling of the uniform droplet process."
- [103] O. Jaber, G. Naterer, and I. Dincer, "Convective heat transfer from molten salt droplets in a direct contact heat exchanger," *Heat and mass transfer*, vol. 46, no. 8–9, pp. 999–1012, 2010.

- [104] G. F. Naterer *et al.*, “Advances in unit operations and materials for the Cu Cl cycle of hydrogen production,” *International Journal of Hydrogen Energy*, vol. 42, no. 24, pp. 15708–15723, Jun. 2017, doi: 10.1016/j.ijhydene.2017.03.133.
- [105] O. A. Jianu, M. A. Rosen, G. F. Naterer, and Z. Wang, “Two-phase bubble flow and convective mass transfer in water splitting processes,” *International Journal of Hydrogen Energy*, vol. 40, no. 11, pp. 4047–4055, Mar. 2015, doi: 10.1016/j.ijhydene.2015.01.074.
- [106] A. Glassner, “The thermochemical properties of the oxides, fluorides, and chlorides to 2500° K,” Argonne National Lab., Lemont, Ill., 1957.
- [107] H. Goldstein, C. Poole, and J. Safko, *Classical mechanics*. American Association of Physics Teachers, 2002.
- [108] “Classical mechanics - New World Encyclopedia.” https://www.newworldencyclopedia.org/entry/Classical_mechanics (accessed Jul. 28, 2020).
- [109] Gy. T. W. vector image was created with Inkscape, *A simplified view on fields of modern physics theories*. 2008.
- [110] “subatomic particle | Definition, Examples, & Classes,” *Encyclopedia Britannica*. <https://www.britannica.com/science/subatomic-particle> (accessed Jul. 28, 2020).
- [111] “The Science of Fluorescence Photography,” *DivePhotoGuide*. <http://www.divephotoguide.com/underwater-photography-special-features/article/science-technology-fluorescence-photography/> (accessed Jul. 28, 2020).
- [112] “Physics - Quantum mechanics,” *Encyclopedia Britannica*. <https://www.britannica.com/science/physics-science> (accessed Jul. 28, 2020).
- [113] C. J. Davisson and L. H. Germer, “Reflection of Electrons by a Crystal of Nickel,” *Proceedings of the National Academy of Sciences of the United States of America*, vol. 14, no. 4, p. 317, 1928.
- [114] R. P. Feynman, *QED: The strange theory of light and matter*. Princeton University Press, 2006.
- [115] E. Schrödinger, “An undulatory theory of the mechanics of atoms and molecules,” *Physical review*, vol. 28, no. 6, p. 1049, 1926.
- [116] OpenStax, “10.5 The Solid State of Matter,” in *Chemistry*, 2016.
- [117] J. W. Rohlf, “Modern Physics from alpha to Z0,” *Modern Physics from alpha to Z0*, by James William Rohlf, pp. 664. ISBN 0-471-57270-5. Wiley-VCH, March 1994., p. 664, 1994.
- [118] S. Harris, *An introduction to the theory of the Boltzmann equation*. Courier Corporation, 2004.
- [119] K. S. Pitzer, “The heat capacity of diamond from 70 to 300° K,” *The Journal of Chemical Physics*, vol. 6, no. 2, pp. 68–70, 1938.
- [120] D. Rogers, *Einstein’s other theory: the Planck-Bose-Einstein theory of heat capacity*. Princeton University Press, 2005.

- [121] P. Debye, "Zur Theorie der spezifischen Wärmen," *Annalen der Physik*, vol. 344, no. 14, pp. 789–839, 1912, doi: 10.1002/andp.19123441404.
- [122] "Comparing Calorimetry Methods," *AZoSensors.com*, May 10, 2017. <https://www.azosensors.com/article.aspx?ArticleID=798> (accessed Jul. 29, 2020).
- [123] R. Mayer, "„Die organische Bewegung in ihrem Zusammenhang mit dem Stoffwechsel“, 1845, S. 3; nachgedruckt in: P," *Buck (Hrsg.):„R. Mayer: Die universelle Anwendung des Prinzips vom mechanischen Äquivalent der Wärme“, Hildesheim, 1980.*
- [124] F. J. Mellencamp, "Application of Gibbs-Helmholtz Equation to Concentration Cells," *Physical Review (Series I)*, vol. 29, no. 4, pp. 329–350, Oct. 1909, doi: 10.1103/PhysRevSeriesI.29.329.
- [125] P. Atkins, "Molecules in motion: ion transport and molecular diffusion," *Physical chemistry*, pp. 819–848, 1978.
- [126] R. E. Barieau, "The Correct Application of the Gibbs—Helmholtz Equation to Reversible Galvanic Cells in which Several Phases Are in Equilibrium at One of the Electrodes," *Journal of the American Chemical Society*, vol. 72, no. 9, pp. 4023–4026, Sep. 1950, doi: 10.1021/ja01165a052.
- [127] G. N. Lewis and M. Randall, *Thermodynamics and the free energy of chemical substances*. McGraw-Hill, 1923.
- [128] O. M. Suleimenov and R. E. Krupp, "Solubility of hydrogen sulfide in pure water and in NaCl solutions, from 20 to 320°C and at saturation pressures," *Geochimica et Cosmochimica Acta*, vol. 58, no. 11, pp. 2433–2444, Jun. 1994, doi: 10.1016/0016-7037(94)90022-1.
- [129] H. Suzuki, A. Inaba, and C. Meingast, "Accurate heat capacity data at phase transitions from relaxation calorimetry," *Cryogenics*, vol. 50, no. 10, pp. 693–699, 2010.
- [130] W. T. Berg, "Low-temperature heat capacities of silver chloride and lithium iodide," *Physical Review B*, vol. 13, no. 6, pp. 2641–2645, Mar. 1976, doi: 10.1103/PhysRevB.13.2641.
- [131] E. D. Eastman and R. T. Milner, "The Entropy of a Crystalline Solution of Silver Bromide and Silver Chloride in Relation to the Third Law of Thermodynamics," *The Journal of Chemical Physics*, vol. 1, no. 7, pp. 444–456, Jul. 1933, doi: 10.1063/1.1749317.
- [132] K. Clusius and P. Harteck, "Über die spezifischen Wärmen einiger fester Körper bei tiefen Temperaturen," *Zeitschrift für Physikalische Chemie*, vol. 134U, no. 1, Jan. 1928, doi: 10.1515/zpch-1928-13419.
- [133] F. C. Brown, "Temperature Dependence of Electron Mobility in AgClf," p. 9.
- [134] A. Maqsood, M. Anis-ur-Rehman, K. Kamran, and I. H. Gul, "Thermophysical properties of AgCl in the temperature range 77–300 K," *Journal of Physics D: Applied Physics*, vol. 37, no. 13, pp. 1845–1847, Jul. 2004, doi: 10.1088/0022-3727/37/13/018.

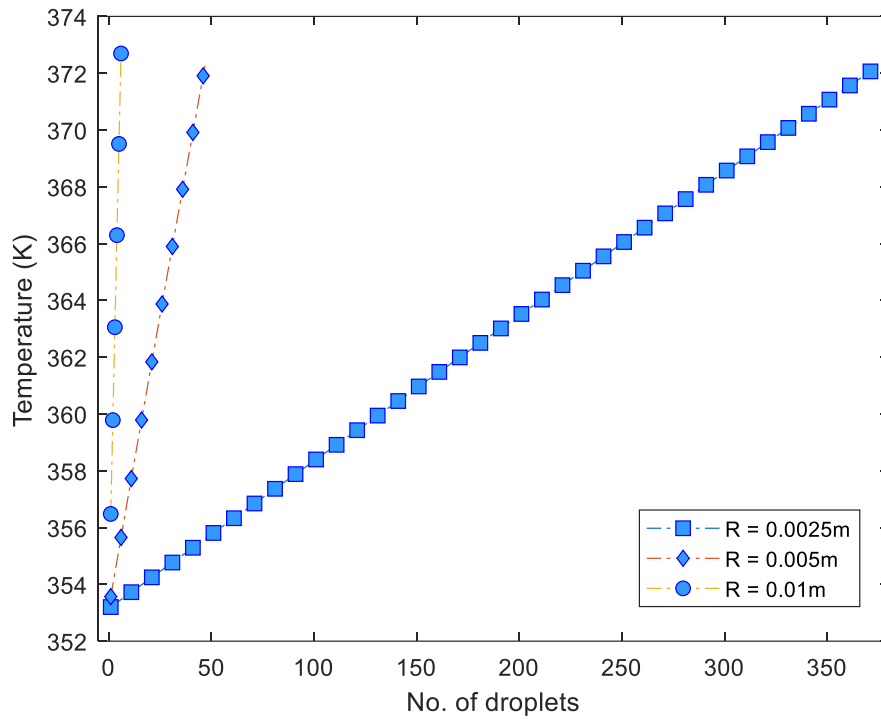
- [135] Ü. Akdere, "Thermal expansion and heat capacities of AgBr and AgCl at solid and liquid phases from molecular dynamics simulation," *International Journal of Modern Physics B*, vol. 29, no. 14, p. 1550091, Jun. 2015, doi: 10.1142/S0217979215500915.
- [136] L. Rycerz, M. Szymanska-Kolodziej, P. Kolodziej, and M. Gaune-Escard, "Thermodynamic Properties of AgCl and AgBr," *Journal of Chemical & Engineering Data*, vol. 53, no. 5, pp. 1116–1119, May 2008, doi: 10.1021/jc700668b.
- [137] W. Jost and P. Kubaschewski, "Spezifische Wärmen von Silber- und Kupfer(I)-Chalkogeniden von -70°C bis zu 550°C ," *Zeitschrift für Physikalische Chemie*, vol. 60, no. 1–6, pp. 69–78, Jul. 1968, doi: 10.1524/zpch.1968.60.1-6.069.
- [138] L. B. Pankratz, *Thermodynamic data for silver chloride and silver bromide*, vol. 7430. US Department of Interior, Bureau of Mines, 1970.
- [139] A. Laskar and M. Reynolds, "Anomalous heat capacity of Agx and the nonlinear temperature dependence of the formation energy of Frenkel defects," *Radiation Effects and Defects in Solids*, vol. 119–121, no. 2, pp. 597–602, Nov. 1991, doi: 10.1080/10420159108220788.
- [140] A. L. Laskar, "Defect properties and diffusion in silver halides," *Philosophical Magazine A*, vol. 64, no. 5, pp. 1043–1057, Nov. 1991, doi: 10.1080/01418619108204877.
- [141] K. Kobayashi, "Heat Capacity and Lattice Defects of Silver Chloride," *Physical Review*, vol. 85, no. 1, p. 150, 1952.
- [142] A. F. Wilde and R. L. Seifert, "Electronic Commutator Method for Determining E° of Formation of Fused Halides," *Journal of The Electrochemical Society*, vol. 108, no. 11, p. 1059, 1961, doi: 10.1149/1.2427947.
- [143] C. R. Metz and R. L. Seifert, "Emf of Isothermal and Nonisothermal Formation Cells of Molten Silver Halides," *Journal of The Electrochemical Society*, vol. 117, no. 1, p. 49, 1970, doi: 10.1149/1.2407437.
- [144] C. M. Mari and G. Terzaghi, "Solid-state galvanic cell for monitoring chlorine partial pressure," *Sensors and Actuators*, vol. 17, no. 3–4, pp. 569–574, May 1989, doi: 10.1016/0250-6874(89)80046-0.
- [145] A. D. Pelton and S. N. Flengas, "Thermodynamics of Molten Silver Chloride-Alkali Chloride Solutions by Electromotive Force Measurements," *Journal of The Electrochemical Society*, vol. 117, no. 9, p. 1130, 1970, doi: 10.1149/1.2407753.
- [146] M. B. Panish, F. F. Blankenship, W. R. Grimes, and R. F. Newton, "Thermodynamic Properties of Molten and Solid Solutions of Silver Chloride and Sodium Chloride," *The Journal of Physical Chemistry*, vol. 62, no. 10, pp. 1325–1331, Oct. 1958, doi: 10.1021/j150568a038.

- [147] M. B. Panish, R. F. Newton, W. R. Grimes, and F. F. Blankenship, "Thermodynamic Properties of Molten and Solid Solutions of Silver Chloride and Lithium Chloride," *The Journal of Physical Chemistry*, vol. 63, no. 5, pp. 668–671, May 1959, doi: 10.1021/j150575a007.
- [148] J. Guion, M. Blander, D. Hengstenberg, and K. Hagemark, "Thermodynamic treatment and electromotive force measurements of the ternary molten salt systems silver chloride-sodium chloride-potassium chloride and silver chloride-sodium chloride-cesium chloride," *The Journal of Physical Chemistry*, vol. 72, no. 6, pp. 2086–2095, Jun. 1968, doi: 10.1021/j100852a035.
- [149] M. Bottarelli, M. Bortoloni, Y. Su, C. Yousif, A. A. Aydın, and A. Georgiev, "Numerical analysis of a novel ground heat exchanger coupled with phase change materials," *Applied Thermal Engineering*, vol. 88, pp. 369–375, Sep. 2015, doi: 10.1016/j.applthermaleng.2014.10.016.
- [150] K. K. Stern, "Electrode Potentials in Fused Systems. III. The Platinum Electrode in Some Halide Melts," *The Journal of Physical Chemistry*, vol. 60, no. 10, pp. 1443–1445, Oct. 1956, doi: 10.1021/j150544a028.
- [151] E. J. Salstrom, "The Free Energy of Reactions Involving the Fused Chlorides and Bromides of Lead, Zinc and Silver," *Journal of the American Chemical Society*, vol. 55, no. 6, pp. 2426–2428, Jun. 1933, doi: 10.1021/ja01333a031.
- [152] W. J. Hamer, M. S. Malmberg, and B. Rubin, "Theoretical Electromotive Forces for Cells Containing a Single Solid or Molten Chloride Electrolyte," *Journal of The Electrochemical Society*, vol. 103, no. 1, p. 8, 1956, doi: 10.1149/1.2430236.
- [153] A. Pelloux, J. Quessada, J. Fouletier, P. Fabry, and M. Kleitz, "Utilization of a dilute solid electrolyte in an oxygen gauge," *Solid State Ionics*, vol. 1, no. 5–6, pp. 343–354, Dec. 1980, doi: 10.1016/0167-2738(80)90033-8.
- [154] B. F. Markov and E. B. Kuzyakin, "Thermogalvanic Cells with a Single Fused Salt," *Russian Chemical Reviews*, vol. 41, no. 3, pp. 250–257, Mar. 1972, doi: 10.1070/RC1972v041n03ABEH002042.
- [155] S. Senderoff and R. I. Bretz, "Ionic Transport Entropy in Nonisothermal Molten Silver Chloride Cells," *Journal of The Electrochemical Society*, vol. 109, no. 1, p. 56, 1962, doi: 10.1149/1.2425326.
- [156] S. Senderoff and G. W. Mellors, "Reversible Chlorine Electrode for the Measurement of Electromotive Force in Molten Salt Cells," *Review of Scientific Instruments*, vol. 29, no. 2, pp. 151–152, Feb. 1958, doi: 10.1063/1.1716125.
- [157] G. J. Janz, *Molten salts handbook*. Elsevier, 2013.
- [158] L. L. Quill, *The chemistry and metallurgy of miscellaneous materials*. ACS Publications, 1950.

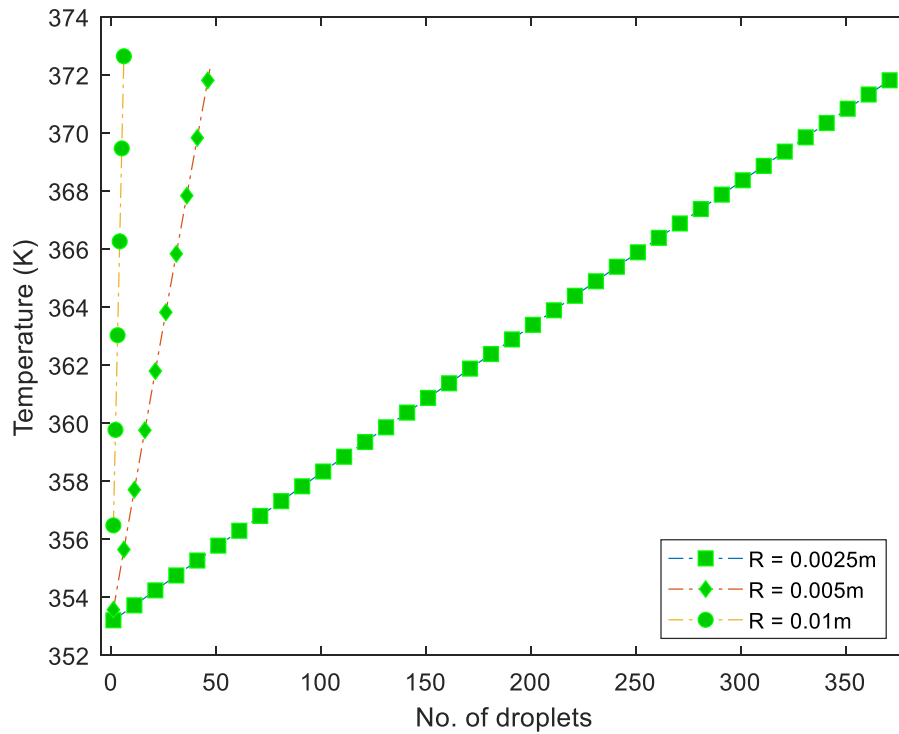
- [159] R. Lorenz and A. Höchberg, "Dichtebestimmungen an geschmolzenen Silberhaloiden," *Zeitschrift für anorganische und allgemeine Chemie*, vol. 94, no. 1, pp. 288–300, Mar. 1916, doi: 10.1002/zaac.19160940116.
- [160] B. Harrap and E. Heymann, "The constitution of ionic liquids. Part 1.—The electric conductivity and viscosity of the molten salt systems, AgCl+ AgBr, PbCl₂+ PbBr₂, AgCl+ PbCl₂, AgCl+ KCl, AgBr+ KBr," *Transactions of the Faraday Society*, vol. 51, pp. 259–267, 1955.
- [161] Z. Vardeny, D. Moses, G. Gilat, and H. Shechter, "Specific heat of CuCl," *Solid State Communications*, vol. 18, no. 9–10, pp. 1369–1371, Jan. 1976, doi: 10.1016/0038-1098(76)90980-7.
- [162] M. W. Chase, "NIST-JANAF thermochemical tables, Fourth edition, Part 1, Al-Co," *Journal of Physical and Chemical Reference Data*, p. 727, 1998.
- [163] J. Avsec, "The calculation of specific heats for some important solid components in hydrogen production process based on CuCl cycle," *Thermal Science*, vol. 18, no. 3, pp. 823–831, 2014, doi: 10.2298/TSCI1403823A.
- [164] I. Barin, O. Knacke, and O. Kubaschewski, *Thermochemical properties of inorganic substances*. Berlin, Heidelberg: Springer Berlin Heidelberg, 1977.
- [165] G. A. Slack and P. Andersson, "Pressure and temperature effects on the thermal conductivity of CuCl," *Physical Review B*, vol. 26, no. 4, pp. 1873–1884, Aug. 1982, doi: 10.1103/PhysRevB.26.1873.
- [166] D. R. Lide, "CRC handbook of chemistry and physics," *Boca Raton: CRC Press*, vol. 1994, pp. 148–155, 1993.
- [167] Z. Glaztzoğlu, "Redox Electromotive Force Measurements in the Molten CuCl-CuCl₂ System and Thermodynamic Properties of Liquid CuCl₂," p. 4.
- [168] Z. Giazitzoğlu, H. Engels, and U. Schiller, "Notizen: Excess Free Energies in Molten CuCl-KCl-LiCl by EMF Measurements," *Zeitschrift für Naturforschung A*, vol. 38, no. 1, pp. 88–89, Jan. 1983, doi: 10.1515/zna-1983-0117.
- [169] Sudworth, "High-temperature battery systems," p. 18, 1996.
- [170] G. F. Naterer, *Hydrogen production from nuclear energy*. New York: Springer, 2013.
- [171] D. R. Lide, *CRC handbook of chemistry and physics*, vol. 85. CRC press, 2004.
- [172] H. K. Gupta and S. Roy, *Geothermal energy: an alternative resource for the 21st century*. Elsevier, 2006.
- [173] Z. Karpas, Z. Berant, and O. Shahal, "Effect of temperature on the mobility of ions," *Journal of the American Chemical Society*, vol. 111, no. 16, pp. 6015–6018, Aug. 1989, doi: 10.1021/ja00198a007.

- [174] N. Calvet, X. Py, R. Olivès, J.-P. Bédécarrats, J.-P. Dumas, and F. Jay, “Enhanced performances of macro-encapsulated phase change materials (PCMs) by intensification of the internal effective thermal conductivity,” *Energy*, vol. 55, pp. 956–964, Jun. 2013, doi: 10.1016/j.energy.2013.03.078.
- [175] J. Dehghannya, M. Ngadi, and C. Vigneault, “Mathematical modeling of airflow and heat transfer during forced convection cooling of produce considering various package vent areas,” *Food Control*, vol. 22, no. 8, pp. 1393–1399, Aug. 2011, doi: 10.1016/j.foodcont.2011.02.019.
- [176] M. Srivastava, “Computational analysis of encapsulated thermal energy phase change storage system: cylindrical and spherical geometry,” p. 7.
- [177] M. Azad, D. Dineshan, D. Groulx, and A. Donaldson, “Melting of phase change materials in a cylindrical enclosure: parameters influencing natural convection onset.,” p. 7.
- [178] E. Oró, J. Chiu, V. Martin, and L. F. Cabeza, “Comparative study of different numerical models of packed bed thermal energy storage systems,” *Applied Thermal Engineering*, vol. 50, no. 1, pp. 384–392, Jan. 2013, doi: 10.1016/j.applthermaleng.2012.07.020.
- [179] N. S. Dhaidan and J. M. Khodadadi, “Melting and convection of phase change materials in different shape containers: A review,” *Renewable and Sustainable Energy Reviews*, vol. 43, pp. 449–477, Mar. 2015, doi: 10.1016/j.rser.2014.11.017.
- [180] “Definition of laminar flow | Dictionary.com,” www.dictionary.com. <https://www.dictionary.com/browse/laminar-flow> (accessed Aug. 24, 2020).
- [181] V. Kurganov, “Heat transfer coefficient,” *A-to-Z Guide to Thermodynamics, Heat and Mass Transfer, and Fluids Engineering*, 2011.

APPENDICES



Appendix 1. Temperature increase of water by CuCl droplets for the quenching height of 20cm



Appendix 2. Temperature increase of water by CuCl droplets for the quenching height of 30cm

VITA AUCTORIS

NAME: Bharanidharan Rajasekaran

PLACE OF BIRTH: Tamil Nadu, India

YEAR OF BIRTH: 1994

EDUCATION: Jawahar Higher Secondary School, Tamil Nadu, India,
2011

Amrita Vishwa Vidyapeetham, B.Tech, Tamil Nadu,
India, 2015

University of Windsor, M.A.Sc., Windsor, ON, 2020